Quantitative and compositional magnetic resonance imaging study of bone marrow oedema-like lesions in knee osteoarthritis

A thesis submitted to the University of Manchester for the degree of Doctor of Philosophy in the Faculty of Biology, Medicine and Health

2021

Henry Noorveriandi

SCHOOL OF BIOLOGICAL SCIENCES

List of Contents

Word count: 44010

List of Tables

List of Figures

List of Abbreviations

2D	2-dimensional
3D	3-dimensional
AMARES	Advanced method for accurate, robust, and efficient spectral
AP	Antero-posterior
BLOKS	Boston-Leeds osteoarthritis knee score
BME	Bone marrow edema
BMI	Body mass index
BMLs	bone marrow oedema-like lesions
BW	bandwidth
CE	contrast enhanced
CE T1-w FS	Contrast enhanced T1-weighted fat suppressed
CI	Confidence interval
CS	Chondroitin sulphate
DCE	Dynamic contrast-enhanced
DESS	Dual-echo steady-state
FF	Fat fraction
FFE	Fast field echo
FISP	Fast imaging with steady state precession
FLASH	Fast low-angle shot
FOV	field of view
FS	fat-suppressed

FSE	Fast spin-echo
FWB	Fat water bone
GE	Gradient echo
GRASS	Gradient recalled acquisition in steady state
ICC	Intraclass correlation coefficient
IP	In-phase
IQR	Interquartile range
IR	inversion recovery
ISRCTN	International standard randomised controlled trial number
IW	Intermediate weighted
jMRUI	Java-based Magnetic Resonance User Interface
JOG	Joint on glucosamine
KL	Kellgren and Lawrence
KOOS	Knee Osteoarthritis Scoring System
MOAKS	Magnetic resonance Osteoarthritis Knee score
MOST	Multicenter osteoarthritis study
MRI	magnetic resonance imaging
MRS	Magnetic resonance spectroscopy
ms	millisecond
NIHR	National institute for health research
NMV	Net magnetisation vector
OA	osteoarthritis
OAI	Osteoarthritis initiative

OP	Out of phase
OR	Odds ratio
PD	Proton density
PDFS	Proton density fat-suppressed
PF	Patellofemoral
ppm	Part per million
PRESS	Point-resolved spectroscopy
RC	Regression coefficient
RCT	Randomised controlled trial
RF	radio frequency
ROI	region of interest
SD	Standard deviation
SDNR	Signal difference-to-noise ratio
SE	Spin-echo
SENSE	Sensitivity encoding
SIP	Signal in-phase
SNR	Signal to noise ratio
SOP	Signal out-of-phase
SPAIR	Spectral adiabatic inversion recovery
SPGR	Spoiled gradient recalled
SPIR	Spectral presaturation with inversion recovery
SSIR	Single slice inversion recovery
STEAM	Stimulated echo acquisition mode

STIR	short tau inversion recovery
T1-w FFE	T1-weighted fast field echo
TE	Echo time
TI	Inversion time
TM	Mixing time
TR	Repetition time
TSE	Turbo spin-echo
VAS	Visual analogue score
VFA	Variable flip angle
VOI	Volume of interest
WATSc	Water-selective cartilage scans
WOMAC	Western Ontario and McMaster Universities Arthritis Index
WORMS	Whole-organ magnetic resonance imaging score
ZA	Zoledronic acid

Abstract

The University of Manchester
Henry Noorveriandi
Doctor of Philosophy

Quantitative and compositional magnetic resonance imaging study of bone marrow oedema-like lesions in knee osteoarthritis

Background: Bone marrow oedema-like lesions (BMLs) detected on magnetic resonance imaging are common in patients with knee OA and have been linked with pain and disease progression. A number of MRI sequences have been used to assess BML size, however there are few data directly comparing sequences and the optimum approach remains unknown. Structural change within BMLs, including an increase in water content, offers a potential alternative approach to the assessment of BMLs using novel compositional MRI methods.

Aim: The overall aim of the thesis was to evaluate the performance of different MRI sequences in the assessment of bone marrow lesions (BMLs) in knee osteoarthritis and to investigate the role of novel compositional MRI methods (mDixon Quant fat fraction and T1 mapping) for BML assessment.

Methods: BML volumes were compared using STIR, PDFS, contrast enhanced T1-w FS, GE T1-w FS and 3D GE mDixon Quant water-only images obtained from patients with knee OA. In a separate study of OA patients, fat fraction was determined using 3D GE mDixon Quant imaging in both normal marrow and BMLs and change in fat fraction over an 8-week period using image registration was compared with change in BML volume. A series of fat-water-bone (FWB) phantoms comprising different fat fractions were made and imaged using 3D mDixon Quant imaging and T1 mapping (Single slice inversion recovery, SSIR and variable flip angle, VFA) and results compared with MR Spectroscopy. A preliminary study of SSIR T1-based measurements in a small number of knee OA subjects was also performed.

Results: Reliability of the assessment of BML size was excellent for STIR, PDFS, contrast enhanced T1-w FS and 3D GE mDixon Quant water-only sequences. There was little difference in BML size assessed using the different sequences apart from the 3D FS GE T1-w sequence which was much less sensitive. Fat fraction from 3D GE mDixon Quant images was significantly lower in BMLs compared to non-BML marrow in subjects with knee OA and change in fat fraction correlated with change in BML size over time. In-vitro fat fraction values from mDixon Quant imaging were similar to those obtained using MR spectroscopy. There was a strong correlation between SSIR and VFA T1 estimates in the phantom. SSIR T1-based measurements of BMLs showed differences compared to marrow without BML in knee OA subjects.

Conclusion: Most conventional fluid sensitive MRI sequences are reliable and sensitive for assessment of BML size. 3D gradient echo Dixon imaging appears a promising technique for the assessment of BMLs in osteoarthritis, allowing both volumetric and compositional assessment, despite previous concerns about gradient echo imaging in the literature. T1 mapping holds promise as a novel approach to imaging BMLs but is less feasible and less well validated than Dixon imaging.

Declaration

No portion of the work referred to in the thesis has been submitted in support of an application for another degree or qualification of this or any other university or other institute of learning.

Copyright Statement

i. The author of this thesis (including any appendices and/or schedules to this thesis) owns certain copyright or related rights in it (the "Copyright") and s/he has given the University of Manchester certain rights to use such Copyright, including for administrative purposes.

ii. Copies of this thesis, either in full or in extracts and whether in hard or electronic copy, may be made only in accordance with the Copyright, Designs and Patents Act 1988 (as amended) and regulations issued under it or, where appropriate, in accordance with licensing agreements which the University has from time to time. This page must form part of any such copies made.

iii. The ownership of certain Copyright, patents, designs, trademarks, and other intellectual property (the "Intellectual Property") and any reproductions of copyright works in the thesis, for example graphs and tables ("Reproductions"), which may be described in this thesis, may not be owned by the author, and may be owned by third parties. Such Intellectual Property and Reproductions cannot and must not be made available for use without the prior written permission of the owner(s) of the relevant Intellectual Property and/or Reproductions.

iv. Further information on the conditions under which disclosure, publication and commercialisation of this thesis, the Copyright and any Intellectual Property and/or Reproductions described in it may take place is available in the University IP Policy (see http://documents.manchester.ac.uk/DocuInfo.aspx?DocID=24420), in any relevant Thesis restriction declarations deposited in the University Library, the University Library's regulations (see http://www.library.manchester.ac.uk/about/regulations/) and in the University's policy on Presentation of Theses.

Acknowledgement

First and foremost, of the long list of those I would like to express my sincere gratitude are my supervisors, Professor Terence O'Neill and Dr Richard Hodgson, for their invaluable support, advice, patience, and encouragement throughout my PhD. Terry and Richard have always given me thoughtful feedback on all of my projects, allowing this thesis to provide beneficial evidence for research in the relevant subject. I could not have completed this thesis without their support.

I am very much indebted to Professor David Felson, Director of Research in Osteoarthritis Manchester (ROAM), for having me in his research group, allowing me access to unpublished ROAM data, and his valuable comments and suggestions on my work.

I am especially grateful to Professor Timothy Cootes, Professor Michael Callaghan, and Dr Matthew Parkes for their invaluable help, support, and constructive suggestions. I also appreciate all the support I received from Ms Helen Williams and her staff in ROAM group.

Additionally, I would like to express gratitude to Professor Stephen Williams for his invaluable support, advice, and suggestions on my MR spectroscopy project. Without his help, it is hard to imagine how I would have managed to complete this study.

My gratitude extends to Professor Susan Astley as my PGR Advisor for her advice and encouragement throughout my PhD.

My appreciation also goes out to Dr Josephine Naish, Dr Damien McHugh, and Dr William Lloyd for their tremendous help on my T1 mappings project. I would also like to thank Dr David Higgins from Philips for his valuable support and Dr Ben Dickie for his kind help and support in making my phantoms. I would not have been able to do this work without their help.

I am also grateful to the staff and radiographers at Manchester clinical research facility (CRF) where the MRI scans occurred, particularly Mr Barry Whitnall, Mr Neal Sherratt, and Ms Sarah Lehmann, for their support to make this research possible.

I would also like to acknowledge Indonesia Endowment Fund for Education (*Lembaga Pengelola Dana Pendidikan*) in the Ministry of Finance of the Republic of

Indonesia for funding my doctoral programme. I would not have been able to do this without this funding.

Finally, I would like to thank my family members for all their love, to my parents for their unlimited support. My beloved wife, Dr Asri Maharani, I owe a massive debt of gratitude for her motivation, encouragement, patience, and support; and my daughters, Nandita and Adinda. Without their tremendous understanding and encouragement in the past few years, it would be impossible to complete my study.

Chapter 1

Introduction

Chapter 1
Introduction

1.1 Summary

This chapter reviews the clinical and public health impact of knee osteoarthritis (OA). Imaging features of knee OA are outlined with a focus on bone marrow oedema-like lesions (BMLs) identified using magnetic resonance imaging (MRI). The broad aim of the work presented in the thesis is outlined. This is followed by a summary of the content of subsequent thesis chapters.

1.2 Knee osteoarthritis

Osteoarthritis (OA) is a chronic degenerative disease affecting the joints which results in chronic pain, stiffness, and disability [1, 2]. It is a major global health problem, affecting millions of people worldwide [1, 3] and one of the leading causes of chronic pain and disability in the elderly population [1, 4, 5]. It can affect any joint though the knee is one of the most frequently affected sites [6]. Around the globe, approximately 250 million people suffer from knee OA [3]. Symptomatic knee OA affects more than 14 million US citizens, with the risk increasing with age [7, 8]. Knee OA is linked with a significant economic costs, largely driven by the requirement for joint replacement surgery [5]. With increasing life expectancy in most developed countries and a rise in the number of people with obesity, an important risk factor, the number of people with knee OA is increasing [9].

On plain radiography, features of knee OA include the presence of osteophytes, joint space narrowing, subchondral bone sclerosis, and subchondral cysts formation.

Additional structural features are present on MR imaging, including bone marrow oedema-like lesions [10].

1.3 Bone marrow oedema-like lesions

Bone marrow oedema-like lesions (BMLs) are common, affecting up to 80% of those with symptomatic OA. On MRI they are seen as ill-defined areas of high signal intensity adjacent to subchondral bone. Histologically they can be shown to represent areas of bone damage. They are of clinical and prognostic significance being and have been shown to be an important predictor of pain [11, 12] and OA progression [12-14]. Given their link with symptom and disease progression, BMLs can be considered potentially important biomarkers in observational studies of patients with knee OA and as outcome measures in clinical trials of interventions in knee OA.

There are a number of different MRI sequences have been used to identify and also assess the size of BMLs, including T2-weighted fat-suppressed [15], proton density-weighted fat-suppressed, short-tau inversion recovery [16], and contrast-enhanced T1 weighted fat-suppressed MRI sequences [17, 18]. To date, though, it is not clear which approach provides the optimum method for assessing BMLs in terms of reliability, accuracy, and sensitivity to change.

Novel application of compositional MR imaging techniques provide a potentially different approach for the assessment of BMLs based on biochemical composition of the tissues, and particularly the assessment of fat and water; these include Dixon techniques [19] and T1 relaxation time measurement (T1 mapping) [20]. To date, however, no data are looking at the use of these techniques in the assessment of BMLs in knee OA.

The broad aim of the work described in this thesis is to determine the optimum method of a quantitative assessment of BML size in patients with symptomatic knee OA and to investigate compositional MRI techniques as an alternative approach to the assessment of BML size in knee OA.

1.4 Outline of thesis

In the next chapter, the background literature relating to BMLs and the assessment of BMLs is reviewed. This is followed by the aims and objectives (Chapter 3) and then the study methods used to address these aims (Chapter 4). In Chapter 5, the results of an analysis looking at the reliability of BML volume assessment using different conventional MRI sequences are described. This is followed by Chapter 6, in which the results of a comparison of novel quantitative gradient echo Dixon imaging with conventional MR imaging for assessing BML volume are reported. In Chapter 7, Dixon fat fraction measurements are investigated in BMLs, and image registration is used to compare fat fraction changes with conventional BML volume change over time. A study of MR spectroscopy, Dixon fat fraction and T1 in a fat-water-bone phantom and a human subject is reported in Chapter 8. The chapter includes the results of a small preliminary study using a novel method for estimating fat fraction from T1 relaxation data. In the last chapter (Chapter 9), the implications of the findings are discussed and some directions for future research provided.

Chapter 2

Background

Chapter 2

Background

2.1 Summary

This chapter begins with an overview of OA of the knee, including its occurrence and aetiology. Clinical and imaging features of the disease are discussed, including plain radiography and MRI imaging. The focus of the thesis is on bone marrow oedema-like lesions (BMLs) associated with knee osteoarthritis. These are described in detail, including their assessment, clinical significance, and histopathologic features. Different MRI sequences which have been used to assess BMLs are summarised, and the literature relating to accuracy, reliability, and sensitivity to change of BMLs assessed using these sequences reviewed. Following this, there is a review of novel compositional MRI/ MR spectroscopy techniques and their potential application in the assessment of OA and BMLs.

2.2 Knee osteoarthritis

2.2.1 Definition of osteoarthritis

Osteoarthritis (OA) can be defined as a complex chronic disease of the entire joints characterised by the deterioration of articular cartilage, in addition to related changes in the adjacent bone, as well as associated inflammation involving ligaments, joint capsule, synovial membrane, and periarticular muscles [21].

2.2.2 Occurrence and aetiology

Osteoarthritis of the knee affects over one in eight men and women over the age of 60 and is a major cause of disability. Prevalence increases with age, and it is more

common in women than men. It is also linked with a significant health care costs largely driven by the requirement for joint replacement surgery with approximately 600,000 knee replacements performed annually in the United States [22].

Genetic factors, constitutional/ environmental, and local factors predispose to the development of knee OA. Different genes have been identified as contributing to susceptibility to OA, including genes for vitamin D receptors, insulin-like growth factor 1 [23], type 2 collagen [24], and growth differentiation factor 5 [25]. Environmental factors include obesity and trauma that linked with occupational/ recreational activity. Being overweight is linked with an increased risk of knee OA [26]. Local factors, including joint malalignment, may also play a role. Pathologically, the disease is characterised by loss of articular cartilage, synovial inflammation and hypertrophy, meniscal damage, subchondral remodelling with marginal osteophytes formation, and bone marrow oedema-like lesions, as well as muscle and ligament abnormalities [27].

2.2.3 Clinical features and diagnosis

Symptoms of knee OA include pain, stiffness, and loss of function. Pain is typically worse with activity and relieved by rest, though over time pain may become continuous and persistent at rest or at night. Loss of function includes impaired mobility and difficulty in a range of activities of daily living. On physical examination, the knee may be increased in size, with evidence of muscle wasting, knee effusion and crepitus. Diagnostic criteria for knee OA based on history and clinical examination, and X-ray findings according to American College of Rheumatology are outlined in table 2.1.

A. Osteoarthritis if (using history and clinical examination): Pain in the knee for most days of the previous month and three of the following: 1. Age more than 50 years 2. Morning stiffness lasting 30 minutes or less 3. Present of crepitus on active joint motions 4. Bony tenderness 5. Bony enlargement of the knee on examination 6. No palpable warmth of synovium
B. Osteoarthritis if (using history, clinical examination, and radiographic findings): Pain in the knee for most days of the previous month and at least one of the following: 1. Age more than 50 years 2. Morning stiffness lasting 30 minutes or less 3. Crepitus on active motions and osteophyte at joint margins on radiographs

* Modified from Altman et al. (1986) [21]

*Table 2.1. Criteria for the diagnosis of OA of the knee**

2.3 Imaging

In this section, imaging of knee OA is reviewed, including plain radiographs and magnetic resonance imaging (MRI). Novel/ advanced MR compositional imaging techniques are also discussed.

2.3.1 Plain radiography

Plain radiography (X-ray) remains the investigation of choice in clinical practice for the diagnosis of OA and to assess disease progression. The technique has some advantages; it is inexpensive, fast, easily available, and can be obtained while the patient is loading their joint (weight-bearing) [28]. It is used to detect bony abnormalities, including marginal osteophytes formation, subchondral bone sclerosis, subchondral cysts formation, abnormal bone contour, and joint space narrowing [29]. Despite its advantages, there are limitations; it provides only an indirect measure of cartilage thickness by looking at the joint space and is unable to provide a direct

evaluation of cartilage and meniscal integrity, as well as synovial tissue. Other disadvantages are radiation exposure and the inability to visualise other soft tissues.

The severity of radiographic OA can be assessed by using semiquantitative scoring systems. Several grading scales exist for the assessment of the severity of OA, including the most widely used Kellgren and Lawrence (KL) classification system-[29]. This system has been developed as a radiological grading of OA for several joints, including knees, hips, and hands. The classification focuses on osteophyte formation, joint space narrowing, and bone sclerosis. It provides five grading scales (0: no abnormality to 4: severe), mostly depending on the osteophyte status and joint space narrowing for the classification. Figure 2.1 shows representative examples of different KL grades at the knee on antero-posterior (AP) radiographs [30].

Figure 2.1. The Kellgren-Lawrence classification. (A) Grade 1. Minimal, doubtful osteophyte is observed at the lateral joint margins. (B) Grade 2 is defined as the presence of at least one definite osteophyte and without joint space narrowing. (C) Grade 3 knee OA shows multiple osteophytes, definite joint space narrowing, and some sclerosis. (D) Grade 4 exhibits some findings: large osteophytes, marked joint space narrowing, severe sclerosis, and definite deformity of bone ends. Reproduced from Proteomic analysis of synovial fluid in osteoarthritis using SWATH-mass spectrometry, Liao, W., Li, Z., Li, T., Zhang, Q., Zhang, H., and Wang, X., Molecular medicine reports,17(2), pp.2827-2836, 2018, licensed under CC BY-NC-ND 4.0.

The Kellgren-Lawrence classification has been commonly used as a screening tool for participants' recruitment in clinical trials, though there are some limitations of radiography for the assessment of joint space narrowing [31]. First, joint space

narrowing may be defined by the evaluation of the distance between the distal femur and proximal tibia at only a point of contact and therefore, any cartilage loss in other areas would not be captured. Secondly, the joint space not only consists of cartilage but also the meniscus [32]. Therefore, joint space narrowing on plain radiography may not necessarily reflect true cartilage loss but may also reflect meniscal damage or combinations of both. Lastly, radiographs are unlikely to be sensitive to evaluate small changes in cartilage over time [33].

2.3.2 Magnetic resonance imaging

MRI can demonstrate BMLs and has revolutionised understanding the pathophysiology and natural history of knee OA [34]. MRI changes of OA may be present before changes on plain radiographs. A case-control study of 155 participants with no radiographic features of knee OA showed that some pathologic features of OA, including osteophytes, cartilage damage, and BMLs, were more commonly detected on MRI of cases than controls [35]. This study further found that the presentation of BMLs may have an important role in the development of knee pain within 15 months of follow-up. In a cohort study, Felson et al. [12] suggested that the presentation of BMLs is one source of knee pain in subjects with or without radiographic OA. In addition, knees with enlarging BMLs at 15 months follow-up had a moderate relationship with the development of knee pain.

BMLs have been recognised as an important feature in knee OA subjects and a promising target in clinical trials. MRI provides a quantitative assessment of BML size (volume or area). Therefore, selecting the appropriate and optimum MRI sequences in clinical trials is crucial in the study of BMLs. A broad range of MRI sequences and BMLs assessments methods (quantitative and semiquantitative scoring systems) are available for BML analysis. In general, fluid sensitive fat-suppressed sequences (such

as T2-weighted, proton density-weighted or intermediate-weighted sequences) are useful for the evaluation of BMLs [15]. The use of fat-suppressed MRI sequences produces a high signal of BMLs and a low signal of surrounding normal fat marrow. Further details about the physics of MRI and the review of different MRI sequences in the imaging of BMLs in the literature are outlined later.

Although the value of MRI for BML assessment in research settings is well recognised, some limitations of MRI may prevent its application in clinical practice, including cost, relatively long acquisition time, the complexity of advanced MRI techniques, and time-consuming nature of quantitative/ semiquantitative analyses. In addition, MRI scanners are very expensive, and running and maintaining the machine is also costly [32, 36] [37].

Furthermore, there are a number of potential hazards of MRI to the human body that mostly related to the interaction of the magnetic fields with metallic substances and electronic devices. MRI involves the use a strong magnetic field, rapidly switching gradient magnetic fields and radiofrequency (RF) fields. Some ferromagnetic (magnetizable) materials within the patient can potentially be affected by the magnetic field, causing tissue damage. Patients with a previous history of eye injury with the risk of metal fragments in the eye should be screened before having an MRI scan with the plain radiographs of the orbits.[38]. Implantable devices such as cardiac pacemakers, cochlear implants (CI), and vagal nerve stimulation (VNS) devices were historically considered as absolute contraindications for MRI because of the risk of injury due to metal displacement and device malfunction. With new generation of the design of the implants, some manufacturers have offered devices which are labelled as MRI conditional/ compatible. Therefore, MR imaging of patients with these devices are now can be performed provided specific protocols or guidelines are followed, as

well as close collaboration with device manufacturer representatives is required [39-41].

Further details about MR imaging principles, including T1, T2 and T2* relaxation, repetition and echo times, and signal localisation are described in section 2.5, fundamental types of MRI sequences in section 2.6 and imaging of BMLs in section 2.7.

2.4 BMLs associated with knee osteoarthritis

As outlined above, BMLs are commonly seen in knee OA. The following sections review BMLs associated with knee OA, including a brief overview of the historical background and occurrence of BML, the clinical significance of BMLs, BMLs and structural progression of knee OA, the pathogenesis of BMLs, and intervention studies that used BMLs as the outcome measures.

2.4.1 Historical background and occurrence

The term "bone marrow oedema" (BME) was reported in the literature for the first time by Wilson et al. in 1988 [42]. The authors examined ten subjects with painful hip or knee joints that showed an area of low marrow signal intensity on T1-weighted MR images and high signal intensity on T2-weighted images. The authors suggested that this imaging finding may represent an increase in water content in the bone marrow. The feature is unique to MRI and cannot be visualised by conventional radiography (X-ray or computed tomography) or ultrasound. As outlined in chapter 1, the features are in fact due to areas of tissue damage rather than simply oedema, and most researchers now prefer the term bone marrow oedema–like lesions or bone marrow lesions (BMLs). Figure 2.2 shows examples of BMLs on MRI images. BMLs are common in knee OA. In a cohort study of 377 patients with symptomatic knee OA,

82% had evidence of BMLs [43]. However, BMLs are not specific to people with known OA and may occur in the absence of disease, with a recent study showing that 13% of healthy middle-age subjects without clinical knee OA had evidence of BMLs [44].

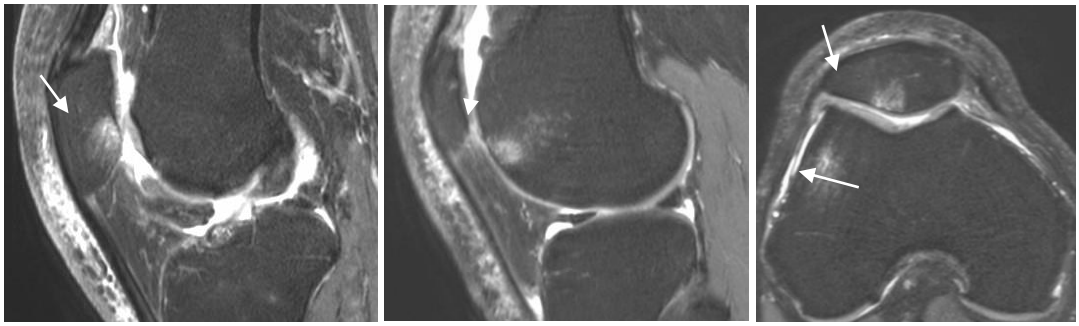

(a) (b) (c)

Figure 2.2. BMLs appear as high signal intensity (arrow) in the patella (a) and anterior femoral region (b) in sagittal PDFS images. Axial PDFS image shows BMLs in the patella and femur (c).

2.4.2 Clinical significance

2.4.2.1 Knee pain

Observational data suggest a strong link between BMLs and knee pain. Felson et al. conducted a cross-sectional study of 401 participants with radiographic knee OA (351 subjects with knee pain and the rest without pain) [11]. BMLs were presented in around 78% of participants with a painful knee and 30% without knee pain. Furthermore, large BMLs were more frequent in those with painful knee OA.

According to Ip et al. [45], in individuals with radiographic OA, there was a significant association between BMLs and pain on climbing stairs. Sowers et al. [46] reported that BMLs which were greater than 1 cm were more frequent in women with painful knee OA compared to women with non-painful knee OA (OR= 5.0; 95% confidence interval= 1.4-10.5).

Data from longitudinal studies suggest that BMLs predict future pain. In a subsample of the MOST study (Multicenter Osteoarthritis Study), Felson et al. [12] reported that that an increase in BML score after a 15-month follow-up was significantly associated with the development of knee pain.

2.4.2.2 BMLs and structural progression

BMLs on MRI have been linked with a higher rate of cartilage loss or degradation [13, 14]. In a study of 217 men and women with primary knee OA followed for 30 months, both the size and change of BML were strongly associated with cartilage loss. Knee compartments with a higher baseline BML score had subsequent greater cartilage loss ($p<0.0001$). An increase in BML size was triggered by limb malalignment and was also strongly related to further cartilage loss at follow-up with a 1-unit increase in BML score associated with an increase of 0.65 units of cartilage loss ($p= 0.003$) [13].

In a longitudinal study of 109 men and women with symptomatic knee OA, BMLs and cartilage were assessed using MRI at baseline and two years [47]. BMLs were graded as 0 to 2 (0= absence of lesion; 1= mild to moderate; 2= severe/large lesion). Those with severe baseline BMLs in the medial compartment of the knee had a reduction in cartilage volume at baseline ($p=0.02$). Severe baseline BMLs were also associated with greater cartilage loss over two years ($p=0.002$) and a higher risk of knee joint replacement over four years (Odds ratio 1.55 (95% CI 1.04-2.29)).

In a further longitudinal study of 377 patients with OA, increasing BML score was associated with higher cartilage loss (OR 2.1 to 5.9) while a lower BML score was associated with a lower risk of cartilage loss over 30 months of follow-up (OR 0.5 to 1.6) [14].

Subchondral cystic lesions may develop within BMLs and have been linked to the regression or resolution of BMLs in the same region [48, 49]. On fluid sensitive MRI sequences, subchondral cysts appear as well-defined areas of high (bright) signal intensity. The formation of subchondral cystic lesions may be caused by the intrusion of synovial fluid into the subchondral bone through defects in the articular surface [50] or micro-contusions of the bone that lead to necrosis [49]. Although subchondral cysts are closely associated with BMLs, previous studies have failed to find an association between subchondral cystic lesions and pain in patients with knee OA [51, 52].

2.4.3 Pathogenesis

The aetiology and pathogenesis of BMLs associated with OA are not known. In a histopathological study of BMLs (based on samples obtained from patients undergoing total knee replacement), it was reported that BMLs mainly consisted of fat marrow tissue with a small proportion (less than 30%) of abnormal tissue consisting of necrosis, fibrosis, marrow oedema, and bone marrow bleeding [53]. In a further study of 7 patients with advanced knee OA, tissue samples obtained at the time of joint replacement surgery showed fibrovascular tissue growth into subchondral bone and also abundant bone remodelling in the samples [54]. The data suggest that BMLs represent areas of damage and repair within the subchondral bone.

2.4.4 Intervention studies

BMLs have recently been used as outcome measures in clinical trials of both mechanical [18] and medical treatments [55, 56]. In a 6-weeks randomised trial of a knee brace in 126 subjects with painful patellofemoral (PF) OA, subjects were randomised to patellar knee brace or no brace group [18]. BMLs were assessed using a 1.5 T MRI scanner and CE T1-w FS images. The PF joint BMLs (those involving

patella or anterior region of the femur) were measured quantitatively at baseline and six weeks. Of 126 subjects, 117 had baseline and six weeks MR images. After accounting for baseline values, the brace group had a reduced PF BML volume compared with the no brace group at six weeks follow up (difference -490.6 mm^3, 95% CI -929.5 to -51.7; p=0.03).

In an RCT of zoledronic acid (ZA) therapy, 59 patients with symptomatic knee OA were randomised to zoledronic acid or placebo and followed for 12 months [55]. The outcomes were pain intensity and BML size. A 1.5T MRI scanner was used to assess BMLs at baseline, 6 and 12 months. All the scanning was performed using 2D PDFS. BML size was measured in mm^2 using Osirix software, applied to the greatest area of each lesion at four sites (medial tibial, medial femoral, lateral tibial and lateral femoral sites) and then were summed to produce a total BML score (mm^2). BMLs were also scored using a semiquantitative scale at each of the four sites. There was a reduction in BML size at six months (in mm^2 total area and a semiquantitative score of BMLs) in the ZA group compared to the control group (β coefficient -175.7, 95% CI -327.2 to -24.3, p=0.024 for volumetric assessment and β coefficient -0.63, 95% CI -1.28 to +0.01, p=0.05 for ordinal scale). The change in visual analogue pain scale (VAS) intensity of ZA group after six months was statistically significant compared to placebo (β coefficient -14.5, 95% CI -28.1 to -0.9, p=0.04).

In a further trial, sixty-nine patients were randomised to receive chondroitin sulphate (CS) or a placebo for six months [56]. Cartilage volume and BMLs were assessed by 1.5 T MRI scanners at baseline, 6 and 12 months. Images were obtained using 3D fast imaging with steady-state precession (FISP) with fat suppression. The BMLs were assessed for global knee and subregions using the whole-organ magnetic resonance imaging score (WORMS) scale. The study found that BML size was significantly

smaller for the lateral compartment (p=0.035) and lateral condyle (p=0.044) in the CS group compared to the placebo group at 12 months follow-up, but not for global knee (p=0.062) and medial compartment (p=0.287), however, at six months, there was no significant difference between these two groups.

2.5 Magnetic resonance imaging

In the last section, the advantages and limitations of MR imaging were considered. In the following sections, the basic principles of MR imaging are described in more detail. Further, some fundamental processes in MRI, including T1, T2 and T2* relaxation, repetition, and echo times, are also covered. Following this, MR signal localisation is also described.

2.5.1 Basic principles of MRI

The basic principle of MRI examination in the clinical setting is to generate images of the human body by detecting the electromagnetic activity of hydrogen nuclei and their interaction with an external magnetic field and radio waves [57]. Hydrogen is the most abundant element in the human body [58]. To perform MRI, when a patient is placed in an MRI scanner, the body is exposed to a main static magnetic field produced by the scanner, and the body then becomes magnetised. In MRI, the main magnetic field is referred to as B_0 and is measured in Teslas (T). MRI systems in common clinical use are 1.5 T, with increasing numbers of 3 T systems being used [59].

Hydrogen nuclei consist of a single (unpaired) proton. The proton possesses a positive electrical charge and constantly spins on its axis, so-called nuclei spin [60, 61]. A moving electrical charge produces a magnetic moment like a little bar magnet. In the absence of an external magnetic field, the spinning hydrogen protons are randomly oriented within the human body [60]. The influence of an external magnetic field and

the interaction of the magnetic fields (the fields of the spinning nuclei and B_0) produce an additional spin or wobble around B_0. This secondary spin is called precession [62]. The protons will precess at a frequency that is directly proportional to the strength of the magnetic field and given as the Larmor equation:

$$\omega_0 = \gamma . B_0$$

Where ω_0 is the Larmor frequency (Megahertz), γ is the gyromagnetic ratio (a constant specific to a particular nucleus), and B_0 is the strength of the magnetic field in tesla (T).

The Larmor equation describes that the precessional frequency is equal to the strength of the B_0 multiplied by the gyromagnetic ratio [62]. Once the magnetic field is applied, the previously randomly orientated nuclei will align with B_0. Some will align anti-parallel, and a slight majority of them align parallel to the direction of B_0 [60]. The cumulative effect of the magnetic moments of all the nuclei is called the net magnetisation vector (NMV) [57].

The terms z-direction and xy plane are frequently used to explain the basic principles of MRI to describe the magnetic fields of MRI. Conventionally, the main magnetic field (B_0) is represented along the z-axis. The xy-plane is perpendicular to the z-axis (see figure 2.3).

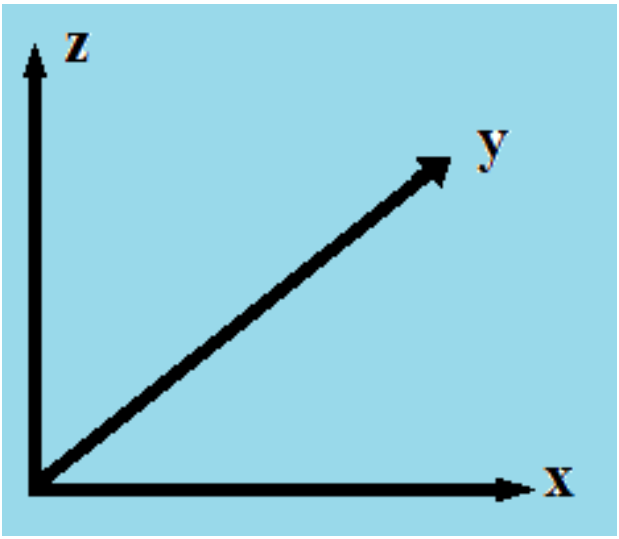

Figure 2.3. The main magnetic field (B_0) is represented by a line directed from bottom to top (z-axis). The other two dimensions are denoted by x and y, with the xy-plane perpendicular to the x-axis.

If a radiofrequency (RF) oscillating magnetic field (also known as the B_1 field) oriented perpendicular to B_0 [61] is applied to the patient using a radiofrequency coil, some of the spins absorb this energy which has the effect of tilting NMV from its previous position toward the transverse plane [61, 63]. Two components of magnetisation will be produced: longitudinal and transverse magnetisation. If the RF pulse is sufficient to produce a 90-degree flip of the NMV, it is called a 90-degree flip angle pulse. As the transverse magnetisation precesses in a receiver coil, a current is induced in the coil, which can be measured as the MR signal [63].

2.5.2 T1 recovery, T2/T2* decay, and relaxation times

As discussed previously, immediately after a 90-degree RF pulse is applied, the longitudinally orientated net magnetisation rotates from the longitudinal axis (also known as the z-axis) to the transverse plane (xy-plane). When the RF pulse is switched off, the net magnetisation will start to realign with B_0; this process is called longitudinal relaxation or T1 recovery, in which the magnitude of the longitudinal magnetisation will recover [61]. There are additional processes that reduces the transverse magnetisation called transverse relaxation. These processes are known as

T2 relaxation. As M_z is slowly restored, the hydrogen nuclei return to the equilibrium state by dissipating their energy to their surroundings (the lattice), so-called spin-lattice relaxation. The time constant for this recovery is called the T1 relaxation time [61, 63].

Immediately after RF pulse excitation, the spins are in phase [57, 63]. Phase refers to the relative positions of magnetic moments of protons on their circular precessional path. Once the RF pulse is off, phase coherence is gradually lost as some spins either fall behind or advance on their precessional paths relative to others. This loss of coherence causes the vector of the net transverse magnetisation to become smaller and smaller and finally disappear. This phenomenon is known as transverse relaxation, which is defined as the decay of the transverse magnetisation [61, 63]. Transverse relaxation differs from longitudinal relaxation in that spins do not need to dissipate their energy to their surroundings but may exchange energy with each other. This type of relaxation is hence called spin-spin relaxation with the time constant for this relaxation is known as the T2 relaxation time [61, 63].

Another factor that contributes to this is dephasing due to magnetic field inhomogeneities. The magnetic field is not exactly the same everywhere. Some places may be stronger, and others are weaker. This magnetic field inhomogeneity or non-uniformity may be the result of intrinsic defects (imperfections) of the main magnetic field (B_0) or field distortions produced by differences in magnetic susceptibility of various tissues within the field. This additional factor contributes to T2* decay with its time constant called T2* relaxation time [61, 63]. Different tissues have different T1, T2 and T2* relaxation time values. Tissues with a strong interaction between hydrogen nuclei and the electromagnetic vibrations of macromolecules, such as the triglyceride appendages of fat molecules have short T1 relaxation times. Other tissues

that have paramagnetic substances such as methemoglobin and gadolinium also have short T1 relaxation times. Fluids, such as synovial fluid and cerebrospinal fluid, contain few large macromolecules and possess very small interaction between macromolecules and the protons of water. Consequently, they have long T1 relaxation time [61].

MRI pulse sequences that emphasize contrast between tissues based on T1 relaxation are called T1-weighted sequences. Tissues with short T1 values such as fatty marrow appear as high signal or white on a conventional spin echo T1-weighted sequence. In contrast, fat tissue in the marrow appears as low signal (dark or black) on fat-suppressed (or fat-saturated) MRI sequences or STIR sequences, while the signal of water-containing areas, such as bone marrow oedema will be bright. Marrow oedema will also enhance on T1-weighted pulse sequences after contrast agent administration as contrast agent will shorten the T1 relaxation time of the tissue due to increased vascularity and capillary permeability. Further details on conventional MRI sequences will be discussed in the next section.

2.5.3 Repetition time and echo time

There are three key intrinsic features of biological tissue (T1 relaxation time, T2 relaxation time, and proton density) that determine tissue contrast in MR images [64]. Proton density is the number of excitable protons of hydrogen nuclei per unit volume of a given tissue. Two key parameters that influence MR image contrast are repetition time (TR) and echo time (TE). TR is described as the time (in milliseconds) measured between the application of an RF excitation pulse and the start of the next RF pulse. TE, also measured in milliseconds, is the time between the application of the RF pulse and the detection of the peak of the echo [57, 63].

When TR is short, the differences in T1 relaxation time between fat and pure water can be detected as fat tissue which has short T1 relaxes quickly and gives a large signal after the next RF pulse. Water or any tissue with a long T1, on the other hand, have relatively little relaxation between two RF excitation pulses and less longitudinal magnetisation is available when the next RF excitation pulse is applied. Thus, these tissues emit less signal than fat [63]. On the other hand, if a long TR is selected, all tissues, including those with long T1, will return close to equilibrium. Hence, the signals differences between fat and water will be small. Therefore, TR affects the T1 contrast on images [57, 63].

The TE determines the influence of T2 relaxation times on image contrast. If TE is short, there is no signal difference between tissues with difference T2 values, as the differences of T2 relaxation times between both tissues are small at the time of the echo collection. With a longer TE, tissues with short T2 have lost most of their signal while tissues with long T2 have stronger signal at the time of echo collection. Thus, by selecting an echo time (TE), the operator can define the degree of T2-weighting of the MR image [63].

2.5.4 MRI signal localisation

The previous section reviewed the role of the repetition and echo times, and how the body can be exited to emit signals. The next sections discuss how signal from one part/ section of the body can be distinguished from the signal emitted from other sections by using a technique called spatial localisation. For this purpose, the MR scanner is equipped with extra electromagnets called gradient coils. These gradient coils cause a gradient in the magnetic field. Gradients are linear variations of the magnetic field strength in a selected direction. By using gradient coils, the magnetic field strength across the body can be controlled [57, 61].

There are three types of gradient coils to produce gradient magnetic fields in three different directions (x, y, and z directions) [57, 63]. The gradient coils are switched at different times and in different directions to perform spatial localisation or encoding. For 2D images, spatial encoding relies on application of three magnetic field gradients, typically a slice-selection, phase-encoding, and frequency-encoding gradient. A slice-selection gradient is the first step of spatial encoding. Slice selection gradients are used to select the anatomical slice or section of interest by producing a non-uniform magnetic field one direction. For example, if the slice selection gradient is applied in the z direction, a proton in the head may spin faster than the middle body part (centre), and a proton at the middle part will spin faster than one in the feet. By choosing a radiofrequency excitation pulse of a particular frequency and bandwidth, it is possible to excite only one corresponding slice of interest without influencing other body parts [61, 63].

To obtain a particular slice thickness, a range of frequencies must be transmitted to produce resonance across the whole slice. This range of frequencies is called the transmitter RF (radiofrequency) bandwidth. Slice thickness is determined by the slope of the slice selective gradient and the transmit bandwidth. A desired slice is excited by transmitting an RF pulse with a centre frequency that correspond to the middle of the slice and a bandwidth and gradient slope according to the thickness of the slice. Each slice has a different centre frequency determined by its position (z) along the slice-selective gradient [65, 66].

After selecting a slice, then the position of each point will be encoded in the other two directions to get information about individual pixels in that slice by applying the phase-encoding gradient and the frequency-encoding gradient. To produce phase encoding, a phase-encoding gradient is switched on for a period after the RF pulse.

This gradient causes the Larmor frequency at one edge of the plane of the slice to be slightly higher than those at the opposite edge of the slice plane. Protons anteriorly, for example, will spin faster than the those more posteriorly. This result in a phase shift between the spins at the end of the phase encode gradient. The process is repeated multiple times with different strengths of phase encode gradient generating different phase shifts across the patient. From this it is possible to determine where signal comes from in the phase encode direction by using Fourier transformation [61, 63].

The remaining step is to determine where the signal comes from in the third direction, e.g. the left, centre, or the right side of the body. This step is achieved by applying the frequency encoding gradient, also called the readout gradient during signal acquisition. After the end of the phase-encoding gradient step, all spins will precess at the Larmor frequency associated with the B_0. The purpose of frequency encoding gradient is to create a gradient of the magnetic field from left to right. This gradient will cause the protons to experience slightly different magnetic fields and precess at different frequencies. The protons on the left-hand side, for example, spin with a lower frequency than the ones on the right. This process will produce an additional phase shift which evolve during the signal acquisition. Signal at a particular frequency and hence arising from a particular position can be determined by Fourier transformation. By using this information in addition to the phase-encoding gradient we can determine the spatial position of MR signal within the selected slice [61, 63].

2.6 Fundamental types of MRI sequences

In clinical practice, imaging is usually not necessary in patients with typical presentation of knee OA. Where imaging is necessary, plain radiography is the first line of investigation. MRI may be considered in cases when the diagnosis is unclear, for example, in patients with severe symptoms but with relatively mild OA on plain

radiographs. In secondary care when surgical intervention for OA is being considered, an MRI scan can be very useful to provide information about the conditions within the knee, including the state of the preserved compartments and the anterior cruciate ligaments that are critical to the surgical plan [67-69].

There are a wide variety of MR sequences used in medical MR imaging. In general MRI sequences can be grouped based on the type of the sequence (for instance spin echo, gradient echo, or inversion recovery) or by image weighting (T1, T2 or PD-weighting) and by some optional features, such as fat-suppressed or gadolinium-enhanced. This section discusses three of the most common conventional MR pulse sequences that are commonly used in musculoskeletal imaging: spin-echo (SE), gradient echo (GE), and inversion recovery (IR) sequences [57]. Other MR sequences will not be discussed in this section.

2.6.1 Spin echo (SE) sequences

Spin echo sequences are produced by applying two RF pulses, a 90° RF excitation pulse and a 180° RF refocusing pulse. A 90° RF pulse is used to flip the net magnetisation vector into the transverse plane. As the transverse magnetisation is gradually dephased, including by a dephasing or prephasing gradient in the read direction, a 180° pulse is then applied at a time equal to half of the echo time (TE) to refocus or rephase the dephasing of spinning nuclei caused by the dephasing gradient (and any other field inhomogeneities). Thus, after the second half of the TE has passed, the nuclei are again spinning in phase (at total TE). An echo is then formed and read [61, 63].

SE is used as the standard MR sequences for acquiring T1-, T2- or PD-weighted images by manipulating TE and TR. As discussed in the previous section, sequences

that have a short TR and short TE are used to obtain T1-weighted images. When both TR and TE are long, then T2-weighted images are produced. Meanwhile, if a long TR and short TE are used, it produces proton-density (PD) weighted images [63].

Spin echo sequences were one of the first MRI sequences developed and are still widely used in the form of the fast spin echo sequence. Fast or turbo spin echo (FSE/ TSE) is a modified SE sequence with much shorter scanning times. FSE is achieved by transmitting a series of 180° RF pulses during each TR interval and recording the corresponding echoes using different phase-encoding gradients. This series of echoes is known as an echo train, and the number of echoes is called echo train length [61, 63].

2.6.2 Gradient echo (GE) sequences

Gradient echo (GE) sequences are a group of MR imaging techniques that are produced by applying two gradient pulses in opposite directions. The first gradient pulse is used to induce transverse dephasing (for example using a negative gradient) of spinning protons and then a second gradient is applied in the opposite direction to rephase (positive gradient) the transverse magnetisation to re-align the dephased protons and hence produce an echo known as gradient echo. This sequence is the basis of some modern MRI techniques [61, 63].

GE sequences differs from SE sequences in several ways. The difference is related to the pulse sequence elements used to generate an MR signal. Firstly, SE sequences use two RF pulses (90° and 180°) while GE sequence is based on a single RF pulse. The TR and TE are often much shorter with GE than SE, and the echo of GE can be recorded at a very short echo time. The short TR allows for rapid scanning time. For this reason, GE sequences are used as the basis of many rapid MR imaging techniques.

Secondly, there is an extra variable added to the usual TR and TE parameters, the so-called tip or flip angle of the spins (denoted by α). The flip angle for the excitation pulse in SE sequences is usually at or close to 90° while GE often uses flip angles of much less than 90°, meaning that less relaxation time is required, and so shorter TR can be used. A larger flip angle may give more T1-weighting. Another different feature of GE, as opposed to SE, is that the dephasing of spinning protons as a result of T2* decay is not refocussed, instead of in SE where only T2 decay is not refocussed and hence GE is susceptible to static magnetic field inhomogeneities [61, 63]. Although the signal is more sensitive to magnetic field inhomogeneities, advanced development of MR scanner hardware and coils permit reliable and reproducible image quality in routine clinical settings [36].

GE sequences are also known as gradient-recalled echo or fast-field echo (FFE) sequences. Different types of GE sequences have been developed by different manufacturers under various acronyms. These include two groups of GE sequences, spoiled GE (SPGR) and refocused (balanced) steady-state GE sequences. SPGR techniques enable us to acquire T1 weighted or intermediate-weighted images. Meanwhile, balanced steady state sequences may be used to provide higher signal to noise ratio and are mostly used to produce mixed T1 and T2-weighted images [70-72].

2.6.3 Conventional inversion recovery

This sequence is a SE sequence with an additional 180° RF preparatory pulse (inversion pulse) that precede the usual 90° and 180° pulse of a conventional SE sequence [63]. The interval between 180° preparatory pulse and the 90° pulse is called the inversion time (TI). During the inversion time tissues regain their longitudinal magnetisation (Mz) at different longitudinal (T1) relaxation rates. Inversion recovery

can discriminate different tissues based on differences in T1 relaxation time by changing the TI. If a very short TI is chosen, there will be no relaxation of any tissues. When TI is very long all tissues will achieve full relaxation and by choosing intermediate TI there will be more relaxation from short T1 tissues than long T1 tissues. This sequence is known as a magnetisation-prepared sequence; a preparatory pulse used to flip longitudinal magnetisation from z-axis into negative z-axis, so it is pointing in the opposite direction [66]. When this pulse is switched off, the spinning nuclei begin to undergo T1 relaxation. This can be used to null the signal of a certain entity of interest, for example fat based on its short T1. When the NMV for fat passes the transverse plane (the null point for fat), then the SE pulse sequence (90° and 180° pulse) is applied. At this TI, the longitudinal magnetisation of fat is very weak, whereas that of non-fat tissues is stronger. When the NMV is flipped by the 90° pulse, there will be no or little transverse magnetisation so little or no signal generated from fat [57]. This sequence is the basic concept of the short-tau inversion recovery (STIR) sequence used to suppress fat signal in clinical MR imaging [61]. Fat tissue has short T1 value and the TI corresponding to fat is approximately 100-200 ms at 1.5 T, such that the NMV of fat passes the null point. Just before the 90° pulse is turned on, there will be no or little longitudinal magnetisation present from fat, and after the 90° pulse, the transverse magnetisation of fat is low or insignificant. Because of this low transverse magnetisation of fat, no signal is generated from fat [61, 73].

2.7 MRI sequences for BMLs assessments

MRI is not routinely used in the diagnosis of knee OA in patients in a clinical setting. However, MRI has become an important imaging tool in the research setting as it offers some benefits over conventional radiographs for the imaging of OA. First, MRI has a greater sensitivity than radiographs to detect bone and soft tissue changes related

to knee OA. Second, MRI is able to directly visualise all the components of the joint and many OA features, including cartilage, menisci, intra-articular ligaments, synovium, bone attrition, bone marrow lesions (BMLs), subchondral cysts, and intra-/ periarticular cystic lesions [74]. Third, MRI also permits tomographic scanning (axial, sagittal and coronal plane) that avoid morphological distortion and superimposition of knee structures as its encountered on radiographs [32]. Finally, MRI has a greater sensitivity to detect some abnormal changes of pre-radiographic OA or earlier stage than radiography [35].

Currently, most studies using MRI to assess BMLs use fast-spin echo (FSE) sequences, such as T2-weighted, proton density (PD) and intermediate-weighted (IW) sequences with fat-suppression (FS) or a short tau inversion recovery (STIR) sequence [75-77]. These sequences are recognised as the most sensitive sequences to detect fluid containing tissues, such as BMLs, that appear as bright or white with normal fatty marrow appearing dark (black) in the background [76, 77].

T2-w sequences need a long echo time (TE) more than 70 milliseconds (ms) with long repetition time (TR) more than 1500 ms [78]. With long TR and long TE, tissues with long T1 and T2 (such as fluid) will emit high signal and appear as bright/ white. There are fat suppression techniques that can be used to suppress (reduce) the signal from fat marrow, including spectral presaturation with inversion recovery (SPIR) and T1-dependent fat suppression or STIR. The SPIR technique employs an initial inverting pulse, known as a frequency-selective pulse that only inverts fat magnetisation since fat and water resonate at slightly different frequencies [79]. By adding this fat suppression, the signal of fat can be suppressed and appears as dark/black (figure 2.4). The same fat suppression techniques can also be applied to IW or PD sequences.

Spectral adiabatic inversion recovery (SPAIR) is an alternative to the conventional fat suppression, in which the fat signal is inverted with an adiabatic spectrally selective pulse, and acquisition is begun after the inversion time (TI) that nulls the fat signal. The longitudinal magnetisation of fat at the time when the excitation pulse is applied is zero, so that fat spins will not contribute to the MR signal. SPAIR offers some advantages over STIR. This technique is insensitive to B1 inhomogeneities and only fat spins are suppressed. Further, it produces a higher SNR than STIR and it does not suppress other tissues with a T1 relaxation time similar to fat T1. A disadvantage of SPAIR is that this technique is sensitive to B0 such that they may have heterogeneous fat suppression, especially at the edges of a large field of view (FOV) [79].

MR pulse sequences can be either two-dimensional (2D), with excitation of one section at a time, or three-dimensional (3D), with a volume of multiple sections obtained in each excitation [76]. Routine MRI protocols for 2D sequences usually are acquired with slice thickness of between 2 and 4 mm. Matrix size is typically of the order of 256x256 pixels to maintain an acceptable acquisition time and a good signal to noise ratio (SNR) [76].

One limitation of FS sequences is artefact related to failed FS may occur, and this phenomenon especially appears in the peripheral region or near a metal object that may produce local magnetic field heterogeneity. This local heterogeneity can subsequently lead to artefact that appears as hyperintense areas that can mimic BMLs [15].

Contrast-enhanced T1-weighted images with fat suppression can also be used to see marrow abnormalities [17]. Gradient-echo sequences such as Dual-echo steady-state (DESS), fast low-angle shot (FLASH), or spoiled-gradient recalled acquisition in steady-state (GRASS) have also been used to visualise BMLs [80].

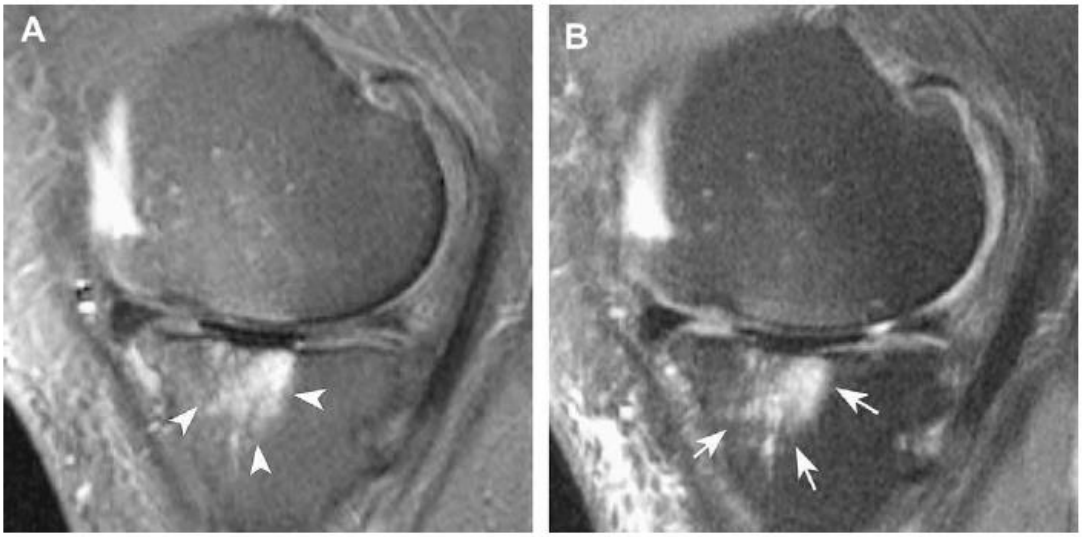

Figure 2.4. Subchondral BML of tibial plateau in sagittal PDFS (A) and T1w FS images after post-contrast administration (B). Reprinted from Osteoarthritis and Cartilage, 17(9), F.W. Roemer, R. Frobell, D.J. Hunter, M.D. Crema, W. Fischer, K. Bohndorf, A. Guermazi, MRI-detected subchondral bone marrow signal alterations of the knee joint: terminology, imaging appearance, relevance and radiological differential diagnosis, Pages No. 1115-1131, Copyright (2022), with permission from Elsevier.

2.7.1 Comparison between MRI sequences: STIR vs contrast-enhanced (CE) T1-weighted sequences

How is the assessment of BMLs influenced by the type of MR imaging approach used? Several studies have compared BML volumes using different MRI sequences, and these are outlined in the next sections (2.71-2.74).

There are no published data on comparison of quantitative (volumetric) BMLs assessments in knee OA between PDFS and STIR sequences. Some authors though have compared quantitative BMLs assessment between STIR and CE T1-w FS sequences.

Schmid et al. [81] compared the utility of STIR and a CE T1-w FS sequences for marrow evaluation using a 1.0 T MR scanner. The study comprised of 51 patients with different foot and ankle diseases of whom three had osteoarthritis. STIR images were obtained with TR 4800, TE 30 ms and with TI 150 ms; T1-w images were obtained

with TR 500-720 and TE 15-20 ms. The signal difference-to-noise ratio (SDNR) of normal bone marrow and BML, as well as volume measurements of the BML were calculated and significant differences between the two sequences were sought. Volume measurements were determined by manual segmentation. Detail about this and other studies which looked at imaging of BMLs/ MR sequences used are shown in table 2.2. Intraobserver agreement in the depiction of ill-defined abnormal bone marrow was fair (kappa values 0.31 to 0.38), while interobserver agreement was moderate (kappa value= 0.49 to 0.55) for both MRI sequences. Mean SDNR of bone marrow oedema was 25% higher with the CE T1-w FS sequences compared to the STIR sequence (125.9 vs 95.4), while the mean volume of bone marrow oedema was slightly bigger (5.25%) with the STIR compared to the CE T1-w FS (8.75; SD 10.7 vs 8.29; SD 9.9) (p-value <0.001). There was a high correlation of the volume of abnormal bone marrow between both sequences (r^2= 0.98).

A similar sequence comparison was conducted by Mayerhoefer et al. in 2005 [17]. Images were acquired from 30 participants with several types of knee problems of whom 8 had osteoarthritis, using 1.0 T (group 1 consisted of 16 participants) and 1.5 T MR scanners (group 2 consisted of 14 participants). MR parameters of 1.0 T for STIR sequences were TR 2500 ms, TE 10 ms with TI 100 ms, and TR 650/750 ms, TE 18 ms for CE T1-w with FS. For 1.5 T, STIR sequences were obtained using TR 4100/4700 ms and TE 26-28 ms with TI 130 ms, while CE T1-w FS sequences were obtained using 740/11 ms. BML volume was assessed as relative volume (percentage of BML from the condyle volume) using a computer-assisted quantitative method. Relative BMLs signal intensity in both sequences was measured and compared for both groups of participants. Mean relative BML volume of group 1 was slightly bigger (7.2%) on the CE T1-w sequence than STIR (16.3±17.6 vs 15.2±17.0; r^2= 0.99) when subjects received contrast media of 0.2 mL/kg body mass, while the mean signal

contrast was almost 37% higher in the CE T1-w than STIR sequence (112.9±81.6 vs 70.7±49.8; r^2= 0.94). In contrast, among 14 subjects (group 2) who received a lower dose of contrast media (mean 0.15 mL/kg body mass) and were scanned with a stronger MR magnetic field had mean BMLs volume slightly bigger (but not statistically significant) on the STIR than the CE T1-w FS (9.3 ±11.9% vs 8.8±11.7%) with a strong correlation between both sequences with correlation coefficient, r^2 = 0.96 ($p<0.01$). In addition, mean signal contrast was 14% stronger in the CE T1-w than STIR (102.1±74.5 vs 88.0±51.5; r^2= 0.86). There was also a moderate correlation between the dose of the contrast media and the relative BML volume (r^2= 0.4; $p<0.01$).

A different volumetric study of BMLs in the femorotibial compartment of 22 medial femorotibial knee OA patients found that BMLs volume on CE T1-w FS (with a gadopentate dose of 0.2 mL/kg body mass) was smaller (mean difference 3.2-3.5%) than on STIR when assessed using manual volumetric assessment. The segmentation of BMLs was limited to the posterior 2/3 of the femoral condyles with two to three central slices of the medial femoral condyle. Intraobserver agreement for manual segmentation was reported as high with the mean difference (bias) -94 mm^3 (95%= -199 to 11 mm^3) for CE T1-w FS and 142 mm^3 (95% CI= -41 to 325 mm^3) for STIR sequences. However, BML volume was larger on contrast-enhanced images than STIR images when measured using computer-assisted segmentation (mean difference 4.1-5.3%) [82].

2.7.2 IW-FS and DESS sequences

Hayashi et al. conducted a cross-sectional study to compare IW-FS, and Double echo steady-state (DESS) sequences using 3.0 T MRI [80]. This study analysed 177 subjects with mild to moderate chronic, frequent knee pain that took part in the Joint

on Glucosamine (JOG) cohort. WORMS was chosen as the semiquantitative scoring method. Of 346 knees that were included in the analyses, there were 200 subregions with BML WORMS score ≥1. BML size was larger using the IW-FS sequence in 186 subregions (93%) compared to DESS. Almost 60% (119 subregions) of BMLs were larger by one grade, 26% larger by two grades and 7.5% by three grades. Only 14 subregions (7 %) were scored with the same grade in both sequences, and 93 (46.5%) subregions with BMLs seen in IW-FS did not show any lesions on the DESS. Interestingly in this study, cysts appeared larger when using the DESS sequence than IW-FS in 36.4% (40 cases).

A similar comparison of IW and DESS sequences was conducted by Raynauld and Colleagues [83]. The study used data from the Osteoarthritis Initiative (OAI) cohort, aiming to assess reliability to detect BMLs and sensitivity to measure BML change on IW-TSE and DESS sequences. There were 144 subjects with symptomatic knee OA who had a 3.0 T MRI scan performed in which BMLs were evaluated using a semiquantitative scoring method (WORMS) at baseline and 24 months follow-up. Intrareader reliability for semiquantitative BMLs assessment was substantial for IW-TSE (kappa values= 0.64) and the DESS (k= 0.78). At baseline, the prevalence of BMLs detected by both MR sequences was slightly different, 80.6 % for IW-TSE and 79.2% for DESS but the mean BML score was significantly lower using DESS than its counterpart for the global knee, compartments, and the subregions (p= 0.001) (figure 2.5). Meanwhile, at 24 months follow up, mean changes of BMLs score were similar in the two sequences.

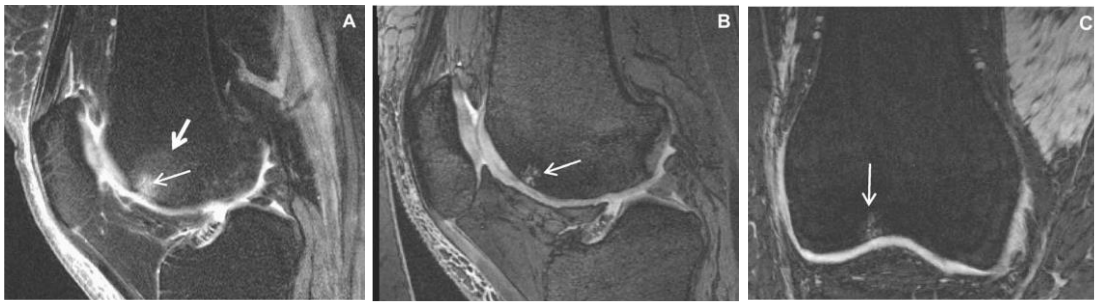

Figure 2.5. Images above are examples of a BML with cystic component in the trochlea (arrows) appears bigger in sagittal IW 2D TSE image (A) compared to sagittal 3D DESS (B) and coronal 3D FLASH (C). Reprinted from Osteoarthritis and Cartilage, 16(12), C.G. Peterfy, E. Schneider, M. Nevitt, The osteoarthritis initiative: report on the design rationale for the magnetic resonance imaging protocol for the knee, pp. 1433-1441, Copyright (2022), with permission from Elsevier.

Another longitudinal study has been conducted [84] in a subsample of OAI study (30 males and females osteoarthritic knees) using IW FS and 3D DESS images at 24 and 48 month visits. BMLs volume were assessed using a semiautomated method (based on the threshold of signal intensity and a dilation filter to merge connected lesions). Intratester reliability for semiautomated BML segmentation was excellent for IW-FS (ICC [3, 1 model] = 0.99) and 3D DESS (ICC= 0.97). The results showed that BMLs volumes on IW FS sequences at baseline were significantly larger by almost tenfold compared to the DESS sequence (BMLs median in IW FS= 1840 mm^3; DESS=191 mm^3; $p< 0.0001$). The study further found that IW FS sequence revealed more BMLs change over 24 months follow up than 3D DESS sequences. This difference was greatest among knees with larger BML volume change.

Furthermore, the BMLs volume at the 24 month visit on IW FS was correlated with BML volume on DESS (r_s= 0.83), but BML volume change on IW FS was not significantly correlated with change on DESS sequences. In relation to pain, BMLs volume on IW FS was significantly correlated with WOMAC (Western Ontario and McMaster Universities Arthritis Index) pain at baseline point (r_s= 0.39), and BMLs volume change was correlated with WOMAC score change on IW FS (r_s= 0.37) but

not on DESS at follow up time. Based on this study, it was concluded that IW-FS are more sensitive in detecting BML change than the DESS sequences. Quantitative BMLs measurement using IW FS provide stronger correlation with knee pain compared to those measured on DESS both at 24 months and 48 months follow-up.

2.7.3 Miscellaneous MR sequences comparison

A prospective cohort study of 297 asymptomatic non-OA adults were examined on 1.5 T MRI scanner using two different sequences, 3D T1-w gradient echo FS and FSE T2-w with FS [85]. The T1-w gradient echo (GE) sequence used TR 58 ms, TE 12 ms and flip angle 55 degrees. BMLs were assessed as present or absent on both sequences at baseline. Medial tibial cartilage volume was measured at baseline and follow-up (2.3 years mean follow up time), while the incidence of knee pain was assessed at follow-up (the average of 2.3 years). The study observed 46 BMLs in 39 participants at baseline. Most of the BMLs (45 BMLs) were visualised on T2-w FS sequences with 34 of them were also visualised on both T2-w FS and T1-w GE FS sequences (11 BMLs on only T2-w FS images, and one BML only detected on T1-w GE sequence). Annual loss of medial tibial cartilage loss was significantly greater in participants with BMLs seen on both sequences compared to those with BMLs visualised only on T2-w FS images (57 mm^3/annum, p= 0.01, standard error of the mean, SEM= 23) after adjusting for age, gender, and BMI. Participants with BMLs in the medial compartment visualised on both sequences at baseline were more likely to develop pain than those with BMLs visualised only on T2-w FS images.

A comparison of three different MRI sequences (non-FS T1-w SE, contrast-enhanced T1-w FS, and PDFS) was performed by Roemer et al [86]. The study assessed 31 patients with knee OA using 1.5 T MRI scanner. The semiquantitative WORMS scale and semiautomated volumetric methods were used for BMLs assessment. The study

found that intraobserver variability of manual volumetry of BMLs was excellent for all three sequences with Person's correlation coefficients of 0.99. BMLs in twenty three out of 31 patients (47 BMLs in total) were visualised on all sequences except one lesion that was not visualised on the non-FS T1-w SE images. The majority of the lesions (83 %) appeared largest on PDFS while only 14.9 % were largest on CE T1-w FS and one lesion was largest on non-FS T1-w SE sequence. Overall, the volumetric assessments were significantly different on three sequences comparison, thus: PDFS > CE T1-w (38 %); CE T1-w FS > non-FS T1-w SE (114 %); PDFS > non-FS T1-w SE (195 %) (p values for all <0.001). This cross-sectional study indicated that the PDFS sequence is more sensitive to visualise BMLs and associated with bigger volumetric measurement compared to CE T1-w FS and non-FS T1-w SE in knee OA. It was recommended that PD-w FS and CE T1-w FS could be used interchangeably.

Another BMLs study using two different MRI sequences was conducted on ex-vivo (bone specimens) from 60 subjects with severe knee OA undergoing total knee replacement surgery. The aim of this study was to characterise BMLs using a combination of two MRI sequences and relate them with histopathology information [87]. BMLs were assessed using a 1.5 T MR scanner with non-FS T1-w SE and PDFS sequences. BMLs were found in 74% of tibial plateaus with 59 % of them detected only by PDFS (defined as BML 1) and 41 % seen on both sequences (BML 2). BML 2 were associated with reduced cartilage volume, more fibrosis, and necrosis in the bone marrow compared to the BML 1 ($p< 0.05$). BML 2 was also associated with a thicker subchondral bone plate. These findings suggested that BMLs detected on non-FS T1-w SE and PDFS may provide further information on different BML phenotypes and identify different degrees of degenerative changes in the subchondral bone. Table 2.2 summaries technical aspects of the MRI sequences and parameters in the studies outlined in this section.

Study (year)	MRI (T)	MR sequences	MR parameters (ms)		
			TR/TE/TI	FOV (cm)	Slice thickness/gap (mm)/ matrix
Cross-sectional study					
Schmid et al. 2002 [81]	1.0	TSE STIR; CE T1-w FS	4800/30/150 500-720/15-20/-	18	3-4/0.3-0.8/-
Hayashi et al. 2011 [80]	3.0	IW-FS DESS	30/3200/- FA 180° 16.3/4.7/- FA 25°	16 14	3/0/313x448; BW 248 0.7/0/384x307; BW 185
Roemer et al. 2010 [86]	1.5	PDFS CE T1-w FS T1-w SE	5080/32/- 720/15/-	18	3.0/0.3/384x282
Muratovic et al. 2016 [87]	3.0	Non-FS T1-w SE PDFS	Not mentioned	-	-
Longitudinal study					
Mayerhoefer et al. 2005 [17]	1.0	STIR CE T1-w	2500/10/100 FA 90° 650-750/18/-	-	4mm/0/256x256
Raynauld et al. 2013 [83]	3.0	IW TSE DESS	3200/30/- FA 180° 16.3/4.7/- FA 25°	16 14	3/0/448x313; BW 248 0.7/0/384x307; BW 248
Zhang et al. 2015 [84]	1.5	IW-FS 3D DESS	3200/30/- 16.3/4.7/- FA 25	16 14	3/0/313x448 0.7/0/307x384
Wluka et al. 2015 [85]	1.5	3D T1-w GE FS T2-w FS	58/12/- FA 55° 3500-3800/50/-	16 13	1.5/0/512x512 3/1/256x192
Nielsen et al. 2016 [82]	1.5	STIR CE T1-w GE FS	5000/29/150 860/20/-	20 16	4/0.4/266x512 4/0.8/512x512

Table 2.2. Direct comparison of MRI sequences and parameters for BMLs assessments

2.7.4 Summary

To summarise, in OA, several publications have reported volumetric BML assessments using different MRI sequences, including T2-w FS, STIR, PDFS, CE T1-w FS sequences and GE sequences (such as DESS). BML volume assessed using different MRI sequences have been compared, many comparing contrast-enhanced (CE) and non-CE MRI sequences. There are no published data that have compared BML volume using both PDFS and STIR sequences.

Most of studies that utilised T1-weighted sequences including T1-w GRE sequences for BML assessments demonstrated that these sequences are not sensitive for depicting BMLs and underestimate the extent of BMLs. There is some evidence that BMLs detected on both of two different MRI sequences (T2-w FS and T1-weighted sequences) are associated with a higher incidence of pain and higher cartilage loss, compared to BMLs seen only on T2-w FS sequences. In addition, BMLs detected on both PDFS and non-FS T1-w sequences were associated with more severe degenerative changes in the subchondral bone. It is possible that BML detection on different MRI sequences may reflect underlying structural or compositional differences in the BMLs. If so, this raises the possibility that the clinical outcomes may also be different.

Notwithstanding the current research, there remains a paucity of studies which have compared BML volume using different sequences and also reliability of assessment and their association with clinical outcomes.

2.8 MRI-based quantitative assessment of BMLs

In the research setting, MRI-based BML assessments consist of two approaches: semi-quantitative and quantitative approaches[86, 88]. The semiquantitative approach uses a

grading system to assess the severity of OA pathological features, typically with scores for each feature ranging from 0 to 2 or 3 based on the extent or size of lesions in predefined regions of the knee. A number of SQ scoring systems have been developed, including the Whole-Organ Magnetic Resonance Imaging Score (WORMS) [88], the Knee Osteoarthritis Scoring System (KOSS) [89], the Boston Leeds Osteoarthritis Knee Score (BLOKS) [90], and the Magnetic resonance Osteoarthritis Knee score (MOAKS) [91]. It has been reported that most of these scoring systems have good inter-reader reliability following training and calibration [89, 92].

MRI-based quantitative assessment of BMLs is typically based on measurement of BMLs size determined by segmenting the lesions on a slice-by-slice basis, either manual or semi-automated/ computer-assisted [17, 81]. The approach is more time-consuming compared to semiquantitative approaches as the segmentation is performed either manually or using semi-automated methods. Semi-automated approaches need specific software from which to extract the relevant measurement from the segmented regions [93, 94]. A comparison study between semiquantitative and quantitative approaches for cartilage and BMLs assessments was conducted in 2011 [95]. The results showed that the quantitative approach was more sensitive in detection of BML volume change during a 24-month follow-up than the semiquantitative approach.

There are a number of different approaches in quantitative assessment of BML size used in the studies that have been discussed in previous sections above. The first quantitative BML assessment associated with OA was conducted by Schmid and colleagues in 2002 on a study of MR Imaging of foot and ankle [81]. Area of the BMLs was calculated for every slice and multiplied by the thickness of the section plus interslice gap. The analysis was undertaken on CE-T1-w FS and STIR images. A

study by Roemer et al. in 2010 used a similar method to Schmid et al. using specialised dedicated 3D segmentation software [86]. They analysed the BMLs on three different MR sequences: non-FS T1-w SE, PDFS and CE T1-w with FS images. A similar approach was used by Callaghan et al. [18] in a randomised clinical trial.

Ratzlaff and colleagues [94] in 2013 developed semi-automated software in their research to measure the BMLs using sagittal STIR images. The BML assessments were preceded by defining an average reference of signal intensity (SI) value plus two standard deviations (SD). SIs above the threshold then were calculated digitally and visualised on the images of each slice as BML. Then, the total 3D volume of BMLs was calculated. Table 2.3. summarises the MRI parameters for the studies on quantitative BMLs assessments.

A simpler method of BMLs volume measurement was applied by Driban and his colleagues [96] in their longitudinal study of knee OA patients by using the product of three linear measurements across a BML. One reader measured BML approximate volume by multiplying three linear dimensions of a BML: antero-posterior (AP), medial-lateral (ML) and superior-inferior (SI) dimension of each BML. This method was selected because it did not require specific software, was relatively quick and provided a continuous measure of BML size. Laslett et al. [55] measured BML area on the slice image where the BML was largest.

Meanwhile, to evaluate BML size, and BML volume changes over 24 months in a longitudinal study in 107 knee OA patients, Raynauld et al. used single dimension BML measurement [97]. To assess BMLs, the reader manually selected the MRI slice that contained the BML with the greatest size, and maximum linear size was then measured in millimetres.

Study (year)	MRI system (Tesla)	MR sequences For BMLs evaluation	MR parameters (ms)		
			TR/TE/TI	FOV (cm)	Slice thickness/gap (mm)/matrix
Cross-sectional					
Schmid et al. 2002 [81]	1.0	STIR CE T1-w FS	4800/30/150 500-720/15-20/-	18	3-4/0.3-0.8
Roemer et al. 2010 [86]	1.5	PDFS CE T1-w FS T1-w SE	5080/32/- 720/15/-	18	3.0/0.3/384x282
Ratzlaff et al. 2013 [94]	3.0	TSE FS IW	3230/30/-	-	3.0/0.3
Observational cohort					
Raynauld et al. 2007 [97]	1.5	3D FISP with FS	42/7/-/- FA 20°	16	1/0/410x512
Driban et al. 2011 [96]	1.5	IW FS	2950/31/-	14	3/0.5/-
Randomised trials					
Laslett et al. 2012 [55]	1.5	PDFS	3875/42/-	16	3-5/0-3/224x448
Callaghan et al. 2015 [18]	1.5	PDFS CE T1-w FS	1500/15/- 500/17/-	16	3/0/3/384x384

Table 2.3. MRI-based quantitative BMLs analysis

2.9 Compositional MRI techniques for BMLs assessment: water-fat separation Dixon techniques

There has been increased interest in advanced quantitative/ compositional MRI techniques (such as T1, T1ρ, and T2 relaxation time mapping) for the evaluation of

OA. Most of the research/ development has focused on cartilage and assessment of matrix composition of cartilage [98-101], with few data on BMLs. In this and the next section (2.10), the aim is to discuss some compositional MR techniques which can potentially be used for the evaluation of subchondral bone marrow, including Dixon MR sequences to quantify fat and water signal and T1 mapping. The next sections will describe the basic principle of the Dixon techniques and T1 mapping (section 2.10), focussing on those relevant to this thesis and discuss their potential in the assessment of BMLs in knee OA.

2.9.1 Technical aspects of Dixon imaging

The basic principle of Dixon technique takes advantage of the different resonance frequency of hydrogen protons in fat and water; a phenomenon called the chemical shift. The original method or two-point Dixon acquires two images with two different TEs to allow the separation of the fat signal from water signal. Since the fat and water spin at different frequencies, the magnetisation vectors precess at different speeds [102]. As the echo time increases the fat and water signal periodically is out of phase and in-phase. One image is acquired when fat and water spins are in phase (signal in-phase: SIP) and the second image is produced at out of phase (signal out-of-phase: SOP). At 1.5 T, approximately the difference of TE between two states is 2.2 ms (out-of-phase TEs:2.2 ms, 6.6 ms, etc.; in-phase TEs: 4.4 ms, 8.8 ms, etc.) and 1.1 ms at 3 T [103]. By obtaining images at different TE values, a voxel that contain a combination of fat and water signals can be decomposed into two different images, fat, and water. Unlike other fat suppression methods, this technique suppresses the fat signal at postprocessing and not during the acquisition. By adding or subtracting these signals it can produce water or fat images since: [79]

W= (SIP + SOP)/2 (water) and F= (SIP-SOP)/2 (fat)

Using this equation, it is possible to generate water-only images with fat suppression and a fat-only image with water suppression. Although the method is insensitive to B1 heterogeneity, the method is sensitive to B0 inhomogeneities that produce water-fat swapping artefacts. To overcome this effect, Glover and Schneider extended the two-point Dixon method by using unwrapping algorithms [79]. They added a third image to compensate at another TE and generated three-phase shifts of 0, +π, and –π between the water and fat.[104] Glover then developed this method into the four-point Dixon method that used four images with phase of 0, π, 2 π, and 3 π [105].

Based on these equations, four sets of images can be produced as:

- A water image (with fat-suppression)
- A fat image (showing only fat)
- An in-phase image (SIP-image without fat suppression)
- An out of phase image (SOP)

Dixon sequences are known by a different name by different MR vendors, such as IDEAL (General Electric healthcare), Dixon (Siemens healthcare), mDixon (Philips healthcare) and WFOP (Toshiba) [79].

In the last twenty years, the 3.0 T MR imaging vendors have developed proprietary reconstruction algorithms to improve the performance of Dixon method allowing more accurate and reliable calculation of fat and water content. In general, the signal intensity in a given voxel can be described using the following equation [106]:

$$s(t) = (W + F\sum a_i \cdot e^{j2\pi t(\Delta f_i)})e^{j2\pi t\psi - (\frac{t}{T_2^*})}$$

Where $s(t)$ is the signal acquired at time t, Δf_i and a_i are the chemical shift and relative amplitude of the ith spectral peak of fat (F) relative to water (W), ψ is the magnetic field inhomogeneity, and T_2^* is the transverse relaxation time. This method of fat-water separation is termed the iterative decomposition of water and fat with echo asymmetry and least-squares estimation (IDEAL) by GE. The latest IDEAL techniques use a six-echo acquisition with a bespoke reconstruction algorithm [107] to calculate fat fraction. IDEAL is used extensively in musculoskeletal imaging, especially in complex and challenging anatomical regions, such as knee, fingers, and neck [108-110]. Multipoint Dixon was developed by Philips and could be used as a two-, three-, or four-point Dixon or more with a different reconstruction algorithm.

2.9.2. Advantages and disadvantages

Given the fact that these techniques are insensitive to B1 (local magnetic field) and B0 heterogeneity, one of the strengths of the Dixon method is it offers homogenous fat suppression compared with STIR or fat-sat techniques. Furthermore, it offers robust fat suppression in regions with high magnetic susceptibility, such as near metallic objects, in complex anatomic regions, and in the extremities of patients [79]. Dixon techniques provide a higher signal-to-noise ratio (SNR) compared with STIR sequences [111]. Furthermore, STIR sequence suppress fat signal based on T1 longitudinal relaxation time difference with water (in which fat has short T1) and may, therefore, suppress signal from other tissues with short T1. For this reason, the STIR sequence is not suitable for use with intravenous contrast agent since gadolinium may shorten T1 values of tissues [79, 112].

Notwithstanding that Dixon method provides important advantages, it has several disadvantages. The primary drawback is increased scan time compared with standard

SE sequence with fat-sat. Typically, the acquisition time is twice as long as a SE sequence with the same acquisition parameters. The second limitation is phase shift artefacts, specific artefacts of Dixon techniques, due to main magnetic field (B0) inhomogeneity discussed above causing fat and water swapping. The three-point Dixon not only provides superior and robust fat suppression, but it may also produce higher SNR [79, 111].

Similar to the IDEAL method, a six-echo acquisition Dixon is available on Philips scanners called mDixon Quant and is used in this thesis. Clinically, it is used mainly for abdomen and musculoskeletal system [79] and it can automatically provide fat fraction maps without off-line processing.

Fat fraction measurements can be biased by factors including T1 and T_2^* relaxation and the presence of multiple fat peaks [113, 114]. This bias can be reduced by choice of acquisition parameters. T1 bias can be minimised by using a low flip angle and/or long TR. Further, T_2^* decay can be incorporated into the signal models and corrected for (as shown in the equation above). The correction of T_2^* is particularly important in organs containing mineralised bone, such as bone marrow where $T_2^*$is short. A predefined fat spectrum model can be assumed to account for the effects of multiple fat peaks [115, 116]. The Philips mDixon Quant sequence from Philips scanners provides inline calculation of a quantitative FF map incorporating measurement and correction of T_2^*.

2.9.3 MRI-based fat fraction quantification

The ability of six gradient-echo Dixon MRI (mDixon Quant) sequences to separate the signals of water and fat has opened a new area of fat quantification allowing estimation of the percentage of fat in each voxel, a feature that has many potential musculoskeletal imaging applications [79, 111].

mDixon Quant sequence has many strengths. This technique is readily available on many clinical scanners and can easily be performed within a reasonable time. As a 3D imaging technique with high resolution and anatomical detail it allows us to assess marrow fat fraction across the entire 3D imaging volume providing anatomical images of fat and water components. This technique also provides potentially accurate measures of fat and water contents that account for T_2^* correction, multiple fat peaks, and magnetic field nonuniformity [113, 117].

Despite these advantages, this technique possesses some limitations. First, the reconstruction algorithm requires an accurate model of the fat spectra. In its current implementation, mDixon Quant utilises prior knowledge of multiple fat peaks for the liver. Potential inaccuracies in the fat, water, and fat fraction map may occur if the lipid spectral profiles of the target organs, such as bone marrow are different from that of liver tissue. Second, the signal model assumes a common T_2^* value for both water and fat components, instead of individual water and fat T_2^* relaxation times. Third, the detail of the algorithms and the postprocessing methods are not available to the users [79, 105, 106, 115].

Dixon MRI have been reported to be useful in discriminating normal and diseased bone marrow and for monitoring disease progression [116]. Results from previous studies have shown excellent agreement with MR spectroscopy in the phantoms [108, 114], liver, pancreas [118], as well as preliminary studies of bone marrow of the spine [119, 120], and proximal femur [113], suggesting that this technique may be accurate for fat fraction estimation even in the presence of trabecular bone. Further studies have also suggested good scan-rescan repeatability in the vertebrae and sacroiliac joints.

Quantitative Dixon imaging has been successfully applied in different organs, including liver to quantify fat deposition in the liver tissue [121], muscle [122], and ankylosing spondylitis of the sacroiliac joints [108]. A study by Fischer et al. used two-point Dixon method to quantify fat infiltration of thigh muscle [122]. A similar method has been used to assess fat composition in Duchenne muscular dystrophy [123]. This method also has been applied to quantify bone marrow infiltration of hematologic disorders. For example, in Gaucher disease, a decreased fat component in lumbar spine represents marrow infiltration by this disease [124].

It has not to date been used in assessment of BMLs in knee OA, however, given the compositional changes within BMLs, fat fraction quantification using Dixon clearly has potential for this and further research is needed.

In summary, quantitative fat-water Dixon imaging has been used to assess fat fraction in different parts of the body, though not as yet in knee osteoarthritis, and has shown excellent agreement with single-voxel magnetic resonance spectroscopy. Further studies are needed in patients with knee OA including looking at fat fractions of BMLs and normal marrow and comparing fat fraction with conventional measures of BML size.

2.10 T1 relaxation time measurements

2.10.1 Biological basis

The T1 relaxation time (also called longitudinal relaxation time or spin-lattice relaxation) is the time constant of protons to recover their longitudinal magnetisation to equilibrium state (along Z-axis) after excitation by a radiofrequency (RF) magnetic field, also known as B_1 field. The T1 value is a characteristic of tissue and longer in an MRI system with stronger magnetic field [125, 126].

T1 values of normal human tissues are influenced their macromolecule component, water binding and water content. They can change in pathologic or abnormal condition, for example oedema around tumours or inflammatory lesions may lead to increased T1, probably due to the increase in water content. T1 may also be effected by the presence of cellular debris [127].

The main components of the bone are cortical and trabecular bone, haematopoietic (red) marrow and fatty (yellow) marrow. The relative proportion of these constituents varies with age and sex. Peak skeletal bone mass maturity is attained at about 25-30 years of age. There might be a small to moderate degree of bone loss until around the age of 40. Following this, there is a decrease of trabecular bone of about 1% per year, which is increased in females at the menopause and continues for several years afterwards. In histopathological terms, this reduction in bone mass is reflected by a decrease in cortical thickness, along with a reduction in the number and diameter of trabeculae. Marrow changes have been noted where the cellular red marrow of vertebral body decreases from approximately 60% of the mass in the first decade to about 30% in the ninth decade [127, 128].

On conventional MRI, cortical and trabecular bone give low signal on all pulse sequences. The signal characteristics of bone marrow on clinical MR images are determined by fat, water, and mineralised matrix. Most fat protons are chemically hydrophobic substances contained in heavy molecules resulting in fat having short T1 relaxation time. An age-related shortening of the T1 relaxation times to approximate that of fat might be expected in adult bone marrow as the relative proportions of red and fatty marrow change [128].

2.10.2. T1 mapping methods

There are many techniques for T1 mapping and a wide range of reported T1 values in human tissues. There are three main T1 mapping methods available: Inversion recovery (which is regarded as the gold standard), Look-Locker and Variable Flip Angle (also called alternative methods) [125].

The gold standard for T1 mapping is considered to be inversion recovery (IR) T1 mapping. The inversion recovery techniques involve inverting the longitudinal magnetisation M_z and sampling the MR signal after an inversion time (TI) using a standard imaging technique that can be spin echo (SE) or gradient echo (GE) [125, 129]. The IR pulse sequence is repeated N times, with different inversion times (TI). For accurate measurement, it is recommended that at least four different TIs that span the range of expected T1 values are performed [125, 130]. T1 values may then be calculated by using nonlinear least-square curve fitting. The procedure is discussed further in Chapter 4 (Methods).

The Look-Locker sequence is similar to inversion recovery in that it applies an inversion pulse to the magnetisation but instead of using a single sample of the recovery curve per TR, this method uses several low flip angle (α) pulses (known as pulse trains) spread across the TR with a certain spacing time (T) [130]. The advantage of this technique is it provides a large number of images that are available for fitting T1 and can produce a 3D image. However, it has the disadvantage that the estimate may differ from the true T1 value depending on several factors, including type of pulse sequence, flip angle, TR, tissue T2 value, RF inhomogeneity, and field strength [125].

Variable Flip Angle (VFA) T1 mapping uses two or more spoiled gradient-echo scans with different flip angles, assuming effective RF spoiling. VFA T1 mapping is less robust than inversion recovery technique. In particular, the signal bias resulting from insufficient spoiling may cause inaccurate T1 estimation [131]. This technique is also sensitive to B1 inhomogeneity and is typically combined with a B1 estimation sequence for the correction of VFA T1 measurements [132, 133].

Despite some limitation, VFA T1 mapping still offers some benefits in research setting. This method can be used to acquire 3D T1 maps [130] with rapid acquisition time, and available in many clinical scanners.

Signal (S) detected with VFA sequence depends on the repetition time (TR), T1 value of the tissue, and the FA (α) as shown in the formula below [134]:

$$S = S_0 \cdot \sin(\alpha)(1-\exp(-TR/T1)) / (1-\exp(-TR/T1) \cos(\alpha))$$

The detail of VFA T1 mapping is further described in the methods chapter (chapter 4).

The T1 relaxation time increases as the external magnetic field strength increases. Fat has a shorter T1 relaxation time than water, approximately 288 ms at 1.5 T and 372 ms at 3 T. A comparison of 1.5 T and 3.0 T for T1 relaxation time measurement on five healthy knees was conducted in 2004 by Gold et al. using the Look-Locker method. They found that T1 values of normal marrow fat were 288 ± 5 ms at 1.5 T and increase substantially to 365 ± 9 ms at 3.0 T [126]. Another study on a healthy human knee to measure T1 values was conducted by Duewell et al on 5 subjects [20]. T1 values were measured with an inversion recovery method at 1.5 T with TR=4000 ms, TE=18 ms and six different TIs (75, 150, 300, 600, 1200, and 2400 ms). Meanwhile, the Look-Locker method was chosen at 4 T with an adiabatic inversion pulse (TR

8400 ms, delay time 200 ms, and flip angle 17°). This study found the T1 values of bone marrow of 0.29±0.009 s at 1.5 T and 0.42±0.031 s at 4 T.

The modified fast inversion-recovery method (MFIR) uses a constant repetition time (TR) and a fast-spin-echo signal acquisition [135] which provides reasonable accuracy and acquisition times. In the MFIR pulse sequence the signal intensity is given by the equation [135]:

$$S = S_0 [1 – 2f.\exp(-TI/T1) – (1 - 2f)\exp(-TR/T1)]$$

Where S_0 is the maximum signal, TI is the inversion time, and f is the inversion efficiency.

In the past, T1 mapping has been used to evaluate tissues throughout the body including brain [136] and myocardium [137] as well as lumbar vertebrae in Hodgkin's disease [138]. Recently, T1 mapping has been successfully used to evaluate bone marrow oedema in sacroiliac joints with ankylosing spondylarthritis [139]. At present, there is little information on MRI T1 mapping of subchondral bone marrow and BMLs in knee OA.

STIR imaging, however, has been used in many BML studies as it provided homogenous fat suppression based on differences in the T1 relaxation time of the tissues. As previously discussed, the preliminary results to date suggest the STIR sequence is sensitive for detecting BMLs and allowing volume quantification of their maximum extent when compared to other sequences [16, 17, 81, 140] but there is little quantitative data on T1 measurement of bone marrow lesions. Previous studies using MR spectroscopy (see also next section – 2.11) have suggested increased water and reduced fat content within BMLs in patients with knee OA [104, 141]. As fat fraction

decreases it might be expected that the bulk T1 relaxation time would increase. However, there may be other effects relating to the T1 of the water component.

In summary, T1 measurement has been used to assess multiple tissues in different parts of the body, however not as yet in knee osteoarthritis although STIR imaging has been used to assess bone marrow lesion size. Further work is needed to better understand the relationship between T1 and fat fraction in complex fat-water-bone systems, and to compare T1 values in BMLs and normal marrow.

2.11 Magnetic resonance spectroscopy

Magnetic resonance spectroscopy (MRS) is a non-invasive method for examining metabolite concentration in human tissues, including fat composition of normal and abnormal bone marrow [142, 143]. MRS is considered the standard of reference in the quantification of fat composition. This section briefly describes the basic principles of MRS technique and its application in clinical studies of bone marrow. The relevance for the work presented in the thesis is that MRS can be used as the standard reference with which to compare other compositional imaging approaches.

2.11.1 Basic concept of MRS

MRS is essentially similar to nuclear magnetic resonance (NMR) spectroscopy, that has been used in chemistry and physics. MRS is the specific term for NMR spectroscopy used in a biological or medical settings. MRS to some extent overlaps with MRI in that MRI detects NMR signals produced by water and fat in tissues to make images. MRS detects NMR signals produced by chemical compounds, including fat and water within a given tissue and evaluate the in-situ biochemistry [144, 145]. In general, similar to MR imaging technique discussed in a previous section (2.5.1), MRS utilises atomic nuclei that are spinning and produce nuclear magnetic fields. MRS has

been commonly used to separate a target tissue into its water and fat components and to estimate fat contents based on the differences in chemical shifts.

There are two main approaches to localise the spectroscopy signal: single voxel spectroscopy, in which the signal of tissue of interest is selected by gradient selection of three orthogonal slices [145], and multiple voxel spectroscopic imaging, which applies spatial phase encoding as in MRI and the signal from multiple voxels is acquired simultaneously [146]. Collection of spectra of single voxel MRS typically use 10 x 10 x 10 mm^3 to 20 x 20 x 20 mm^3. This volume of interest (VOI) is manually localised in the tissue target, for example bone marrow or a BML using multiplanar localising images. Shimming is then applied to achieve a homogeneous magnetic field across the VOI. After successful shimming a spectroscopic sequence is performed. Two MRS sequences are commonly used: point-resolved spectroscopy (PRESS) [147] and stimulated echo acquisition mode (STEAM) MRS pulse sequences [148]. Both sequences are suitable for estimation of fat fraction. The STEAM consists of three 90° pulses, while PRESS uses 90°-180°-180° pulses.

In performing MR spectroscopy for fat fraction calculation, neither water nor fat saturation should be used, as the signal from both components are required to calculate fat fraction. The analysis of collected spectra requires expertise and must be performed offline using specialised software. A description of the analysis of the MR spectra for fat fraction calculation is described in chapter 8.

The MR spectrum is a two-dimensional plot of frequency on the horizontal axis and intensity of the signal on the vertical axis. MRS signals from different atomic nuclei are distinguished by their unique frequencies at a particular magnetic field strength [149].

2.11.2 MRS-based quantitative assessment of bone marrow

There have been a number of MRS studies to investigate anatomic, age and gender variance of bone marrow fat content and to characterise bone marrow changes in different pathological states [150, 151]. Altered fat content has been linked to skeletal fragility, osteoporosis [151], diabetes mellitus [152], and Gaucher disease [153].

MRS-based bone marrow water and fat fraction measurements have been validated against chemical analysis [114] and histology studies [154]. This technique has been reported to have good reproducibility in the spine [155] and the proximal femur [156].

Previous work has used spectroscopy as a gold standard to validate Dixon imaging in fat-water phantoms. Dixon fat fractions have been compared with MR spectroscopy in the spine [119, 120] and proximal femur [113, 115], suggesting that water-fat imaging with T2* correction was accurate for fat fraction quantification. A study of MR spectroscopy in knees of patients with ACL injury showed significant differences in water content between areas of bone marrow oedema and adjacent bone marrow [141]. Further, previous work using MR spectroscopy has shown significant differences in water content between BMLs in OA patients and normal bone marrow in control healthy subjects [104]. The increased water content was consistent with a previous histology study that showed oedema was observed within the BMLs [53].

In summary, MRS is the method of choice to measure fat content accurately, but it suffers from lower spatial resolution, relative long acquisition times, and difficulty covering the whole knee. Furthermore, MRS analysis requires expertise and specialised software for offline postprocessing and analysis. Previous studies have validated six-point Dixon sequences against spectroscopy in simple fat-water phantoms with promising results in human subjects suggesting Dixon offers potential

advantages for calculating fat fraction in abnormal bone marrow. The assessment of bone marrow fat content and fat changes of BMLs has the potential to be very important to better understand the pathophysiology of OA.

2.12 Summary

BMLs are common in symptomatic knee OA and considered to be an important feature of osteoarthritis. They appear as high signal intensity lesions with ill-defined borders on fluid sensitive MRI sequences, such as fat suppressed proton density or STIR sequences. Studies have linked BMLs to pain and disease progression and suggest they are a potential imaging biomarker for knee OA.

Previous work has focussed on assessing BML size using semiquantitative or quantitative approaches. Quantitative approaches are recognised as more time-consuming but are considered more accurate and reproducible. Quantifying BML volume accurately is difficult due to poorly defined borders of BMLs, and it is therefore subject to observer error which may potentially introduce misclassification. The choice of MRI sequence to allow optimal differentiation of abnormal and normal bone marrow is important.

To date, however, there are few comparative data looking at how BMLs vary in size based on the MRI sequences used in imaging. Several studies have compared BMLs volume using different pulse sequences, but mostly fluid sensitive non-CE vs CE pulse sequences. IW/ PDFS, STIR, and CE T1-w FS images are typically recommended for assessing BMLs in OA of the knee. Based on previous studies, PDFS sequences appear best validated for demonstrating the full extent of BMLs, however, it has been suggested it can be interchanged with CE T1-w FS images. STIR may also produce similar results although direct comparison with PDFS is as yet lacking. Studies on

gradient echo sequences such as T1-w FS GE or DESS suggested that these sequences produced smaller BML volumes and were less sensitive than fluid sensitive or CE sequences. The use of gradient echo images has been generally discouraged for assessing the full extent of BMLs due to their sensitivity to T2* effects in trabecular bone. However, gradient echo images do have some potential advantages (e.g., fast 3D imaging) and there are a wide variety of gradient echo imaging techniques with widely different properties. A gradient echo technique which has been optimised for BML imaging (e.g., by minimising sensitivity to T2* and effects of multiple spectral peaks of fat) has yet to be tested against IW/ PDFS images for BML assessment. Future studies to compare multiple different sequences against PDFS images for BMLs assessments are necessary, including their reliability and also their relation to clinical features in particular pain.

The development of novel compositional MRI techniques provides an alternative approach to conventional MRI sequences, by characterising BMLs based on parameters which depend on their biochemical composition, including fat fraction and T1 relaxation time. Although work to date has generally focussed on assessing BMLs maximum extent, there are increasingly suggestions that other properties of BMLs including fat fraction and T1 may be important. Fat fraction in knee OA has been previously investigated using spectroscopy, however Dixon imaging is a potentially more practical method in vivo and has been widely used in the liver in particular. There has been some preliminary validation in other bones against spectroscopy. Dixon imaging has also been tested in fat-water-bone phantoms against a wide range of fat fractions although there is little comparative work with spectroscopy. T1 differences form the basis for STIR imaging and T1 measurement is another potentially useful quantitative technique. Both water-fat Dixon imaging and T1

mapping have been used successfully in different parts of the body including bones, for example in ankylosing spondylitis, though not to our knowledge in knee osteoarthritis. In knee OA, simple binary characterisation of BMLs based on their presence on 2 different sequences suggest parameters such as T1 and fat fraction may be useful for discriminating BMLs. These quantitative techniques could provide alternative methods for monitoring BMLs based on bone marrow composition rather than BML extent. Such techniques offer the potential to reduce segmentation requirements and bias by following the compositional changes in a region of bone marrow over time.

Further work remains to be done to investigate the behaviour and reliability of Dixon fat fraction and T1 measurement techniques in fat-water-bone systems compared to spectroscopy. There is little published work looking at these techniques in OA of the knee and comparative data between BMLs and normal-appearing bone marrow is lacking. It remains to be seen how such compositional measurements relate to conventional assessments of BML size.

Chapter 3

Aims and Objectives

Chapter 3
Aims and objectives

3.1 Summary

This chapter summarises the aims and objectives of the thesis.

3.2 Aims

The broad aim of the thesis is to compare the performance of conventional MRI sequences in the assessment of subchondral bone marrow oedema-like lesions (BMLs) in knee osteoarthritis and to investigate the role of novel application of compositional MRI methods (mDixon Quant fat fraction and T1 relaxation time).

3.3 Specific objectives

3.3.1 To compare conventional MR sequences for BML volume measurement (Chapter 5):

(1) to determine the intraobserver reliability of volumetric BML assessment of BMLs in patellofemoral knee OA using four established MRI sequences; proton density fat-suppressed, STIR, contrast-enhanced T1-weighted with fat suppression, and 3D gradient echo T1-weighted fast field echo sequences.

(2) to determine the influence of MRI sequence on BML volume and the correlation between BML volume assessed using four established MRI sequences.

(3) to determine the correlation between BML volume assessed using four established MRI sequences and knee pain.

3.3.2 To compare novel quantitative gradient echo mDixon Quant imaging with conventional imaging in assessment of BML volume (Chapter 6)

(1) to compare BML volume assessment in subjects with symptomatic knee OA using novel 3D mDixon Quant water-only sequences and conventional 2D fat-suppressed proton density (PDFS) sequences
(2) to determine for each MRI sequence the association between BML volume and knee pain

3.3.3 To investigate the use of fat fraction in assessment of BMLs using novel quantitative gradient echo mDixon Quant imaging

(1) to validate fat fraction estimates from quantitative gradient echo mDixon Quant imaging against MR spectroscopy using fat-water emulsion phantoms with and without bone granules (Chapter 8)
(2) using water-fat separation MRI imaging (quantitative mDixon Quant sequences) to compare fat fraction (%) of BMLs and normal marrow in patients with symptomatic knee OA (Chapter 7)
(3) to compare a novel approach to assessment of change in BMLs over time using image registration and mDixon Quant fat fraction measurement with conventional BML volume change (Chapter 7)

3.3.4 To investigate T1-based measurements in fat-water-bone phantoms and BMLs in knee osteoarthritis (Chapter 8)

(1) To assess the feasibility and limitations of methods for quantification of T1 and fat fraction using phantoms with varying amounts of fat and bone and a subject with a BML, specifically:

a. to compare T1 quantification using single slice inversion recovery monoexponential T1 mapping and a 3D gradient echo VFA sequence.
b. to compare T1 estimates, and fat faction estimated using a novel biexponential inversion recovery T1 procedure against MR spectroscopy and previously validated mDixon Quant techniques.

(2) To compare T1 measurements and fat fraction assessed using the novel biexponential inversion recovery T1 procedure between BMLs and normal appearing bone marrow in subjects with knee OA.

Chapter 4

Methods

Chapter 4

Methods

4.1 Summary

This chapter outlines the methods used to address the aims and objectives of the thesis. There were four separate experiments/ studies and the methods for each are described in turn. Details of the cohorts from which the subjects who contributed data to study 1-3 are described, followed by a summary of the MRI sequences used in those studies and MRI image analysis. Details about creation of the phantoms used in the last experiment are described and also the imaging protocol which was used. The broad approach to data analyses for the separate studies is outlined at the end of the chapter. Additional information about methods and analysis are included in later (results) chapters.

4.2 Study 1- Comparison of different conventional MRI pulse sequences for volumetric BML assessment

4.2.1 Aims and study cohort

The aims of this study are i) to compare BML volume in subjects with painful knee OA using four established MRI sequences, ii) to determine the reliability of volumetric BML assessment using these sequences, and iii) to determine the correlation between BML volume assessed using the sequences and knee pain.

Subjects who contributed data to the analysis had been recruited from a clinical trial of knee brace therapy (‘Brace trial’) in patients with symptomatic patellofemoral (PF) knee OA [18]. In brief, in the trial men and women aged 18 and over with painful knee

OA were invited to attend for screening. Those who agreed to take part were randomised to a patellofemoral knee brace or no therapy. After a period of 6 weeks therapy was stopped. After a 2 week wash out period, subjects crossed over to the alternative treatment (brace or no therapy) and continued for a further 6 weeks. Subjects had MRI performed at the start of the study using four established MRI sequences (see below). They were asked about knee pain in the past week using a visual analogue scale (0-10) at baseline and follow up. The study in this thesis (Study 1) was a secondary analysis of 76 subjects recruited to the Brace Trial. MRI images taken at baseline were included in the analysis.

4.2.2 Imaging protocol

Subjects were scanned using a 1.5 T Gyroscan Intera MRI scanner (Philips, Best, Netherlands). Axial images of the patellofemoral joint were obtained using four established MRI sequences: proton density fat-suppressed (PDFS), STIR, contrast-enhanced (CE) T1-w fat-suppressed, and 3D T1-w FFE sequences (detail of the MRI sequences' parameters are summarised in Table 4.1 and also in chapter 5).

4.2.3 Image analysis

The images were firstly anonymised and randomised by an independent statistician before image analysis. The reader (the author [HN]) who was blinded to the patients' identification (ID) and pain score, performed the segmentation of BMLs. Images acquired using different sequences in the same subject were not evaluated together and the reading order of the MRI pulse sequences was randomly assigned. Each MRI sequence was evaluated independently and separately to minimise recall bias.

Intra-reader repeatability for volumetric BML assessment was assessed by re-evaluation of MR images from 15 subjects who were randomly selected from the data. The images were assessed with a minimum of 4-weeks between the two assessments.

Volumetric BML assessment was performed by manual segmentation using Osirix. BMLs were defined as ill-defined areas of high signal intensity in the subchondral region directly adjacent to articular cartilage. The study focused on the assessment of BMLs in the patellofemoral (PF) regions (patella and trochlea of the femur) using the four different established MRI sequences (baseline visit only). Any BML in the patella and trochlea were included in the analysis. The PF region was defined using the Boston-Leeds Osteoarthritis Knee Score (BLOKS) [90] anatomical delineation (figure 4.1). Manual segmentation was performed using the freehand ROIs tool.

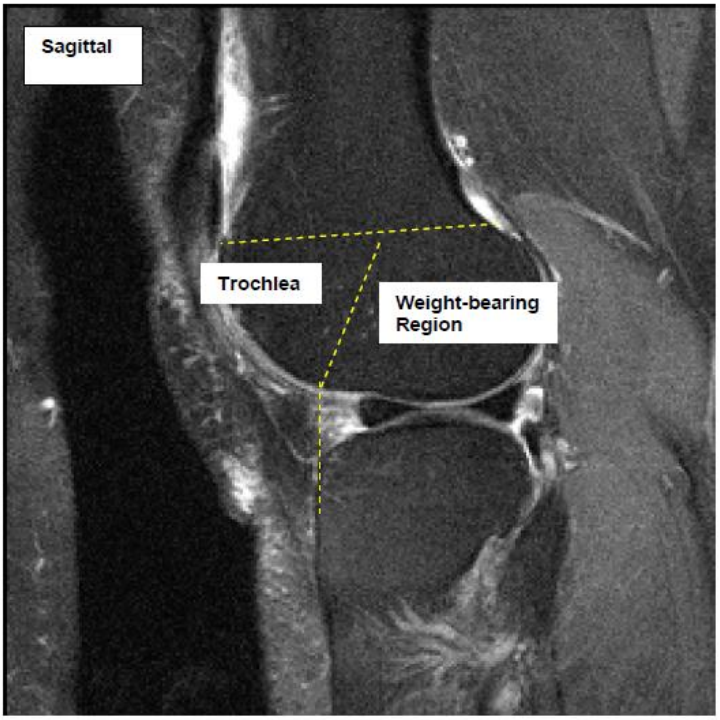

Figure 4.1. Anatomical delineation of femur into trochlea and weight-bearing regions according to BLOKS. Reproduced from [The reliability of a new scoring system for knee osteoarthritis MRI and the validity of bone marrow lesion assessment: BLOKS (Boston–Leeds Osteoarthritis Knee Score), D J Hunter, G H Lo, D Gale, A J Grainger, A Guermazi, P G Conaghan, 67(2), pp.206-211, copyright notice 2022] with permission from BMJ Publishing Group Ltd.

Before segmentation of BMLs was performed, in order to be consistent in defining the trochlear region for all images across patients, the axial MR images that represent the trochlear region were defined (upper and lower boundaries of the region) by the following steps:

- A sagittal WATSc sequence was used to define the upper and lower boundaries. The upper boundary of the trochlea was defined by the anterior upper most cartilage or the anterior epiphyseal line (at the anterior femur) (figure 4.1).
- The lower boundary was defined by the intersection of a line parallel to the anterior aspect of the proximal tibia at the margin of the tibial plateau with the femoral surface. (figure 4.1).
- Axial MR images that lie within these two lines were included in the analysis, meaning that any BML that appeared below or above these boundaries was excluded from the analysis.

BMLs were delineated on each MRI sequence using Osirix software. Freehand ROIs were drawn around the areas of BMLs carefully avoiding normal appearing bone. Cystic components within BMLs were included in the segmentation. Any bone cysts without oedematous bone marrow component were excluded from the segmentation. BML volume (in mm^3) was calculated by multiplying the area of BML identified within a slice with the slice thickness plus slice gap and summing the values over all the slices of the BML.

4.3 Study 2- Comparison between 3D mDixon Quant and PDFS sequences for volumetric BML assessment

4.3.1 Aims and study cohort

The aim of this study was to compare novel gradient echo mDixon Quant water-only imaging with conventional imaging in the assessment of BML volume. Subjects who contributed data to this analysis had been recruited for a randomised clinical trial of participants with painful knee (DISKO Study; ISRCTN Number: 96920058). In this trial, subjects with painful knee OA and evidence of a BML had been randomised to either treatment with Denosumab or placebo. MRI scans were performed at baseline and follow up after an interval period of 6 months. The study in this thesis (Study 2) was a secondary analysis of a subset of 30 subjects who had had mDixon Quant and PDFS MRI sequences performed at the baseline visit.

4.3.2 Imaging protocol and images analysis

Subjects were scanned using a 3T scanner based at the Manchester CRF. Details about the MRI protocol for the DISKO study and image analysis (Study 2) are outlined in chapter 6. A summary of the MRI sequence parameters is presented in Table 4.1.

BML volume measurement was performed by manual segmentation using Osirix (see section 4.2.3). To minimise reading biases, the order of the subjects and MR images (for the two images – mDixon Quant and PDFS) were randomly assigned using a random permutation planner available online (www.randomization.com). The reader who was blind to individual subject characteristics then measured the BML volumes.

4.4 Study 3- Quantification of fat fraction in BMLs and normal marrow using the mDixon Quant MRI and image registration

4.4.1 Aims and study cohort

The aim of the study was to compare fat fraction (%) of BMLs and normal marrow in patients with symptomatic knee OA using a novel gradient echo mDixon Quant technique and to compare a novel approach to assessment of change in BMLs over time using image registration and mDixon Quant fat fraction with conventional BML volume change.

The subjects who contributed data to this study had been recruited for participation in a randomised controlled trial of a lateral wedge insole. Subjects with painful knee OA were randomised to receive either the lateral wedge insole or a neutral shoe for 8 weeks with a wash over period before they received the alternative intervention (ISRCTN: 55059760) [157]. As part of the trial, subjects had MRI images at baseline and after a follow up of eight weeks. Subjects without BMLs at baseline were excluded from the trial. The study in this thesis (Study 3) was a secondary analysis of a subset of 17 subjects who had had mDixon Quant images on two visits separated by seven to nine weeks.

4.4.2 Imaging protocol and images analysis

A six-echo 3D gradient echo sequence (mDixon-Quant) with equidistant echo spacing was obtained for fat fraction quantification and proton density weighted images with fat suppression (PDFS) were acquired for volumetric BML assessments. Details of the MRI protocol and sequence parameters is outlined in chapter 7. Information about the sequences is presented in Table 4.1.

MR images were anonymised before the analysis, and volumetric BML assessment was performed on sagittal PD SPAIR sequences at the baseline and follow up visits. The images in each subject were assessed paired though the reader was blinded to visit order to minimise reading biases. BMLs then were manually segmented using in-house built segmentation software (developed by Timothy. F. Cootes, Professor of Computer Vision, University of Manchester).

The assessment of the mDixon Quant images was conducted once the volumetric BML assessments had been completed for all subjects. The images in each subject were initially randomly allocated using a balanced sampling method to define which images (initial or follow-up) in each subject were to be used for manual segmentation of BMLs and also normal bone marrow. To estimate the fat fraction, the region of interests (ROIs) of BMLs and nearby normal-appearing marrow were manually segmented on the mDixon Quant water images at either initial or follow-up visits depending on the random allocation. Sagittal STIR images were used together with mDixon Quant water images to identify BML extent. The detail of post-processing of MR images is described further in chapter 7. To permit fat fraction calculation from corresponding ROIs at both visits, image registration of the mDixon Quant images was performed using in-house built software.

Study	MRI Scanner	MRI Sequences	TR (ms)	TE (ms)	TI (ms)	slice thickness (mm)	slice gap (mm)
1	1.5 T	PDFS	1500	15	-	3	0.3
		STIR	3700	14	140	3	0.3
		CE T1-w FS	500	17	-	3	0.3
		3D T1-w FFE	39	5.2	-	3	slice overlap: 1.5
2	3 T	PDFS	4200	40	-	3	0.3
		mDixon Quant	15	TE first ~1.4, echo spacing ~1.1	-	1	0
3	3 T	mDixon Quant	15	TE first: ~1.4; echo spacing: ~1.1	-	1	0
		STIR	4300	50	200	3	0.3
		PD SPAIR	2900	30	-	3	0.3
4	3 T	mDixon Quant	30	TE first: 0.95; echo spacing: 0.9	-	1.5	0
		FSE-IR	8000	43 or 30	100, 300, 700, 1500, 3000 or 50, 100, 200, 400, 800, 1600, 3200, 5000	2.5	-
		In-phase VFA	7.4	TE 2.3;	-	1.5	0
		MRS STEAM	315, 600, 1000, 1500, 2000, 3000, 5000	15	-	Voxel size: 8 x 8 x8 mm^3	Spectra BW: 2000; samples 512

Table 4.1. MRI and MRS parameters for each study

4.5 Study 4- Compositional MRI Approaches: fat fraction and T1 relaxation times measurements in fat-water-bone phantoms and clinical feasibility study in subjects with knee osteoarthritis

4.5.1 Study aims

The aims of this study were i) to compare fat fraction estimates from mDixon Quant imaging against MR spectroscopy using oil-water-bone phantoms, ii) to compare T1 relaxation time measurements using single slice monoexponential T1 mapping and a 3D gradient echo VFA sequence and to study the behaviour of T1 with differences in fat fraction and bone, iii) to compare fat fraction estimates from a novel biexponential inversion recovery T1 method against MR spectroscopy and mDixon Quant techniques in fat-water-bone phantoms and a subject with a BML, and iv) to compare T1 relaxation times and fat fraction measured using a biexponential inversion recovery method between BMLs and normal-appearing marrow of knee OA subjects. The in vitro study used phantoms of agar-based oil-water emulsion of varying concentration of peanut oil and water (with and without bone matrix). The phantoms with different fat fractions values (0% to 100%) were constructed using basic laboratory equipment and components, including distilled water, agar, water-soluble surfactant, sodium benzoate, peanut oil, and oil-soluble surfactant. Further details are outlined below.

4.5.2 Phantom construction

There were two groups of phantom components: the first group included fat-water emulsions without bone granules with fat fraction from 0% to 100%, while the second group included oil-water emulsions with fat fraction of 0.0 %, 19.1%, 38.6%, and 58.6% with the addition of bone granules (100 and 150 mg/ ml) to simulate the in vivo

condition of human femoral and tibial bone marrow. Each phantom component was placed in a 5 mL plastic tube with inner diameter of 14 mm.

The construction of the phantom adopted the standard approach put forward by Bray et al [108]. For each tube, the appropriate volume of peanut oil with sodium dodecyl sulphate (surfactant; Sigma-Aldrich, St. Louis, Missouri, USA) was added to the peanut oil and gently mixed to form an initial emulsion. Appropriate volumes of 3.0% weight/ volume agar solution were then added to the oil solution in order to create homogeneous fat-water emulsions using a magnetic stirrer hotplate heated to 90°C. The appropriate mass of bone granules (NuOss granules, particle size 250-1,000 μm, Henry Schein, London, UK) were added to reflect the trabecular bone density with the value of 100 and 150 mg/cm^3.

4.5.3 Phantom scanning procedure

The phantom study was performed on a 3T MRI scanner (Achieva, Philips Healthcare, Best, Netherlands). The phantom components were placed in a plastic container and immersed in water agar solution with 3% by weight of agar. All phantoms were imaged together using a knee coil. The tubes were oriented horizontally and perpendicular to the main magnetic field (i.e., perpendicular to the z axis). The images of the phantoms were acquired in a sagittal plane perpendicular to the long axis of the tubes of the phantoms.

The imaging protocol for the phantom study consists of:

a) Sagittal single slice fast spin echo inversion recovery (FSE-IR) sequences were obtained using the following parameters: TR = 8000 ms, TE= 43 ms, TI = [100, 300, 700, 1500, 3000 ms], BW = 675 Hz/pixel, matrix size= 288 x 225, FOV= 220

x 220 mm^2, and slice thickness= 2.5 mm. The slice position was through the centre of the phantom perpendicular to the long axis of the tubes.

b) A mDixon Quant sequence for fat fraction quantification was obtained using a six-echo sagittal 3D gradient echo sequence with equidistant echo spacing using the parameters: TR 30 ms; six echoes, TE_1 set to 0.95 ms; echo spacing set to 0.9 ms; flip angle 3°; slice thickness 1.5 mm with 0 mm slice gap; acquisition matrix 256x128 with 128 slices; voxel size 1.5x1.5x1.5 mm; bandwidth 1822.8 Hz/pixel.

c) A 3D in-phase (IP) variable flip angle (VFA) sequence was acquired for T1 relaxation time measurements with parameters: TR=7.4 ms; TE= 2.3 ms; BW 1847.4 Hz/pixel; FOV 192 x 168 mm^2; matrix 128 x 112; 120 slices with slice thickness of 1.5 mm and slice gap 0 mm. IP VFA sequence was performed with six flip angles (α)= 3°, 5°, 7°, 10°, 20°, 30°, with imaging time lasting in around 2 minutes and 19 seconds per flip angle.

d) A Sagittal B1 mapping sequence was acquired prior to IP VFA acquisition with the following parameters: TR/TR extension /TE= 30/ 120/1.92 ms, flip angle 60°, bandwidth 383 Hz/pixel, FOV 192 x 168 mm^2, 72 slices of 5 mm and 2.5 mm overlap between adjacent slices, with an acquisition time of 10 minutes and 13 seconds.

e) Magnetic Resonance Spectroscopy (MRS) sequences for T1 and fat quantification were acquired using a STEAM volume selection technique without water suppression after volume localised shimming (shim size 25 x 25 x 25 mm^3) with the TE 15 ms with an array of TRs (315, 600, 1000, 1500, 2000, 3000, 5000 ms) with voxel size 8x8x8 mm^3. Each signal was sampled with 512 points and a sweep width of 2000 Hz. The VOIs were acquired at the centre of each phantom. Two sets

of acquisitions at two different centre frequencies (one set on the main fat peak and one on the water peak) were performed to each tube.

4.5.4 Study cohort and imaging protocol for clinical feasibility study

The subjects who contributed to this preliminary study were a subsample of knee OA subjects who had taken part in the lateral wedge insole study as outlined in section 4.4.1 (study 3). Six participants (4 females, two females, aged from 51 to 66 years) with a multiple inversion time single slice inversion recovery sequence were included in the analysis.

The imaging protocol for the clinical feasibility study consisted of a sagittal fast-spin echo single slice inversion (FSE-IR) recovery sequence with the parameters: TR/TE= 8000/30 ms with eight different inversion times (TI) (50, 100, 200, 400, 800, 1600, 3200, 5000 ms), section thickness= 2.5 mm, matrix size= 352x352, pixel size= 0.625 x 0.625, and BW: 623 Hz/pixel.

4.5.5 Image analysis

For T1 relaxation measurements, the images were analysed using in-house code written using Matlab (MathWorks, Natick, MA). The details of the image analysis are described in the following sections.

The mDixon Quant fat fraction values of the phantoms were measured from fat fraction (FF) maps automatically reconstructed by the scanner. A rectangular ROI (the size of the ROI was set to be identical to that used for MRS) was drawn using Matlab in the centre of each phantom in the location that matched the VOIs of the MR spectroscopy. Mean fat fraction values of the voxels within ROIs were calculated as percentage (%) fat fraction.

There are two different quantitative MRI-based approaches for measuring T1 of the phantoms: inversion recovery and variable flip angle (VFA) sequences. The monoexponential T1 relaxation time from inversion recovery was calculated by performing a fit for each pixel at the different inversion times to the following equation:

$S = S_0 [1 – 2f.\exp(-TI/T1) – (1 - 2f)\exp(-TR/T1)]$ [135]

Where S= signal vector, S_0= maximum observable signal intensity, TI= inversion time, f= inversion efficiency.

Similarly, fat fraction was estimated by assuming separate fat and water components with a known fixed T1 for fat and an unknown T1 for water using [135]:

$$S = S_0[ff \{1-2f.\exp(-TI/T1_{fat}) - (1-2f)\exp(-TR/T1_{fat})\} + (1-ff) \{1-2f.\exp(-TI/T1) - (1-2f)\exp(-TR/T1)\}]$$

Where TI is the inversion time, f is inversion efficiency, ff is fat fraction, $T1_{fat}$ is the T1 relaxation time of fat, T1 is the T1 relaxation time of water.

To get T1 and fat fraction values from the phantom, a rectangular ROI (the ROI was set to visually match that used for MRS) was manually drawn at the centre of each tube on the monoexponential T1 and fat fraction maps.

The second technique for T1 measurement involved in-phase (IP) VFA images using the equation [134]:

$S = S_0 . \sin(\alpha)(1-\exp(-TR/T1)) / (1-\exp(-TR/T1) \cos(\alpha))$

Where S is the signal intensity, α is the FA, TR is the repetition time, and S_0 is a constant depending on the proton density, the coil sensitivity, and T2* relaxation. From multiple IP VFA images acquired with a series of different FAs, a T1 map was

calculated on a pixel-by-pixel basis by using a linear fitting method. The actual FA is position dependent because of radiofrequency field (B1) inhomogeneity. The B1-corrected FA was therefore used in the pixel-by-pixel fitting process for calculating the T1 map described above. T1 values (reported as mean values in milliseconds) were measured from the T1 maps after B1 correction. ROIs were drawn in the regions that matched VOIs of MR Spectroscopy.

The sagittal single slice inversion recovery images of human subjects were acquired through a slice in the knee with a large BML on the PDFS sequence. ROIs were drawn in the areas of BML and nearby normal appearing bone marrow on the IR images with an inversion time of 200 ms. The selected ROI of the BMLs consisted of the area judged to be the maximum size of BMLs. ROIs of normal marrow were outlined in normal-appearing bone marrow in the same region or compartment as the BMLs or in the opposing bone if not possible. The T1 values were reported as the median and interquartile range (IQR) of T1 from all pixels inside the ROI.

4.5.6 MRS-based T1 and fat fraction quantification

The spectra acquired from study 4 were exported and analysed at an offline computer using the AMARES (advanced method for accurate, robust, and efficient spectral fitting) algorithm included in the jMRUI software package. The spectrum of water (4.65 ppm) and multiple fat spectral peaks (0.9, 1.3, 2.06, 2.82, and 5.26 ppm) data was reconstructed and corrected for phase, baseline, and frequency shift. A manually selected resonance frequency and line width of water and fat peaks were used as starting values in the nonlinear least-squares fitting algorithm. Line widths of unsuppressed water and lipid peaks, as determined with jMRUI, were measured as an indicator of overall spectral quality. The T1 relaxation times were measured with an

array of TRs (315, 600, 1000, 1500, 2000, 3000, 5000 ms). Peak fitting was performed for the spectra at individual TRs. Water (4.7 ppm) areas were corrected for T1 decay using non-linear least squares fitting. The computed areas under each spectral peak were plotted against TR, and a monoexponential saturation recovery was used for fitting with the equation:

$S_I = S_0 (1- \exp (-TR – (TE/2) – TM)/T1))$

where S_I is the peak spectral area for a given TR, S_0 is the equilibrium value, TR is the repetition time, TE is the echo time, and TM is the mixing time.

The fat fraction (as a percentage) was determined using combined spectra (water peak acquired with centre frequency of water and the methylene peak acquired using the centre frequency of the methylene fat peak). MRS fat fraction was calculated as the ratio of the methylene peak area (after correction for the ratio of the methylene to the total fat peaks) to the sum of the corrected methylene peak and water peak areas. The detail of the MR spectroscopy and fat fraction analyses are described in chapter 8.

4.6 Statistical analysis

The broad approach to the analysis of data in the studies included in the thesis are outlined below. Further details are included in chapters 5-8. Descriptive statistics were used to summarise subject characteristics including means and standard deviations for continuous data and frequency (%) for categorical data. Where the data were non-normally distributed non-parametric summary statistics (median and interquartile range (IQR)) were used. t-tests were used to compare the distribution of two unrelated variables and paired t-tests were used to compare distribution of two related variables. For non-normal data the non-parametric equivalent statistics were used (Wilcoxon rank sum and signed rank test). Intraclass correlation coefficient ($ICC_{3,1}$) was used to

assess intrareader reliability. In study 1, comparisons between four different MRI sequences were analysed using regression techniques and in particular a random-effects panel linear regression model. Post-hoc pairwise comparisons were undertaken using Bonferroni-corrected 95% confidence intervals. Relationships between BML volume on different MRI sequences were tested using Spearman's correlation. Linear regression was used to evaluate the association between BMLs volumes on different MRI sequences and pain. In study 2, comparison of BML volumes between mDixon Quant and PDFS sequences was evaluated using Wilcoxon signed-rank test and Spearman's correlation coefficient. The association between BML volumes and knee pain was tested using linear regression. In study 3 the relationships between change in BML volume and change in BML fat fraction was assessed using the Spearman's correlation coefficient. In Study 4, Bland-Altman plots were used to compare assessments of fat fraction and T1 measurements by MRI and MRS. The difference between means (bias) between MRI and MRS assessments and 95% confidence interval around the mean difference were reported. The relationship between the known fat fraction (using the phantoms) and MRI/ MRS based FF, and between MRI and MRS techniques were tested using Pearson correlation coefficients (r). T1 and FF values in the clinical study (study 4) were reported as the median and interquartile range (IQR) for averaging across voxels in each subject. The difference of the values between BML and normal bone marrow was tested using Wilcoxon signed-rank test. Statistical significance for all analyses was set at the 5% significance level. All statistical analyses were performed using Stata 14.0 (StataCorp, TX, USA).

4.7 Personal contribution to achieving thesis aims

This section outlines the role of the author in achievement of the aims and objectives of the thesis. The author was ***not*** involved in the design or collection of data for any of

the clinical trials outlined in the thesis (Study 1-3). He was involved though at all stages in the studies presented in the thesis (Studies 1-4). This included reviewing and summarising the literature to identify the current state of the art in the field and also gaps in the field. Also, preparation of the images for analysis, and undertaking all of the morphometric and other assessments required. In addition, the author sourced the material for the phantoms, drafted the experimental protocol and undertook imaging and analysis of images from the study. Finally, the author involved in the statistical analysis of data acquired as part of the assessments, interpretation of the findings, and writing up the results.

4.8 Research Ethics

All the clinical studies outlined in this thesis were approved by NHS research ethics committees and the patients recruited to the trials provided informed consent to participate.

Chapter 5

Study 1

This chapter is based on the paper published online:

Noorveriandi, H., Parkes, M.J., Callaghan, M.J., Felson, D.T., O'Neill, T.W. and Hodgson, R., Assessment of bone marrow oedema-like lesions using MRI in patellofemoral knee osteoarthritis: comparison of different MRI pulse sequences. The British journal of radiology (2021). https://doi.org/10.1259/bjr.20201367

Chapter 5

Assessment of Bone Marrow Oedema-like Lesions using MRI in Patellofemoral Knee Osteoarthritis: Comparison of Different MRI Pulse Sequences

Henry Noorveriandi, MD, MSc [1], Matthew J Parkes, PhD [2], Michael J Callaghan, PhD, MPhil, MCSP [3, 4], David T Felson, MD, MPH [5, 6], Terence W O'Neill, MD [6, 7, 8], Richard Hodgson, PhD [9]

[1] Division of Musculoskeletal & Dermatological Sciences, School of Biological Sciences, Faculty of Biology, Medicine & Health, the University of Manchester, UK
[2] Division of Population Health, Health Services Research & Primary Care, School of Biological Sciences, Faculty of Biology, Medicine and Health, the University of Manchester, Manchester, UK
[3] Faculty of Health, Psychology, and Social Care, Department of Health Professions, Manchester Metropolitan University, Manchester, UK
[4] Manchester University NHS Foundation Trust, Manchester, UK
[5] Boston University School of Medicine, Boston, Massachusetts, USA
[6] Centre for Epidemiology Versus Arthritis, Faculty of Biology, Medicine and Health, Manchester Academic Health Science Centre, the University of Manchester, UK
[7] NIHR Manchester Biomedical Research Centre, Manchester Academic Health Sciences Centre, Manchester University NHS Foundation Trust, Manchester, UK
[8] Department of Rheumatology, Salford Royal NHS Foundation Trust, Manchester, UK
[9] Division of Informatics, Imaging & Data Sciences, School of Health Sciences, Faculty of Biology, Medicine & Health, the University of Manchester

Abstract

Objective:

To compare bone marrow oedema-like lesion (BML) volume in subjects with symptomatic patellofemoral (PF) knee OA using four different MRI sequences and to determine reliability of BML volume assessment using these sequences and their correlation with pain.

Methods:

Seventy-six men and women (mean age 55.8 years) with symptomatic patellofemoral knee OA had 1.5 T MRI scans. PD fat-suppressed (FS), STIR, contrast-enhanced (CE) T1-w FS, and 3D T1-w FFE sequences were obtained. All sequences were assessed by one reader, including repeat assessment of 15 knees using manual segmentation and the measurements were compared. We used random-effects panel linear regression to

look for differences in the log-transformed BML volume (due to positive skew in the BML volume distribution) between sequences and to determine associations between BML volumes and knee pain.

Results:

Fifty-eight subjects had PF BMLs present on at least one sequence. Median BML volume measured using T1-w FFE sequence was significantly smaller (224.7 mm^3) than the other three sequences. BML volume was greatest on the CE sequence (1129.8 mm^3) though not significantly different from volume when assessed using PDFS and STIR sequences (960.3 mm^3 and 1056.3 mm^3). There were strong correlations between BML volume on PDFS, STIR, and CE T1-w FS sequences (ρs= 0.98). Correlations were lower between these three sequences and T1-w FFE (ρs= 0.80 - 0.81). Intraclass correlation coefficients were excellent for PDFS, STIR, and CE T1-w FS sequences (0.991 to 0.995), while the ICC for T1-w FFE was good at 0.88. We found no significant association between BML volume assessed using any of the sequences and knee pain.

Conclusion:

T1-w FFE sequences were less reliable and measured considerably smaller BML volume compared to other sequences. BML volume was larger when assessed using the contrast enhanced T1-w FS though not statistically significantly different from BMLs when assessed using PDFS and STIR sequences.

Advances In Knowledge:

This is the first study to assess BMLs by four different MRI pulse sequences on the same data set, including different fluid sensitive sequences and gradient echo type sequence.

5.1 Introduction

Magnetic resonance imaging (MRI) has been widely used in knee osteoarthritis (OA) research as it permits the evaluation of abnormal changes in the joint associated with

disease, including subchondral bone marrow lesions (BMLs). BMLs are common in symptomatic knee OA and are considered to be an important imaging marker which has been associated with pain [11, 12] and progression of disease [13, 14, 35, 158]. Their appearance, however, is influenced by the MRI imaging technique/ sequence used. A number of MRI pulse sequences have been used to assess BMLs in clinical and research studies, including; i) fluid sensitive sequences (T2-weighted, proton density (PD)-weighted, intermediate-weighted sequences with fat suppression) [16, 88, 159, 160], and short-tau inversion recovery (STIR) sequences [16, 17, 81], ii) contrast-enhanced T1-weighted MRI sequences with fat suppression [17, 18, 81, 82, 86], and iii) gradient-echo (GE) sequences such as Dual-echo steady-state (DESS), fast low-angle shot (FLASH), or spoiled-gradient recalled acquisition in steady-state (SPGR) [80, 85]. There are, however, relatively few data comparing these sequences and those published have looked at BML volume assessed typically using a contrast enhanced (CE) vs. non-CE pulse sequence [17, 81, 82, 86]. Further, most studies looked at BML volume on a relatively small number of osteoarthritis patients or a heterogeneous patient population and used two or three different MRI pulse sequences only. Using data collected as part of a trial of brace therapy in patients with symptomatic patellofemoral OA, we assessed BML volume in the patellofemoral joint using four different pulse sequences including three different fluid sensitive MRI pulse sequences and a fat-suppressed gradient echo sequence. Our aims were: i) to determine the reliability of BML volume assessment for each of the sequences, ii) to compare the proportion of subjects identified with BML, and size of the BMLs, iii) to determine between sequence correlations in BML volume, and iv) to determine for each sequence the association between BML volume and knee pain.

5.2 Methods and materials

5.2.1 Subjects

This study was a secondary analysis of a completed randomised clinical trial of a patellar brace in participants with painful patellofemoral knee OA (Trial registration number: ISRCTN50380458) [18]. The clinical trial was carried out from August 2009 to September 2012. Participants were clinically assessed by an experienced physiotherapist for knee pain on some nominated aggravating activities, such as stair climbing, kneeling, prolonged sitting or squatting [18] and those with pain score of 4 or above on 0-10 cm visual analogue scale (VAS) were enrolled in this trial.

5.2.2 MRI pulse sequences parameters

MR images were obtained on a Philips 1.5 T Scanner (Philips, Best Netherlands) using an 8-channel knee coil (SENSE-Knee 8). Images of the patellofemoral joint were obtained in the axial plane using the following MRI sequences: (1) fat suppressed fast spin-echo (FSE) (TR/TE, 1500/15 ms; field of view (FOV), 14 cm; 256x256 pixels and 24 slices; slice thickness, 3 mm with 0.3 mm gap), referred as proton density fat-suppressed (PDFS) hereafter; (2) short tau inversion recovery (TR/TE, ~3700/14 ms; TI, 140 ms; FOV 14 cm; 320x320 pixels and 24 slices; slice thickness, 3 mm with 0.3 mm gap), referred to as STIR; (3) Fat suppressed post intravenous contrast agent (TR/TE, 500/17 ms; FOV 14 cm; 320x320 pixels and 24 slices; slice thickness, 3 mm with 0.3 mm gap) referred to as contrast enhanced T1-weighted sequence with fat suppression or CE T1-w FS; and (4) 3D T1-weighted gradient echo pulse sequence with fat suppression (TR/TE, 39/~5.2 ms; flip angle, 45°; FOV, 14 cm; 256x256 pixels and 53 sections; slice thickness, 3.0 mm; and overlap between adjacent slices, 1.5 mm) referred to as 3D gradient echo T1-weighted fast field echo sequence (T1-w FFE).

There were small parameter differences in 2 participants with some changes to the field of view (increased to 15 cm) and matrix size.

5.2.3 BML assessment

BML assessment was performed by a trained reader (HN) who was blinded to the pain score. Images acquired using different sequences in the same participant were not evaluated together. BMLs are defined as ill-defined high signal intensity areas adjacent to articular cartilage or cartilage loss on 2 or more contiguous slices. We used manual segmentation to calculate BMLs volume and focused on BMLs in the patella and trochlea of the femur (patellofemoral joint). The patella and the opposing region of the anterior femur (trochlea) were defined using regions derived from Boston-Leeds Osteoarthritis Knee Score (BLOKS), the inferior margin of the femur was the intersection between a line drawn parallel to the anterior aspect of the proximal tibia and the femoral surface [90] on sagittal 3D water-selective cartilage scans (WATSc).

Patellofemoral (PF) BMLs were delineated on each MRI slice in Osirix software, and total PF BMLs volume integrated over all slices. In the case of multifocal BMLs, the segmentation was performed for all BMLs and the total PF BML volume (in mm^3) was calculated by adding the volume of all PF BMLs in a knee. Figure 5.1 shows and example of the manual segmentation of multifocal BMLs. Cystic changes within BMLs were included in the BMLs volume measurements. However, simple cysts without associated oedema-like features, solitary cysts, ganglion cysts or high signal intensity within osteophytes were not included in the analysis.

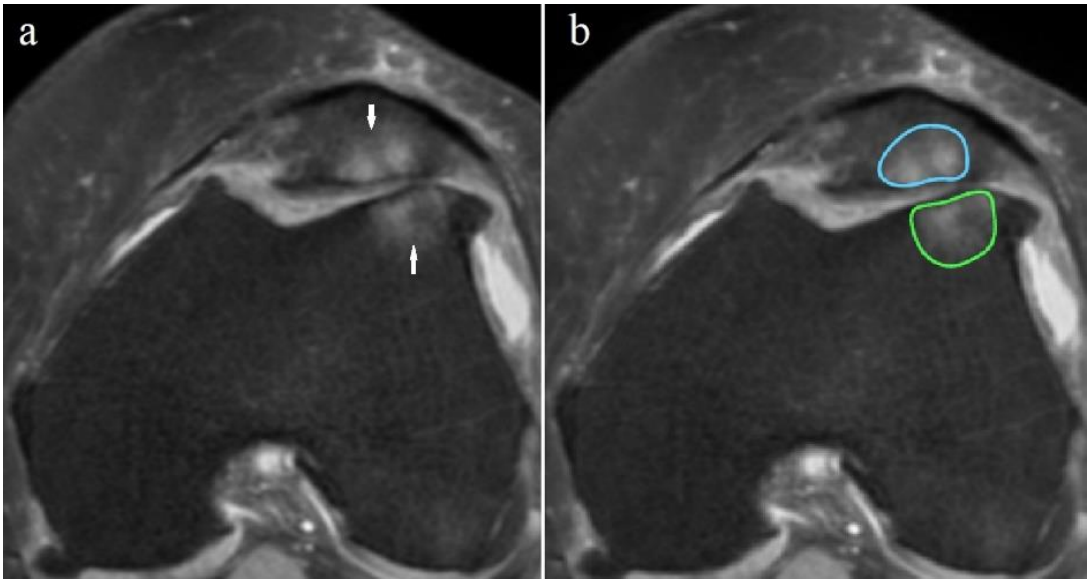

Figure 5.1. Manual segmentation of BMLs. Axial PDFS image (a) shows BMLs in the patella and trochlea (white arrows) with area of interests were drawn for volume measurement (b).

Intrareader reliability for manual segmentation of BML volume was investigated by the reader repeating assessment of 15 knees of four different MRI sequences with a minimum of 4 weeks between assessments. The reader was not aware which images were repeats.

5.2.4 Statistical analyses

The intraclass correlation coefficient (ICC [3,1 model]) [161] was used to determine intrareader reliability in BML volume for each sequence separately. ICC values range from 0 to 1, where <0.5 indicates poor reliability, 0.5 to <0.75 moderate, 0.75-0.9 good, and >0.9 excellent reliability [162]. The statistical analyses were limited to those 58 patients who had a BML on at least one of the sequences. PF BML volumes were assessed using each of the 4 different pulse sequences. We used a random-effects panel linear regression model to look for differences in BML volume assessed using these different sequences. Post-hoc pairwise comparisons were undertaken using Bonferroni-corrected 95% confidence intervals [163]. As the distribution of the BML volume was positively skewed, the BML volumes were first log-transformed, the

model run on these transformed volumes, and the subsequent regression coefficients back-transformed to give coefficients in terms of proportions and predicted back in mm^3. Bivariate analysis was performed using Chi-squared and Wilcoxon rank sum test to compare subject characteristics between those with BMLs on all sequences and with BMLs on some but not all sequences. The association in BML volume between pulse sequences was determined using Spearman's correlation coefficient (ρs) [164]. We used linear regression to evaluate the association between log BML volume on different MRI pulse sequences and VAS pain scores. A type-I error rate of 0.05 was used to assess statistical significance. All statistical analyses were performed using Stata 14.0 (StataCorp, TX, USA).

5.3 Results

5.3.1 Subjects

There were 76 subjects (36 male, 40 female) with four suitable MRI pulse sequences that fulfilled the inclusion criteria. Subjects ranged in age from 41-70 years (mean 55.8 years; SD 7.4) and BMI 30.4 (SD 5.0) kg/m^2. Mean visual analogue scale (0-10 cm) pain score at baseline was 6.2 (SD 2.2) cm.

5.3.2 Intrareader reliability of BML volume

Table 5.1 shows the intraclass correlations coefficient ($ICC_{3,1}$) for BML volume in 15 knees for the four sequences. The ICCs were excellent for PDFS, STIR and CE T1-w FS sequences (all 0.99), while the ICC for T1-w FFE was lower at 0.88.

MRI Pulse Sequences	ICC values (95% Confidence Interval)
PDFS	0.994 (0.981 to 0.998)
STIR	0.995 (0.981 to 0.999)
CE T1-w TSE	0.991 (0.973 to 0.997)
T1-w FFE	0.88 (0.582 to 0.962)

ICC, Intraclass correlation coefficient; PDFS, proton density fat-suppressed; STIR, short tau inversion recovery; CE T1-w FS, contrast enhanced T1-weighted fat-suppressed; T1-w FFE, T1-weighted fast-field echo.

Table 5.1. Intra-reader reliability for manual segmentation of BMLs (n= 15)

5.3.3 Detection of BMLs and comparison of BML volume between different MRI pulse sequences

Among the 76 subjects with complete data, 58 had PF BMLs present on at least one sequence. BMLs were present in all 58 patients when assessed using PDFS, STIR and CE T1-w FS sequences; the T1-w FFE sequence did not demonstrate BMLs in 4 patients.

Compared to the 54 patients where BMLs were present in all sequences, those in whom a BML was not seen on The T1-w FFE sequence were of similar median age (60.5 yrs vs 55.0 yrs), body mass index (28.9 Kg/m^2 vs 30.4 Kg/m^2), and pain score (5.9 vs 6.3). The volume of BMLs, assessed using the other three sequences, was smaller for these subjects. For example, using the PDFS sequence median BML volume was 206.9 mm^3 for 4 subjects without BML (on T1-w FFE) compared to a median BML volume of 1117.9 mm^3 for the other 54 subjects.

Examples of BMLs using the four MRI sequences are shown in figure 5.2.

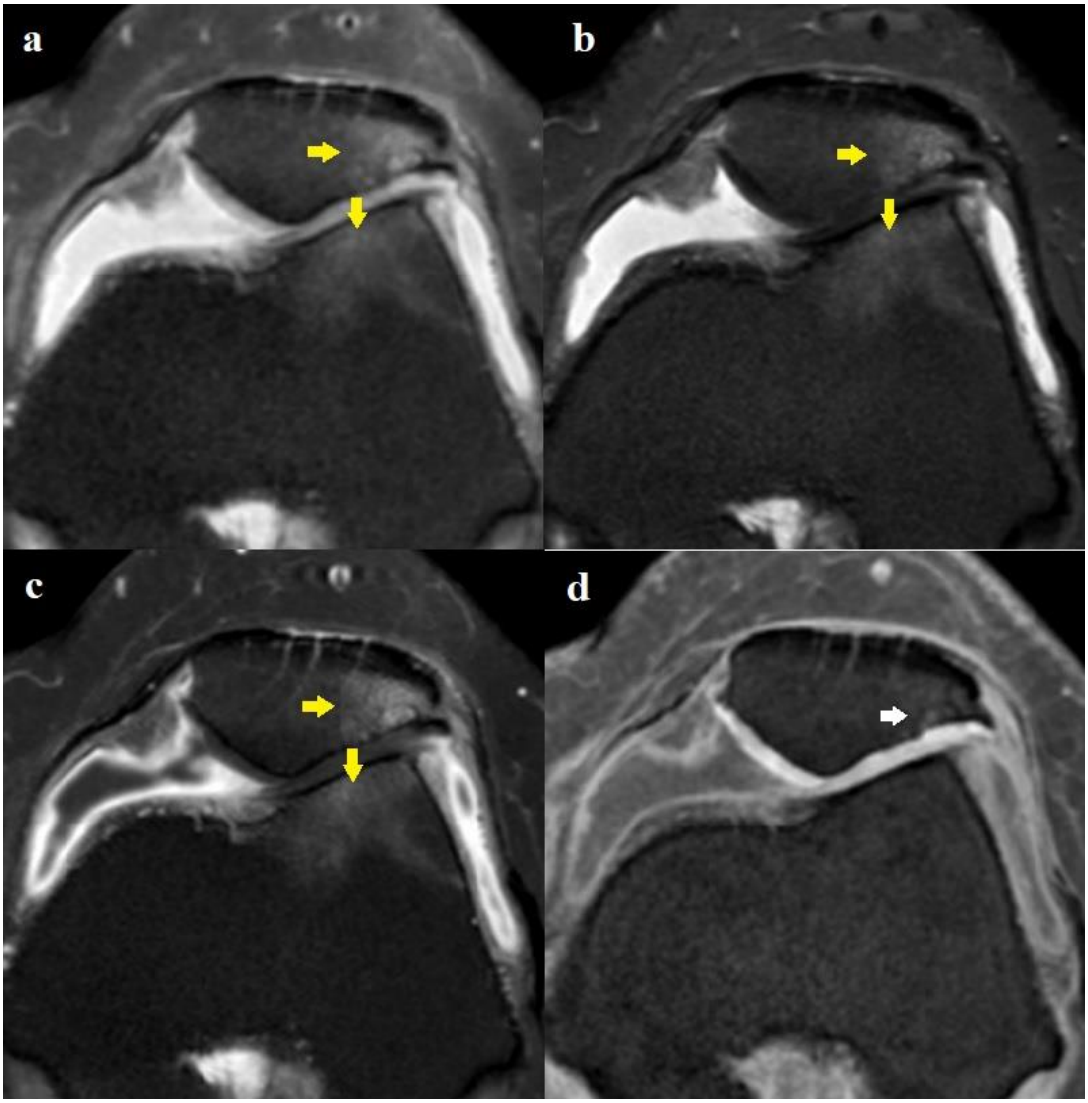

Figure 5.2. Axial PDFS sequence (a) shows BMLs in the patella and femoral trochlea of the knee (yellow arrows). A similar appearance was also visible on STIR (b) and CE T1-w FS (c). However, T1-w FFE sequence (d) of the same knee shows only BML in the patella (white arrow) with no BML clearly visible in the femur.

The median PF BML volume was greatest using the CE T1-w FS sequence, and smallest using the T1-w FFE sequence (table 5.2 and figure 5.3).

MRI Pulse Sequences	Number of patients	Median BML volume (IQR)
PDFS	58	960.30 (316.47; 2705.34)
STIR	58	1056.33 (369.60; 2645.61)
CE T1-w FS	58	1129.76 (467.28; 3166.02)
T1-w FFE	58	224.70 (82.50; 607.95)

PF, patellofemoral; IQR, interquartile range.

Table 5.2. Summary of PF BML volumes (mm^3) on different MRI pulse sequences

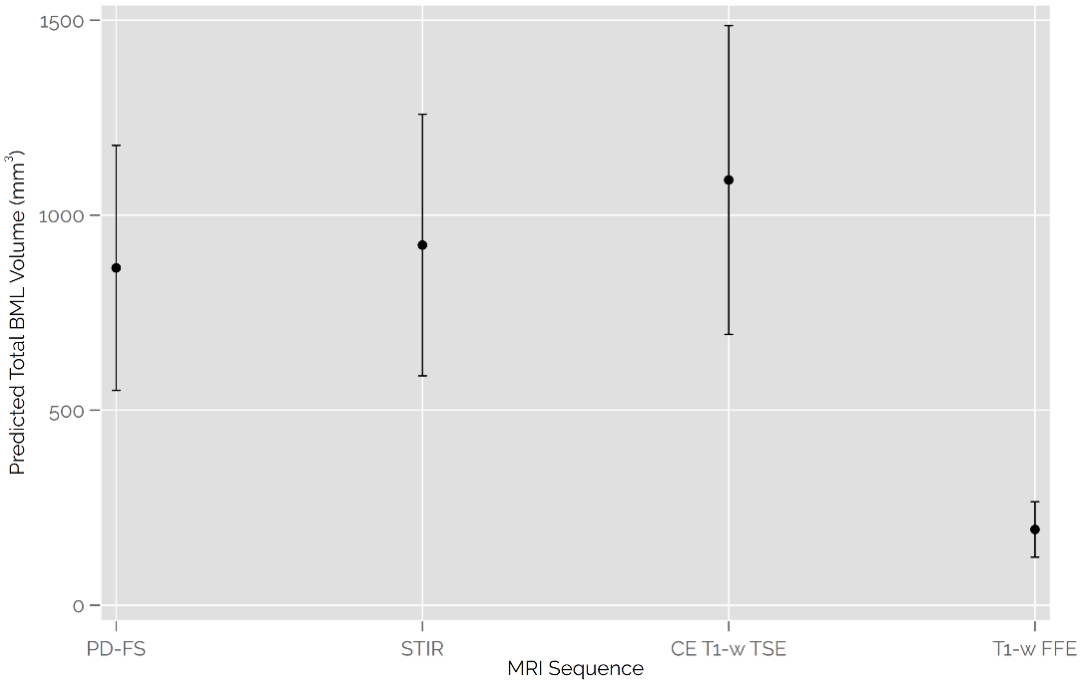

Figure 5.3. Comparison of BML volumes between MRI pulse sequences, taken from the panel linear regression model, after back-transformation onto the mm^3 scale.

Post-hoc pairwise comparisons following the random-effects panel linear regression established that BML volume was similar when assessed using the PDFS, STIR, or CE T1-w FS sequences (table 5.3). BML volumes assessed on T1-w FFE sequence were, on average, between 4 and 6 times lower those from any of the other three pulse sequences.

Comparison between pulse sequences	Proportional difference (Exponentiated coefficient)	Bonferroni-corrected (95% Confidence Interval)
PDFS vs STIR	0.94	(0.74; 1.19)
PDFS vs CE T1-w FS	0.79	(0.62; 1.01)
PDFS vs T1-w FFE	4.45	(3.48; 5.70)
STIR vs CE T1-w FS	0.85	(0.67; 1.08)
STIR vs T1-w FFE	4.75	(3.71; 6.09)
CE T1-w FS vs T1-w FFE	5.61	(4.38; 7.19)

Table 5.3. Comparison of BMLs volume between MRI pulse sequences

5.3.4 Correlation between different MRI pulse sequences

The Spearman's correlation coefficients (ρs) [164] of BML volume between sequences was very strong when assessed using PDFS, STIR, and CE T1-w FS (all ρs= 0.98). The correlation was strong between these sequences and T1-w FFE (ρs ranging from 0.80-0.81) (table 5.4).

Pulse Sequences	STIR	CE T1-w FS	T1-w FFE
PDFS	0.98*	0.98*	0.81*
STIR		0.98*	0.80*
CE T1-w FS			0.81*

*p value <0.05

Table 5.4. Association between BML volume assessed using different MRI sequence: Spearman's correlation coefficients (ρs)

5.3.5 Association between MRI pulse sequences and pain

In a linear regression featuring severity of knee pain (measured on a 10-cm VAS for a patient-nominated aggravating activity) as the outcome and the log-transformed baseline PF BML volume as a predictor for each of the 4 sequences, no association was found for any of the MRI pulse sequences (table 5.5). The amount of pain variance explained by PF BML volumes was low for all sequences.

MRI Sequences	Proportional change (Exponentiated coefficient) (95% CI)	R^2	ρ_S (95% CI)
PDFS	0.91 (0.62; 1.35)	0.004	-0.07 (-0.32; 0.20)
STIR	0.90 (0.59; 1.36)	0.005	-0.06 (-0.31; 0.21)
CE T1-w FS	0.95 (0.64; 1.43)	0.001	-0.03 (-0.29; 0.23)
T1-w FFE	1.30 (0.82; 2.06)	0.025	0.10 (-0.17; 0.35)

ρ_S = Spearman's Correlation Coefficient

Table 5.5. Association between baseline pain score and log-transformed PF BMLs volume assessed using different MRI sequences.

5.4 Discussion

In this study intrareader reliability for BML volume measurement was excellent when assessed using PDFS, STIR and CE T1-w FS ($ICC_{3,1}$= 0.991-0.995) and good for assessment using the T1w-FFE sequence ($ICC_{3,1}$= 0.88). Approximately three quarters of subjects (58 of 76) had evidence of PF BMLs that were present on PDFS, STIR and CE T1-w FS sequences. BMLs were not seen in four of these subjects when assessed using the T1-w FFE sequence. We found that BML volume was larger using the contrast enhanced sequence though was not statistically significantly different from BMLs assessed using the PDFS or STIR sequences after Bonferroni correction. On T1-w FFE images the BML volume was significantly smaller than the other three sequences. Significant correlations were observed between BMLs measured with all sequences. Correlations between PDFS, STIR and CE T1-w FS were very strong (ρs= 0.98); correlations between T1-w FFE and the other sequences were lower (ρs ~0.80).

Several studies have compared BML volume in subjects with knee OA assessed using different MRI sequences, although to our knowledge there are no studies which have looked at BML volume using both STIR and PDFS sequences. Most have compared contrast enhanced sequences with one or two other sequences [17, 81, 82, 86]. Roemer

et al [86] in a study of 32 patients with knee OA reported that BMLs assessed using PD-w FS were larger (38%) than when assessed using T1-w FS CE sequences, though as in our study there was a strong correlation between them. Nielsen et al [82] found BML volume measured from STIR images of the tibiofemoral compartments was slightly larger (~3%) compared to T1 post contrast sequences using manual segmentation. Other studies with relatively small proportions of OA patients have also shown small differences between STIR and contrast enhanced T1-w FS sequences [17, 81]. In our study BML volume was greater when assessed using CE T1-w FS compared to other sequences. There are a number of possible reasons for the apparent difference from previous studies. In our study TR values were shorter than the study by Roemer et al [86] on both PDFS (1500 ms vs 5080 ms) and CE T1-w FS (500 ms vs 720 ms) which could potentially result in BMLs appearing relatively smaller on PDFS and larger on CE T1-w FS images. Because the edge of BMLs is inherently poorly defined, delineation is subjective and other details of the imaging sequence may also be important in determining the precise BML volume. These details include timing of scan post contrast administration [165], relaxivity, and dose of contrast agent [17], efficacy of fat suppression, and signal to noise ratio [166]. This highlights the importance of using standardized protocols including both image sequence and imaging parameters when assessing BML volume in research settings. Given the greater potential for variability using CE sequences there may be advantages to using PDFS and STIR sequences for routine assessment.

In our study we found that T1w-FFE sequences detected BMLs in a smaller number of people (54 vs 58) and that the full extent of BMLs shown on other sequences was not captured by the T1-w FFE sequences. Furthermore, the correlation between BML volume measured on T1-w FFE and other sequences was lower (~0.80) and the intra-

reader reliability was also lower. There is little literature on the value of these sequence for assessing BMLs in OA. DESS sequences, however, have been studied and have also shown much lower volumes than intermediate-weighted fat suppressed images (median BML volume: DESS= 191 mm^3; IW FS= 1840 mm^3), though there was a good correlation between both sequences with a Spearman's correlation coefficient of 0.83 [84]. While both DESS and T1-w FFE sequences have been used to segment articular cartilage volumes, neither appears suitable for segmenting the full extent of BMLs visualized on other sequences. However, it is possible that as with DESS, T1-w FFE sequences may be valuable for discriminating cystic components [15, 80].

Among our subjects we found no significant association between BMLs volume, and a patient nominated VAS pain score. Further, there was no significant difference in pain scores between those with BMLs compared to the smaller number of people (n= 18) without BMLs (data not shown). The small sample size means we cannot exclude type 2 error. Also, all of those who took part in the original clinical trial had significant knee pain (≥ 4 cm VAS) at baseline.

There are some limitations to consider in interpreting the results of the study. The sample size was relatively small, yet we were able to show differences in BML volume across the different sequences assessed and the number of subjects studied was larger than in many previous studies [17, 81, 82, 86]. Because of the standardised imaging protocol, we did not look at the influence of contrast dose or timing on BML volume and other imaging sequence parameters which may potentially have an impact on outcome and for which further studies are needed. Our study was cross-sectional, and we did not look at sensitivity to change or correlation with treatment response factors which may be important in determining an optimum imaging sequence.

Finally, our data relate to BMLs assessed at the patellofemoral compartment and caution is required before generalizing the findings to other sites.

In conclusion, we found that T1-w FFE sequences were less reliable and measured considerably smaller BML volume compared to other sequences. BML volume was larger when assessed using the contrast enhanced T1-w FS sequence though not statistically significantly different from BMLs when assessed using PDFS and STIR sequences.

5.5 Conflict of Interest:

The authors have no conflicts of interest.

5.6 Acknowledgements:

Henry Noorveriandi is supported by a grant from the Indonesian Government (Indonesia Endowment Fund for Education). The authors acknowledge the support of the NIHR Manchester Biomedical Research Centre at the University of Manchester for funding support. The views expressed are those of the author(s) and not necessarily those of the NHS, the NIHR or the Department of Health. The research was supported also by Versus Arthritis (Grant number= 21755).

Chapter 6

Study 2

Chapter 6

Comparison between proton density fat-suppressed and water-fat separation mDixon Quant MR images for volumetric assessment of subchondral bone marrow oedema-like lesions in the knee

Abstract

Purpose:

To compare BML volume assessed on proton density fat-suppressed images and water-fat separation mDixon Quant images in knee joints of patients with osteoarthritis and to assess the correlation between BML volume assessed using these sequences and knee pain.

Material and Methods:

Men and women with symptomatic knee OA (mean age 65.4 ± 8.3 years) had MRI scans with 2D proton density weighted fat-suppressed (PDFS) and 3D gradient echo six-point mDixon Quant images of the knee. Images from 30 patients with evidence of a BML on PDFS were included in the analysis. BMLs were manually segmented on both sequences. BML volumes assessed using the two sequences were compared using the Wilcoxon signed-rank test and the correlation between them was assessed using Spearman's correlation coefficient (ρs). The association between BML volume (both sequences) and knee pain assessed using a numerical rating score (0 – 10), was determined using linear regression.

Results:

BML volume was larger when assessed using PDFS compared to the mDixon Quant sequence, however, the difference in absolute terms was relatively small (6498.7 vs

6084.9 mm^3, $p<0.05$). There was a significant correlation between BML volume assessed using the two sequences ($\rho s=0.995$, $p< 0.05$). There was no significant association between BML volume assessed on either of the sequences and knee pain.

Conclusion:

BML volume measurements using PDFS and water-only mDixon Quant image were broadly similar and strongly correlated. This suggests mDixon Quant could be used for measuring BMLs with the potential advantages of thin-slice 3D images, robust fat suppression and fat fraction.

Keyword**:**

Magnetic resonance imaging, knee osteoarthritis, bone marrow oedema-like lesions, Proton-density fat-suppressed, mDixon Quant imaging.

6.1 Introduction

Dixon imaging is rapidly gaining acceptance in routine clinical scanning. It can provide better fat suppression than conventional techniques [167-170] and has the potential to replace multiple sequences [171-173], for example for assessing the sacroiliac joints in spondyloarthropathy [174]. In addition, Dixon imaging allows for quantitative assessment using in-phase/ out-of-phase imaging or by calculating fat fraction and sometimes T2* [169, 171, 175]. For clinical musculoskeletal applications, fast spin-echo Dixon images are often preferred [169] as they provide similar contrast to conventional fast spin echo images. However, gradient echo Dixon images offer a number of potential advantages including fast 3D imaging, accurate fat quantification and T2* calculation and correction. 3D gradient echo Dixon imaging has been tested in multiple studies in the liver [116] as well as other tissues including the sacroiliac joints in spondyloarthropathy [108].

Bone marrow oedema-like lesion (BML) volumes in osteoarthritis (OA) studies are commonly assessed on fluid sensitive MRI sequences such as fat-suppressed T2-weighted, fat suppressed proton density weighted (PDFS), fat suppressed intermediate weighted (IW) or short tau inversion recovery (STIR) [88]. 3D imaging is attractive for assessing bone changes in osteoarthritis as isotropic images could reduce partial volume and registration errors for BMLs and are well suited to the assessment of certain other features such as osteophytes and bone shape [176]. Furthermore, fat fraction and T2* from 3D gradient echo Dixon images may be useful for characterising BML composition and trabecular structure [108]. However, gradient echo imaging sequences including DESS, GRASS and FLASH have often been considered unsuitable for measuring BML volume due to susceptibility effects in trabecular bone reducing T2* [77] and BMLs have been shown to appear smaller on 3D-DESS and T1-w FS 3D gradient echo sequences compared to standard IWFS images in several studies [80, 83-85, 140]. However, recommendations are mixed with one large community study finding T1W FS gradient echo images and T2-w FS images to be similar [177], one concluding DESS [83] was suitable and another suggesting a combination of fluid sensitive and GRASS sequences may be best [85]. Gradient echo sequences have also been used in several dynamic contrast-enhanced (DCE)-MRI studies of bone marrow lesions [178-181].

3D gradient echo (GE) quantitative Dixon imaging has different MR characteristics to many other gradient echo sequences and has been successfully used in the liver, even when T2* is shortened due to iron overload [182]. However, there are few published studies looking at whether such sequences are suitable for assessing BML volume in the knee.

The aim of this study was to compare BML volume assessed on proton density fat-suppressed MRI images and water-fat separation mDixon Quant images in the knee joints of patients with osteoarthritis and to assess the correlation between BML volume assessed using these sequences and knee pain.

6.2 Materials and methods

6.2.1 Patients and imaging

MRI Images from 30 subjects who had participated in a in a clinical trial of denosumab therapy were used in the analysis (ISRCTN Number: 96920058). The study was approved by the institutional review board and written informed consent was obtained from each patient. Inclusion criteria for the trial included knee pain (at least a score of 3 or more on a numeric rating scale (0-10)), plain radiographic evidence of osteoarthritis, and evidence of a BML on PDFS MRI. Participants were excluded if they had either very mild or severe radiographic OA (Kellgren Lawrence score of 1 or 4).

6.2.2 MRI pulse sequences parameters

MR images were acquired on a 3 T MRI system (Achieva, Philip Medical Systems, Best, Netherlands) using a 16-channel knee coil (SENSE-knee 16). Images of the knee joint were obtained in the sagittal plane using the following MRI sequences: (i) 2D proton density SPAIR sequence (PDFS) with: TR/ TE= 4200/ 40 ms; Field of view (FOV)= 160 x 288.5 mm; acquisition matrix= 292 x 504 pixels; bandwidth= 434.3 Hz/pixel; echo train length= 12; number of slices= 36 slices; slice thickness= 3 mm; and slice gap= 0.3 mm, and. (ii) A six-echo 3D gradient-echo mDixon Quant sequence with equidistant echo spacing: TR= 15 ms; TE1 set to shortest (~1.4 ms); echo spacing

set to shortest (~1.1 ms); flip angle= 3°; Slice thickness= 1 mm; slice gap= 0 mm; acquisition matrix size= 376 x 156 with 160 slices; bandwidth= 1293 Hz/pixel. Water-only images reconstructed automatically by the scanner were used for analysis.

6.2.3 Image analysis

MR images were anonymised and assessed by a radiologist with experience of BML segmentation [140] using Osirix software (see figure 6.1). The order of MR images in every patient was randomly assigned with at least one week gap between the readings of the two sequences in the same patient. Subchondral BMLs were defined as ill-defined high signal intensity in the subchondral bone in the lateral and medial femoral condyle, medial and lateral tibial plateau, and patella. Cystic changes within BMLs were included in the volume measurements. BMLs in the subspinous region or osteophytes were excluded from the assessment. BMLs present on at least two consecutive slices were manually segmented slice-by-slice on each sequence. BML volumes were integrated over all slices and the total volume calculated in mm^3.

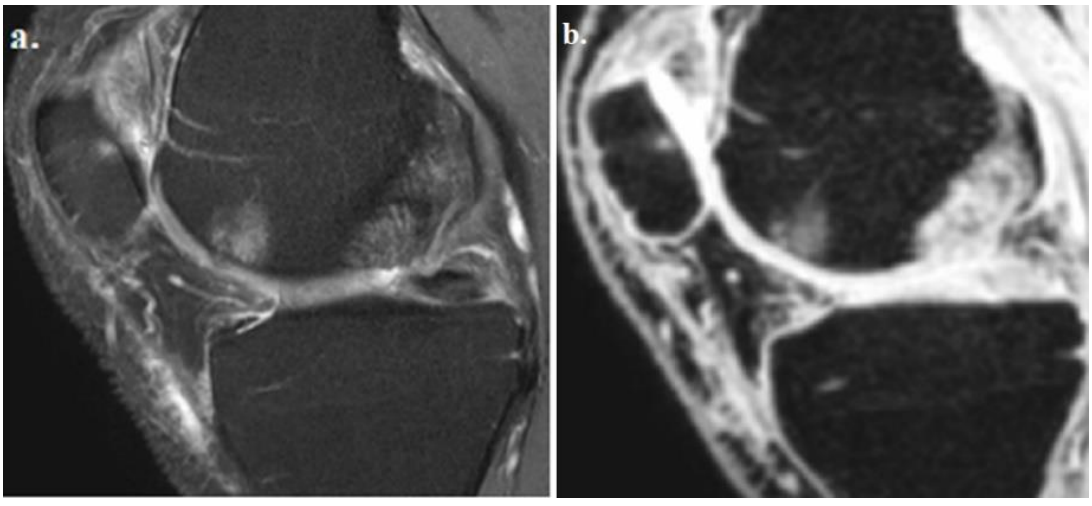

Figure 6.1. Sagittal PDFS sequence (a) shows BMLs in the anterior region of the distal femur and patella (white arrows). (b) shows a similar slice from a water-only mDixon Quant image.

6.2.4 Statistical Analysis

Descriptive statistics were used to characterise the distribution of BML volumes assessed using the two MRI sequences (2D PDFS and 3D mDixon Quant). Differences in the volumes were compared using the Wilcoxon signed-rank test. The association between BML volumes assessed on the two sequences was assessed using the Spearman correlation coefficient (ρ). The correlation coefficients were interpreted as follows: less than 0.3 = poor, 0.3 to 05 = fair, 0.6 to 0.8 = moderately strong, and at least 0.8 = very strong [183]. The association between BML volumes (both sequences) and knee pain was assessed using linear regression. Statistical Analyses were performed using Stata 14.0 (StataCorp, TX, USA).

6.3 Results

6.3.1 Subjects

The mean age of the 30 subjects included in the analysis was 65.4 ± 8.3 years (range 40-81), and the majority (17) were men. Mean body mass index was 29.2 ± 4.3 kg/m^2. Mean numerical rating scale (0-10) pain score at baseline was 6.2 (SD 1.7).

6.3.2 BML Volume assessed using PDFS and mDixon Quant Sequences

Mean BML volume assessed on the PDFS images was 6498.7 mm^3 (SD= 6050.4) (median= 5387.0 mm^3; IQR= 2375.7-8855.9), while for the mDixon Quant sequence the mean BML volume assessed was 6084.9 mm^3 (SD= 5559.5) (median= 4869.4 mm^3; IQR= 2298.4-8462.1). The mean difference in volume was relatively small 413.9 mm^3 (SD= 885.6) Using the Wilcoxon signed-rank test, the difference between the volumes assessed using the two sequences was, however, significant ($p< 0.01$).

There was a strong correlation between BML volumes assessed using the two sequences (ρs= 0.995; p< 0.01), see Figure 6.2.

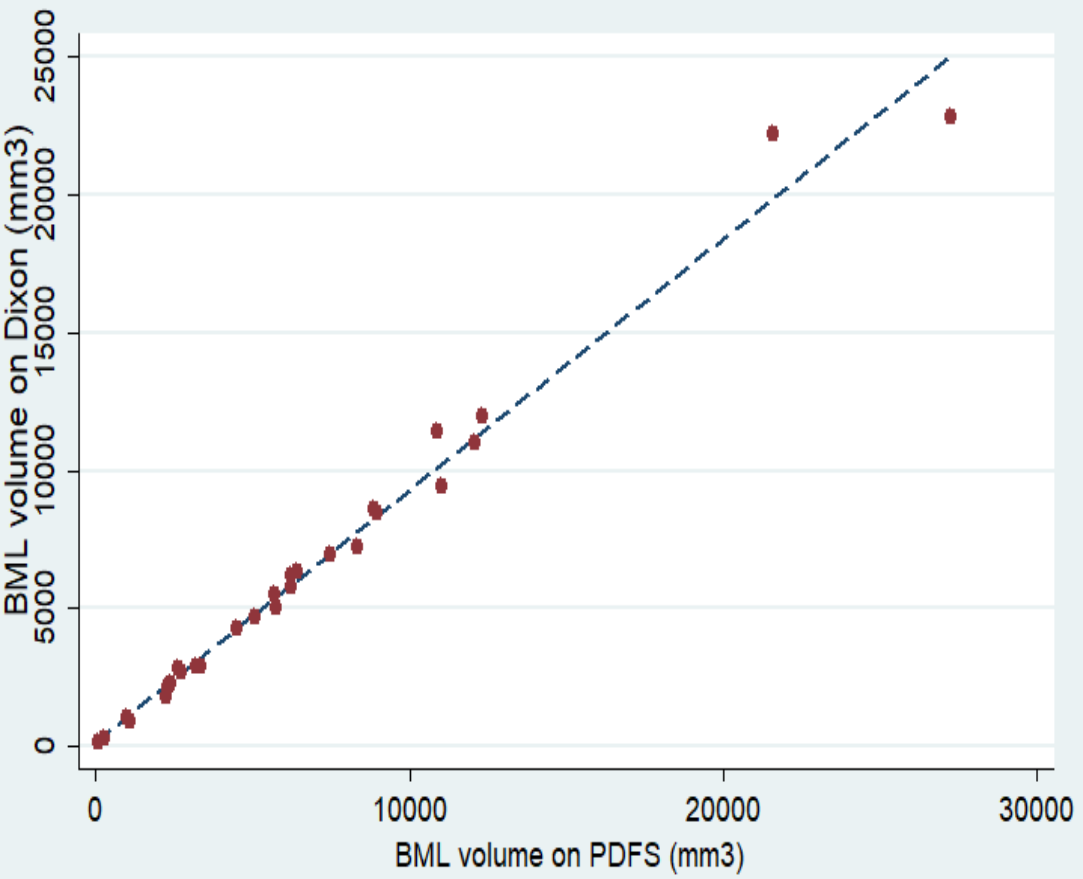

Figure 6.2. Scatterplot of BML volumes measured on PDFS vs mDixon Quant MRI sequences. Linear correlation between BML volume determined by PDFS and mDixon Quant sequences (dashed line; ρs= 0.995, p< 0.01).

6.3.3 Association between BML volume and knee pain

There was no significant association between knee pain severity (measured on a 0 to10 numerical rating scale) and BML volume for either MRI pulse sequences (p> 0.05). (p> 0.05).

6.4 Discussion

In this analysis, BML volume was assessed using two MRI images, conventional PDFS and 3D GE water-only mDixon Quant images. BML volumes assessed on these

images were strongly correlated. Mean BML volume was lower when assessed on the mDixon Quant images, however the magnitude of the difference was relatively small (mean difference just over 400 mm^3) suggesting the mDixon Quant sequence may be a feasible alternative for measuring BML volume.

Some gradient echo imaging sequences including DESS, and FLASH have been considered unsuitable for measuring bone marrow lesion volume due to susceptibility effects in trabecular bone and reduced T2* [77], supported by studies showing substantially smaller bone marrow lesions on DESS and T1-w 3D gradient echo sequences compared to standard fluid sensitive sequences. In contrast, in the analysis outlined in this chapter, BML volumes assessed using the 3D GE mDixon Quant sequence were broadly similar in absolute terms compared to those measured from 2D FSE PDFS images.

Some of the features of the mDixon Quant sequence designed to allow robust fat fraction quantification may also facilitate sensitive BML detection. Susceptibility effects are reduced with a high bandwidth, short first echo time and multiple closely spaced echoes with the potential for T2* correction. The strong, uniform, reliable fat suppression incorporates multiple fat spectrum peaks, unlike alternative methods of fat suppression [184]; this may be particularly important for gradient echo images due to echo time dependent dephasing [117]. Partial volume effects at BML edges are minimised by thin slices. T1 effects are reduced by using a small flip angle (see chapter 8). 3D low flip angle gradient echoes minimise magnetisation transfer effects [185].

The broad agreement between PDFS and mDixon Quant imaging in this study is consistent with previous work concluding 3D GE Dixon was a suitable alternative for

assessing bone marrow oedema in the hands of patients with rheumatoid arthritis after intravenous gadolinium-based contrast agent [186]. In addition to appearing useful for BML volume measurement, the image contrast, multiple images (fat, water, in-phase, out-of-phase) and isotropic resolution of the Dixon sequence may make it suitable for assessing other aspects of the bone such as the bone shape [176]. The T2* map may be useful for differentiating oedema from cysts [80, 83], while the fat fraction map offers the potential to better characterise the bone marrow lesions [Chapter 7]. However, other tissues are poorly assessed on the 3D gradient echo Dixon images due to the lack of T1 or T2 contrast which limits differentiation of fluid from articular cartilage and assessment of meniscal damage.

No association was observed in the analysis between BML volume and knee pain severity for either sequence. Previous studies have differed in whether such a relationship was observed [11, 46, 187, 188]. The restriction to subjects with moderate OA (Kellgren Lawrence grade 2-3) and the exclusion of those with none or mild pain may have reduced the chance of finding a significant association.

Although fluid sensitive sequences such as the PDFS sequence used in the study are widely used and recommended for BML assessment [75, 77], there has been limited histological correlation [53, 54] and the sequence or combination of sequences for ideally characterising BMLs remains unclear [85, 87]; while this study suggests mDixon Quant imaging is similar in sensitivity to the most sensitive sequences, further work will be necessary to determine whether quantitative fat fraction maps which are also available from mDixon Quant imaging can further stratify BMLs in a similar way to T1-w images [85, 87].

There are a number of limitations which need to be considered when interpreting the findings. The study was cross-sectional and did not look at longitudinal change. Cystic and non-cystic bone marrow lesions were not differentiated, and the potential of the T2* map for discrimination between them was not investigated. There are many differences between the mDixon Quant and PDFS sequences used (2D vs 3D, SPAIR vs mDixon Quant, slice thickness, in-plane resolution, spin-echo vs gradient echo, 2D vs 3D geometry correction, bandwidth etc.) so the effects of individual differences are hard to assess. The differences of slice thickness between 2D and 3D images may introduce bias to the volumetric measurements due to partial volume effect. The small different volumes of BML obtained may partly be due to this. However, the mean BML volume obtained by both sequences was significantly correlated.

In conclusion, BML volume measurements using PDFS and water-only mDixon Quant images were broadly similar and strongly correlated. This suggests mDixon Quant could be used for measuring bone marrow lesions with the potential advantages of thin-slice 3D images, robust fat suppression and fat fraction quantification.

6.5 Acknowledgments

This work was sponsored by NIHR and Versus Arthritis. Henry Noorveriandi was funded by Indonesia Endowment Fund for Education (Ministry of Finance of the Republic of Indonesia).

Chapter 7

Study 3

This chapter is based on the paper:

Noorveriandi, H., Cootes T. F., Parkes, M.J., Felson, D.T., O'Neill, T.W. and Hodgson, R. Quantification of fat fraction in subchondral bone marrow in knee osteoarthritis using Dixon MRI and image registration (Under revision for Osteoarthritis Imaging)

Chapter 7

Quantification of fat fraction in subchondral bone marrow in knee osteoarthritis using mDixon Quant MRI and image registration

Henry Noorveriandi, MD, MSc[1], Timothy F Cootes, PhD[2], Matthew J Parkes, PhD[3], David T Felson, MD, MPH[4, 5], Terence W O'Neill, MD[5, 6, 7], Richard Hodgson, PhD[2]

[1]Division of Musculoskeletal & Dermatological Sciences, School of Biological Sciences, Faculty of Biology, Medicine & Health, the University of Manchester, UK
[2]Division of Informatics, Imaging & Data Sciences, School of Health Sciences, Faculty of Biology, Medicine & Health, the University of Manchester
[3]Division of Population Health, Health Services Research & Primary Care, School of Biological Sciences, Faculty of Biology, Medicine and Health, the University of Manchester, Manchester, UK
[4]Boston University School of Medicine, Boston, Massachusetts, USA
[5] Centre for Epidemiology Versus Arthritis, Faculty of Biology, Medicine and Health, Manchester Academic Health Science Centre, The University of Manchester, Manchester, UK
[6]NIHR Manchester Biomedical Research Centre, Manchester Academic Health Sciences Centre, Manchester University NHS Foundation Trust, Manchester, Manchester, UK
[7]Department of Rheumatology, Salford Royal NHS Foundation Trust, Manchester, UK

Correspondence to Henry Noorveriandi, School of Biological Sciences, The University of Manchester, Stopford Building, Room G.538A, Oxford Road, M13 9PL, Manchester, UK; henry.noorveriandi@postgrad.manchester.ac.uk.

Abstract

Objectives:

To evaluate fat fraction of subchondral bone marrow oedema-like lesions (BMLs) and nearby normal-appearing marrow in knee osteoarthritis (OA) using mDixon Quant MR imaging and to compare conventional volume measurements of BML change with an alternative technique using mDixon Quant MRI and image registration.

Methods:

We analysed 3T MR images from 17 symptomatic knee OA subjects (mean age: 61.3 years). BML volume was measured by manually segmenting sagittal fat-suppressed proton density (PD) weighted images at two visits. In addition, regions of interest

(ROIs) from BMLs and nearby normal-appearing marrow were manually segmented on mDixon Quant water images at either the initial or follow-up visit; image registration of the mDixon Quant images at different time points was performed to allow calculation of median fat fraction from corresponding ROIs at both visits. The fat fraction of BMLs was compared with normal-appearing marrow using the Wilcoxon signed rank test and Spearman's correlation coefficient (ρs) was used to assess the association between change in BML volume and change in fat fraction.

Results:

Fat fraction within BMLs was significantly lower than that of normal-appearing marrow (72.5% vs 92.1%, p= 0.003). The change in volume of BMLs over time was negatively correlated with change in fat fraction (ρs= -0.58; p= 0.016).

Conclusions:

Estimation of BML fat fraction in patients with knee OA using mDixon Quant imaging combined with image registration provides a potential alternative approach to volumetric BML assessment.

Keywords:

Osteoarthritis; Subchondral bone marrow; Magnetic resonance imaging; Dixon imaging; Fat fraction

7.1 Introduction

Bone marrow oedema-like lesions (BMLs) are common in those with symptomatic knee osteoarthritis (OA). They are typically identified as ill-defined areas of high signal intensity in the subchondral bone on fat-suppressed T2 weighted or proton density (PD) weighted MRI sequences [88, 158]. The precise appearance of a BML depends on the MRI sequence used [17, 81, 86].

BMLs are typically assessed on the basis of their size using semi-quantitative or quantitative approaches [88-91]. Quantitative volume measurement is more time

consuming, but is considered to be more accurate and reproducible [94, 189, 190]. There are, however, challenges in the quantitative assessment of BML volume because of their ill-defined boundaries and because their size and appearance vary depending on which MRI sequence is used [15, 75]. BML volume measurements are potentially subjective and time consuming, which is of particular importance if the aim is to look at change in BMLs over time. Further, conventional imaging techniques may vary across images and from scan to scan, for example due to inhomogeneous fat suppression, limiting direct comparison of signal intensity from one scan to the next.

Fat fraction estimates from quantitative Dixon water-fat separation MR imaging have been shown to be useful for discriminating between healthy and diseased bone marrow, as well as for monitoring disease progression, though not to our knowledge in knee osteoarthritis [116]. In hip osteoarthritis fat fractions using Dixon MRI were reported to be slightly lower in BMLs [191]. Results from Dixon imaging have shown excellent agreement with single-voxel magnetic resonance spectroscopy (MRS) (e.g. $r^2 \geq 0.95$ in liver) [118, 121]. Fat fraction measurements from Dixon imaging provide a potential alternative approach for BML assessment in clinical research studies of osteoarthritis and have the potential to improve comparison between time points. Dixon imaging has been used in hip osteoarthritis to look at large, fixed regions of subchondral bone; while this avoids manual segmentation of bone marrow lesions it may lack sensitivity to BMLs [191]. An alternative approach, in this study, is to segment BMLs at a single time point and use image registration to compare the same region of interest at multiple time points; this has the potential advantage of improving sensitivity by focussing on bone marrow lesions while reducing variability between time points due to differences in manual segmentations.

The aim of this study was firstly to apply 3D gradient echo mDixon Quant imaging to compare fat fraction in BMLs and nearby normal-appearing bone marrow in patients with knee OA. The second aim was to assess the association between BML volume measured using conventional methods compared to changes in fat fraction measured using mDixon Quant imaging with the single time point segmentation with registration technique.

7.2 Methods

7.2.1 Subjects

The subjects who contributed data to this study participated in a randomised controlled trial of lateral wedge insole in participants with painful knee OA (ISRCTN55059760) [157]. Participants had clinical and radiographic evidence of medial tibiofemoral osteoarthritis. This study was approved by National Research Ethics Service Committee North West (Preston, UK). We looked at a subset of 17 subjects (15 male, 2 female, mean age 61.3 ± 8.3 years) who had taken part in the study, had evidence of BMLs and had the appropriate MRI sequences.

7.2.2 MR imaging protocol

Subjects were imaged using a 3.0 T Philips MR scanner. Participants with mDixon Quant MR imaging on two visits separated by seven to nine weeks (mean 8.1±0.6 weeks) were included in the study. The Dixon sequence was obtained using a six-echo 3D gradient echo sequence (mDixon-Quant) with equidistant echo spacing using one of two sequences (TR 15 ms; six echoes, TE_1 set to shortest (~1.4ms); echo spacing set to shortest (~1.1 ms); flip angle 3°; slice thickness 1mm; acquisition matrix either 376x307 with 201 slices or 376x160 with 160 slices; voxel size 1x1x1 mm; bandwidth 1293 Hz/pixel). The mDixon Quant image was used to quantify fat fraction. Subjects

also had 2D fast spin-echo SPAIR images (TR 2900; TE 30 ms; acquisition matrix, 292x448; number of slices 36; slice thickness 3 mm; interslice gap 0.3 mm; echo train length 14; pixel size 0.55 x 0.71 mm; bandwidth 476 Hz/pixel) and STIR images (TR 4300; TE 50 ms; TI 200 ms; acquisition matrix 212x220; number of slices 30; slice thickness 3 mm; interslice gap 0.3 mm; echo train length 10, pixel size 0.75 x 1.1 mm; bandwidth 621 Hz/pixel). The SPAIR sagittal sequence was used to assess BML volume. The mDixon Quant water-only images were used to define BMLs to assess fat fraction with reference to the STIR images.

7.2.3 Post-processing of MR images

7.2.3.1 BMLs volume assessment

Subchondral BML volume was evaluated on conventional sagittal SPAIR images. Subchondral BMLs were defined as ill-defined areas of high signal intensity directly adjacent to articular cartilage or cartilage loss and present on at least two slices. We excluded any cystic component within BMLs, BMLs in the subspinous region or osteophytes, as well as ligament based BMLs. A radiologist experienced in BML segmentation segmented all subchondral BMLs present in the knee joint on a slice-by-slice basis on both visits using in-house segmentation software which allowed interactive windowing. The reader was blinded to the order of the images and clinical data.

7.2.3.2 Fat fraction assessment

mDixon Quant images were automatically reconstructed into water-only and fat fraction images by the MRI scanner. Water-only and fat fraction images were exported as DICOM files and were analysed on a separate workstation using in-house software.

ROIs of normal-appearing marrow and all subchondral BMLs were manually segmented on sagittal mDixon Quant water-only images at either the initial or the follow up image (randomly chosen), slice by slice. Sagittal STIR images were used together with the mDixon Quant water-only images to identify BML extent. ROIs of normal-appearing marrow were also manually outlined (minimum size of 2 cm^2) in the subchondral bone region in the same bone that contained the BML (the same region with the largest BML if there was more than one BML in the knee) on five consecutive sagittal slices (figure 7.1), or in the marrow of the opposing bone if the BML was too extensive.

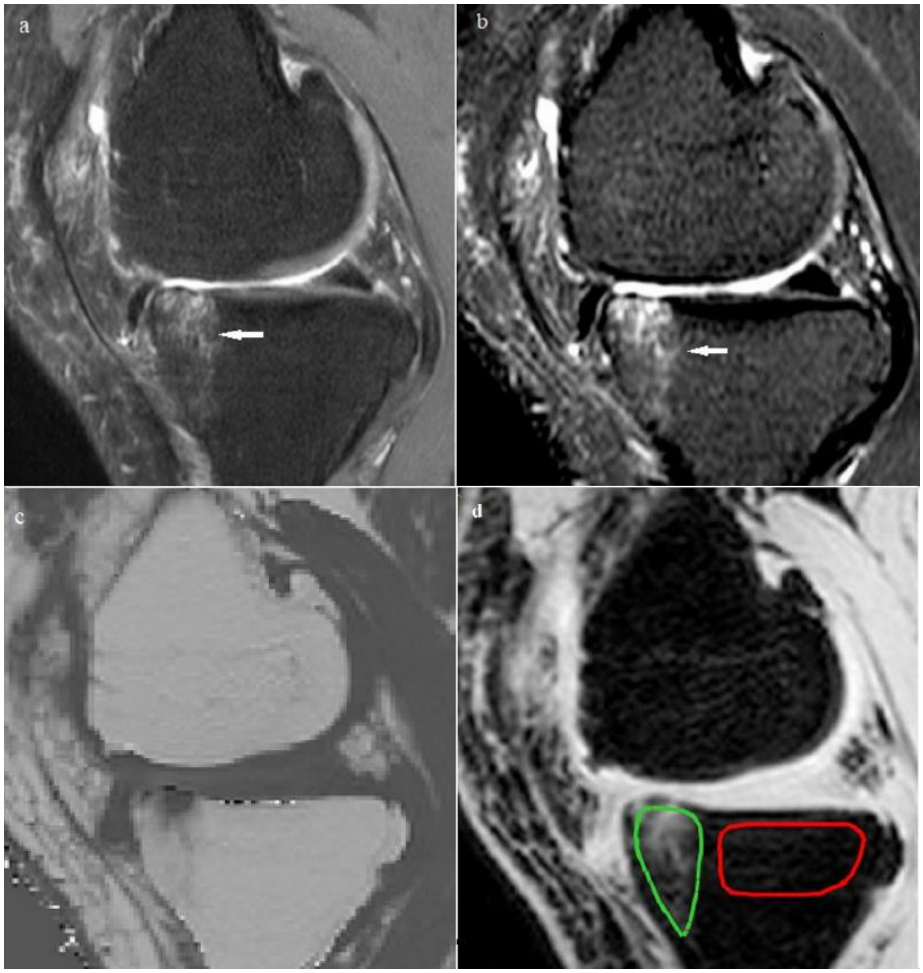

Figure 7.1. Sagittal fast spin echo SPAIR image (a) and STIR image (b) show subchondral BML (white arrows) in the anterior medial region of the proximal tibia. Sagittal mDixon Quant fat fraction image (c) shows the reduced fat fraction in the BML. (d) shows BML (green line) and normal marrow (red line) on mDixon Quant water-only image.

Images of the same patient at different time points were registered using a rigid body transformation. In house software enabled the reader to select a volume for registration in one image. The software performed a coarse to fine search to locate the equivalent region in the other image, optimising a measure based on normalised cross correlation of intensity features within the regions on the two images. Results were visually checked by the reader. This allowed the fat fraction corresponding to where BML was located in the segmented image to be assessed in equivalent regions of the bone at both time points. Fat fraction values were obtained from the image stored values (fat fraction= (SV x RS) + RI; where SV=stored value; RS = rescale slope, DICOM header element 2005, 140A; RI = rescale intercept, header element 2005, 1409, (Philips)).

7.2.4 Statistics

Descriptive statistics were used to characterise the BML volume on the initial and follow-up images. In each patient the median fat fraction was calculated of the voxels in the segmented regions (ROIs) of BMLs, and also for the ROIs of normal marrow. The fat fraction across all patients was expressed as the mean ± standard deviation and the range across all patients was also reported. Because the data were not normally distributed, differences between fat fraction of normal appearing marrow and BMLs were compared using a nonparametric test (Wilcoxon signed rank test). The median fat fraction of the ROI corresponding to the BML was also calculated using the registered image at the other time point. The relationship between change in BML volume and change in fat fraction over time was assessed using the Spearman's correlation coefficient (ρs). The change in BML volume and fat fraction over time was calculated as change= follow up – initial visit. A p value of less than 0.05 was

considered significant. Data were analysed using Stata 14 (Stata Corporation, College Station, Texas, USA**).**

7.3 Results

7.3.1 Volumetric BMLs assessment

The mean (± SD) total BML volume at initial visit was 9033 mm^3 (± 6780) (range 852 to 26633 mm^3). The mean follow-up total BML volume was 8895 mm^3 (± 5386) (range 678 to 23993 mm^3).

7.3.2 Fat fraction in normal appearing marrow and BMLs

The mean (± SD) of the fat fraction values within the manually segmented (non-registered) BML ROI across all patients was 72.5% (± 8.6) (range 52.8 to 88.5%). BML fat fraction was significantly lower than that in nearby segmented normal-appearing marrow (92.1 ± 2.5%, range 87.3 to 95.5%; p= 0.003), see figure 7.2.

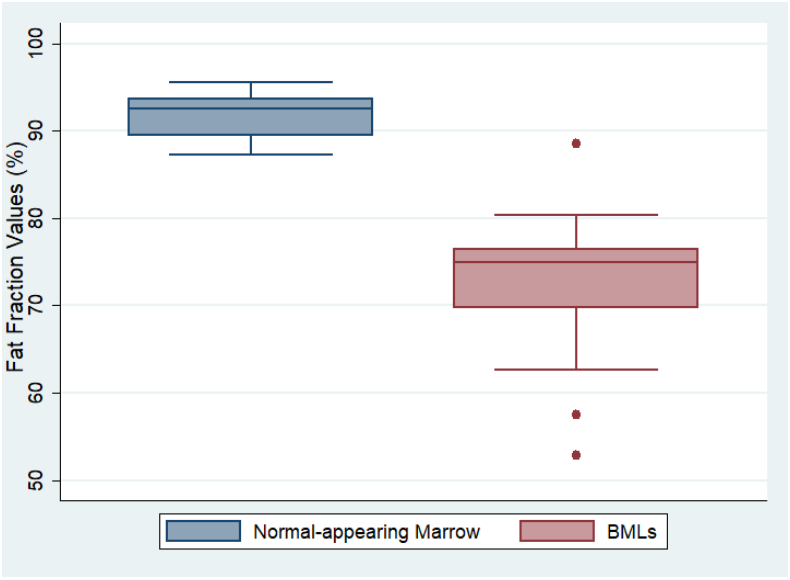

Figure 7.2. Box plot of the fat fraction values within the segmented ROIs of normal-appearing marrow and BMLs.

The fat fraction of the registered normal bone marrow at the other time point in the equivalent region to the normal appearing bone marrow ROI was 91.6 (± 2.5) %

(range 88.0 to 95.5 %), not statistically significantly different from the manually segmented time point (p= 0.15, Wilcoxon signed rank test).

7.3.3 Change in fat fraction and BML volume over time

There was a moderate negative correlation between change in BML volume between the first and second visit and the change in estimated fat fraction between these visits (ρs= -0.58, p = 0.016) (figure 7.3) [192].

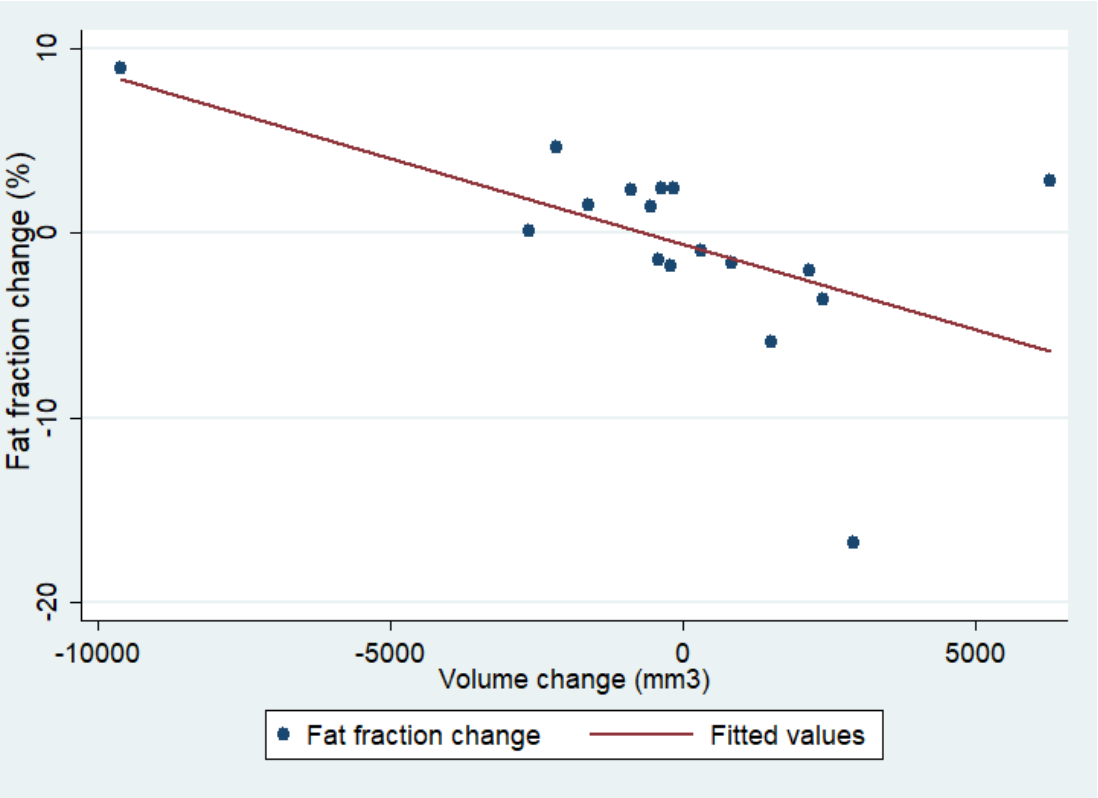

Figure 7.3. Scatterplot with regression line showing the correlation between fat fraction change and BML volume change (Spearman's correlation coefficient= -0.58; p= 0.016).

7.4 Discussion

This study found a significant difference between fat fraction in BMLs and nearby normal-appearing marrow. This suggests fat fraction measurements from mDixon Quant imaging may be useful for differentiating normal marrow from BMLs in knee osteoarthritis.

Two previous studies using MR spectroscopy showed higher water content inside BMLs compared to outside BMLs in patients with OA of the knee [104, 141], although they did not reach statistical significance, unlike the current study; this may possibly reflect either smaller numbers (10 subjects with OA) or the proximity of normal marrow to the BML and relatively large voxel size of spectroscopic imaging. A previous spectroscopy study showed significant differences between areas of bone marrow oedema and adjacent bone marrow in knees of patients with ACL injury (21.4 ± 9.1% vs. 13.0 ± 5.2%, p= 0.001) [141]. Further work using MR spectroscopy demonstrated significant differences in water content between BMLs in OA patients and normal bone marrow in healthy subjects (7.5 ± 5.8% vs 2.2 ± 0.8%, p= 0.02) [104]. Dixon imaging has been used to look hip osteoarthritis, with slightly lower fat fraction reported in BMLs (75%), although statistical significance was not reported as the study focussed on larger regions of interest and there were relatively few images containing BMLs [191].

We also found that changes in fat fraction correlated with changes in BML volume. Image registration was used to align mDixon Quant images from the two different visits to allow fat fraction measurements at multiple time points using a single time point ROI segmentation. A similar approach using image registration has been proposed for dGEMRIC quantification of articular cartilage in knee OA; such techniques have the potential to reduce bias and segmentation time [193].

Currently, BML assessment is typically based on size; however, this relies on accurately identifying an edge that is inherently poorly defined; this makes the process challenging and subjective and requires homogeneous fat suppression. Furthermore, size measurements may ignore important changes deep within the BML. Dixon imaging has a number of potential advantages for assessing bone marrow composition.

It is relatively insensitive to B_0 and B_1 inhomogeneity and can produce fat fraction maps, which are physiologically meaningful and may be less variable than conventional intensity measurements [79]. Compared to MR spectroscopy, images which cover the entire joint can be acquired with high resolution in reasonable times and are straightforward to acquire on many clinical scanners [116]. This study supports the potential of Dixon imaging to provide useful quantitative measurements of BML composition.

Previous work has compared Dixon fat fractions with the gold standard spectroscopy in vivo in spine [119, 120] and proximal femur [113, 115], and with known fat fractions in ex vivo phantoms [108, 114], suggesting that water-fat imaging with T2* correction was accurate for fat fraction quantification in the presence of trabecular bone. Previous studies have also suggested good scan-scan repeatability in the vertebrae [119] and sacroiliac joints [108]. Further studies are needed to define both accuracy and repeatability of the technique in patients with knee OA.

Fat fraction measurements from Dixon imaging have previously been used in patients with ankylosing spondylitis of the sacroiliac joints [108] and also myeloma [116]. To our knowledge this is the first study to look at mDixon Quant imaging in the setting of knee OA. There are, though, a number of limitations that need to be considered in interpreting the findings. The number of patients was relatively small (n=17), however despite this was sufficient to detect a significant difference in fat fraction between BML and normal-appearing bone marrow and also a significant association between change in fat fraction and change in BML volume. In our study the echo times were set to minimum, so were not optimised or fixed, however the values are within typical ranges suggested in the literature [116]. The fat fraction image was calculated by the scanner using a single T2*; approaches using multiple T2* components are an

alternative but may suffer from poor noise performance [119]. The relatively high resolution required in the knee may lead to greater eddy currents. A dedicated fat spectrum from bone marrow was not obtained; previously published work differs in whether a bone marrow spectrum was used [119] or not [108]. Other potential sources of error include edge effects, susceptibility, and chemical shift. Because BMLs are focal, subchondral features, these may be more important than in more homogeneous conditions such as fatty liver and may lead to non-physiological voxel outliers in the fat fraction map, although careful delineation of BMLs was performed, a high bandwidth was used, and median values were used to average across a BML. The registration process may also influence edge effects. T_1 may affect accuracy, although a low flip angle was used [116]. The single time point segmentation with image registration may miss BMLs visible at only one time point, although it has the advantage of focussing more on BMLs than larger ROIs (e,g, the entire subchondral region) in which BML change may be diluted by large amounts of normal marrow [191].

In conclusion, in this small study using mDixon Quant imaging in patients with symptomatic knee OA, BMLs had a significantly lower fat fraction than normal-appearing bone marrow. Estimation of BML fat fraction combined with image registration provides an alternative approach to volume measurement for bone marrow assessment.

7.5 Acknowledgements

The authors would like to thank Dr David Higgins from Philips for valuable support.

7.6 Authors contributions

HN, TWON, and RH contributed to the design of the work. HN, TFC, TWON, RH, and MJP contributed to the analysis of the data. All authors contributed to drafting of the manuscript in addition to revising the content and critical appraisal. All authors have approved the final version.

7.7 Role of the funding source

Henry Noorveriandi was supported by a grant from the Indonesian Government (Indonesia Endowment Fund for Education). This research was funded by NIHR Manchester Biomedical Research Centre. The research was also supported by Versus Arthritis. The views expressed are those of the author(s) and not necessarily those of the NHS, the NIHR or the Department of Health.

7.8 Conflict of interest:

No conflict of interest to declare for any of the authors.

Chapter 8

Study 4

Chapter 8

Compositional MRI approaches: fat fraction and T1 relaxation times measurements in fat-water-bone phantoms and clinical feasibility study in subjects with knee osteoarthritis

Abstract

Purpose:

To assess: i) the accuracy of water-fat mDixon Quant imaging and biexponential T1 mapping of single slice inversion recovery (SSIR) sequences for the assessment of fat fraction (FF) in a fat-water phantom with and without bone granules, compared with single voxel magnetic resonance spectroscopy (MRS), ii) To investigate the feasibility of a 3D gradient echo variable flip angle (VFA) sequence to quantify T1 values with 2D T1 mapping of single slice inversion recovery fast spin echo (SSIR) as the reference standard, and iii) To investigate whether monoexponential T1 mapping and biexponential T1-based fat fraction estimation using inversion recovery could differentiate between bone marrow and bone marrow lesions (BMLs) in subjects with symptomatic knee osteoarthritis.

Methods:

MR imaging and spectroscopy was performed on a Philips 3-T scanner. mDixon Quant, single slice inversion recovery (SSIR), 3D gradient echo variable flip angle (VFA), and single-voxel MR Spectroscopy measurements were performed on a series of phantoms with differing known fat fractions with and without bone granules. The quantitative MR imaging results were compared to the MRS-based results. Preliminary in vivo examination of monoexponential T1 mapping and biexponential fat fraction estimation from inversion recovery sequences was performed in six subjects with knee osteoarthritis.

Results:

Using the phantoms, FF assessed using the mDixon Quant and biexponential T1 mapping was very strongly correlated with MRS FF values, with the Pearson correlation coefficient values (r) 0.991 and 0.932 respectively. FF assessed using mDixon Quant images was slightly higher when compared to the assessment using MRS (mean difference: 3.4 %) while FF assessed using SSIR was higher than MRS FF (mean difference of 18.2 %). T1 values of the phantoms obtained using VFA and SSIR sequences were well correlated (r=0.993), slightly higher using VFA compared to monoexponential SSIR with mean difference of 62.7 ms (95% CI –1.8 to 127.3). In the feasibility study of six subjects with symptomatic knee OA, T1 relaxation time of BMLs determined by monoexponential T1 mapping was significantly longer than that observed in normal bone marrow (798.1 vs 399.0; $p < 0.05$) and the FF from biexponential T1 mapping of BMLs was significantly lower (52.7 % vs 90.8 %; $p < 0.05$).

Conclusion:

FF quantification can be assessed accurately using 3D mDixon Quant imaging. FF assessed using biexponential SSIR tended to overestimate FF when compared to MRS or mDixon Quant methods. T1 mapping in knee OA subjects shows differences between BMLs and normal-appearing marrow and offers an alternative approach for the assessment of BMLs in knee OA.

8.1 Introduction

Magnetic resonance imaging (MRI) is the modality of choice to detect and monitor abnormal bone changes associated with knee osteoarthritis (OA), including subchondral bone marrow oedema-like lesions (BMLs) [15, 18, 189]. MRI is sensitive to both the water and fat components in marrow disorders [194]. To date assessment of BMLs has focused on the size of these structures assessed either semiquantitatively [88-91] or quantitatively [17, 18, 81, 86]. Quantitative/ volumetric BML assessment using standard MRI sequences is considered to be accurate and reproducible. However, there are challenges in this approach due to poorly defined borders of

BMLs. The true extent of the BMLs and their appearance may varies depending on which MRI sequence is used. Furthermore, volumetric BML assessment is potentially subjective and time consuming, in particular if the aim is to evaluate BML change over time.

In knee OA, characterisation of BMLs based on their presentation on two different MRI sequences [85, 87] suggest parameters, such as fat fraction and T1 relaxation time may be useful to discriminate BMLs based on these compositional values. In addition, previous studies using MR spectroscopy found reduced fat fraction inside BMLs compared to bone marrow outside BMLs [104, 141]

Magnetic resonance spectroscopy (MRS) is regarded as the non-invasive reference standard in the evaluation of compositional changes in tissues, including fat fraction and T1 relaxation time measurements [113, 151, 155, 195, 196]. MRS can directly separate the signal of fat marrow into its water and fat components and calculate fat fraction. MRS collects the signals of water and fat as a function of their resonance frequency. The collection of spectra for fat fraction calculation requires an appropriate acquisition technique. The analysis of the spectra must be performed offline and requires a substantial amount of postprocessing and expertise. Furthermore, MRS suffers from lower spatial resolution than MRI, resulting in difficulty conforming to BMLs. Therefore, MRS may be less practical in some clinical settings compared to MR imaging techniques for fat fraction estimation [113].

Advanced MR imaging techniques such as water-fat mDixon Quant sequences, monoexponential, and biexponential T1 mapping using inversion recovery (IR) sequences [19, 116, 196] which can assess fat/water composition and T1 relaxation times, offer potential advantages in the evaluation of BMLs. Dixon sequences have

been proposed as an accurate and reliable imaging technique for in vivo fat fraction (FF) quantification in different tissues such as liver and lumbar vertebra [118, 120, 121].

Biexponential T1 and T2/T2* mappings have been widely used to assess different tissues, including white matter [197], muscle [198], and articular cartilage [199], and have been successfully used to estimate fat fraction in the muscle [198]. Because marrow fat has a much shorter T1 relaxation time than water [126] and BMLs associated with knee OA have been shown to have reduced fat content [53, 104, 141] (Chapter 6), marrow damage and concomitant marrow replacement in the BMLs would be expected to substantially increase T1 relaxation time of the BMLs. Therefore, quantitative measurements of T1 and FF could potentially be used to differentiate between normal bone marrow and BMLs.

To determine T1 in tissues, monoexponential T1 mapping from 2D inversion-recovery (IR) and 3D variable flip angle imaging are typically employed [125]. Furthermore, by assuming a 2-component model with a fixed, known, short relaxation time for the fat component and a longer unknown relaxation time for the water, biexponential fitting of inversion recovery images could be used to estimate fat fraction. To date there are no data concerning the assessment of monoexponential and biexponential T1 mapping using inversion recovery images of bone marrow in knee OA. In preparation for application in clinical / research studies, it would be appropriate to evaluate the accuracy of MRI-based T1 and FF measurements techniques in a phantom.

The aims of this study were i) to compare the accuracy of 3D mDixon Quant Imaging and 2D biexponential fitting from SSIR for measuring fat fraction using fat-water emulsion phantoms of varying fat/water composition and phantoms with bone to

simulate the in vivo femur and tibia, with single voxel magnetic resonance spectroscopy as the reference, ii) to investigate the feasibility of 3D gradient echo variable flip angle (VFA) sequences to quantify T1 of the phantoms with 2D monoexponential T1 mapping of inversion recovery (IR) images as the reference standard, and iii) to investigate monoexponential and biexponential inversion recovery for T1 and fat fraction measurement in the knee joints of subjects with symptomatic knee OA.

8.2 Methods

Seventeen oil-water emulsion phantoms covering a fat content ranging from 0 to 100% were made. These phantoms enabled comparison of different quantitative MR techniques with MRS as the reference standard. Pixel-by-pixel maps of fat fraction and T1 were produced for each MR imaging method with the aim of comparing the results with MRS. In vivo feasibility study of inversion recovery sequences was undertaken on a small number of subjects with symptomatic knee OA to investigate T1 and fat fraction of BMLs and nearby normal-appearing bone marrow.

8.2.1 Phantom study

A series of fat-water emulsion phantoms consisting of peanut oil and distilled water with varying concentration of peanut oil were prepared as previously described [108]. Agar (3% by weight) and sodium dodecyl sulphate (Sigma-Aldrich, St. Louis, Missouri, USA) were used to stabilise the emulsions. No contrast agent was added to the water. The emulsions were prepared slowly over a heat-stir plate and subsequently cooled to allow the mixture to set. This phantom consists of nine 5 mL plastic tubes with FF measurements ranging from 0 to 100% and eight tubes (5 mL) with the range of FF (0-60%) and decellularised bovine trabecular bone matrix (NuOss granules,

particle size 250-1,000μm, Henry Schein, London, UK) with two different concentrations (100 and 150 mg/cm^3) similar to the previous study [108] with the aim of simulating the range of normal and abnormal marrow in the femur and tibia. FF values in the phantom are calculated by weight assuming the density of peanut oil is 0.916 g/cm^3 and are subsequently referred to as the known FF. The fat fraction by weight is calculated using the equation below:

FF by weight= [fat fraction by volume] * peanut oil density / ([water fraction by volume] + [fat fraction by volume] * peanut oil density)

The resultant fat fractions were 0.0%, 9.5%, 19.1%, 28.8%, 38.6%, 48.5%, 58.6%, 68.8%, and 100.0%. Figure 8.1 shows photographs of the fat-water emulsions phantom. The phantom was placed in a plastic box, as shown in figure 8.1b and immersed in agar gel for scanning. The phantom was stored at room temperature in the same room with the MR scanner for 24 hours before the examination. Before scanning, the phantom was placed on the MR scanner perpendicular to the main magnetic field.

(a) (b)

Figure 8.1. Fat-water and fat-water-bone (FWB) phantoms. (a) Examples of 0%, 58.6% and 100% FF tubes with no bone granules (BG) and with the addition of bone. (b) shows set up of the oil-water phantom in the plastic container.

To evaluate the repeatability of the MRI and MRS methods for T1 and fat fraction estimations in a human volunteer subject, a participant with a BML underwent two series of MR examinations on the same scanner with an interval of 10 days between scanning. The MRI and MRS protocols were similar to those used for the phantom.

8.2.2 Clinical feasibility study

Six subjects with symptomatic knee OA who had taken part in a trial looking at the influence of a lateral wedge insole in patients with painful knee OA had single slice inversion recovery (SSIR) imaging performed. Using these images, monoexponential and biexponential T1 fitting was performed to estimate T1 and FF of normal-appearing marrow and BMLs.

8.2.3 MRI and MRS protocol for phantom study

Phantom experiments were performed at room temperature on a Philips 3-T scanner (Achieva, Philips Healthcare, Best, Netherlands). During the scanning, the long axis of the phantom components was placed perpendicular to the long axis of the main magnetic field (i.e., perpendicular to the z-axis). Images of the phantom were acquired axially through the phantom components.

Three-dimensional (3D) gradient echo mDixon Quant chemical shift-encoded images with six-echoes were acquired with the following parameters: TR= 30 ms; first echo time (TE_1)= 0.95 ms; echo spacing= 0.9 ms, FA= 3°; slice thickness= 1.5 mm, interslice gap= 0 mm; matrix size= 256 x 128 with 128 slices; FOV= 384 x 192 mm; bandwidth= 1822.8 Hz/ pixel with imaging time of 4 minutes 28 seconds.

Two different quantitative MRI sequences for calculating T1 were acquired: 2D sagittal single slice fast spin echo inversion recovery (FSE-SSIR) and 3D gradient echo variable flip angle (VFA). SSIR sequences with 5 inversion times were acquired

with the following parameters: TR/TE= 8000/ 44 ms, matrix size= 320 x 240, FOV= 256 x 288 mm, slice thickness= 2.5 mm, BW= 607.6 Hz/ pixel, and TI= 100, 300, 700, 1500, 3000 ms, echo train length= 15. The total acquisition time for five inversion times was 12 minutes (2 min 24 seconds for each inversion time).

Similar images were acquired from the participant with a BML at the first examination. At the second MRI examination, additional oversampling was automatically added by the scanner (50 mm head, 50 mm foot), resulting an acquisition matrix of 320x233 and an acquisition duration of 3 minutes 4 seconds.

T1 relaxation times from SSIR images were calculated by performing monoexponential curve fitting of the signal intensities at different inversion times using 3-parameter fitting to the following equation [135]:

$$S = S_0 [1 – 2f.\exp (-TI/T1) – (1 - 2f)\exp (-TR/T1)]$$

Where S= signal vector, S_0= maximum observable signal intensity, TI= inversion time, f= inversion efficiency, TR= repetition time.

Similarly, with the biexponential fitting procedure using SSIR, fat fraction measurement were estimated using [135]:

$$S = S_0[ff \{1 - 2f.\exp(-TI/T1fat) - (1-2f)\exp(-TR/T1fat)\} + (1-ff) \{1 - 2f.\exp(-TI/T1) - (1-2f)\exp(-TR/T1)\}]$$

Where TI is the inversion time, f is inversion efficiency, and ff is fat fraction. T1 was constrained between 500 and 6000 ms. The biexponential fitting for FF measurements of the phantom used the fixed T1 relaxation time of peanut oil (T1fat) derived from the monoexponential fitting of peanut oil (100% fat).

3D gradient echo VFA sequences with six flip angles (FAs= 3, 5, 7, 10, 20, 30°) were acquired with the following parameters: TR/TE= 7.4/ 2.3 ms, slice thickness= 1.5 mm, slice gap= 0 mm, matrix size= 128 x 112, FOV= 192 x 168 cm. The T1 of VFA sequence with six FAs was calculated based on the equation [200]:

$$S(\alpha) = S_0 \cdot \sin(\alpha)(1-\exp(-TR/T1)) / (1-\exp(-TR/T1)\cos(\alpha))$$

Where $S(\alpha)$ is the signal intensity, α is the FA, TR is the repetition time, and S_0 is a constant depending on the proton density, the coil sensitivity, and T2* relaxation. From VFA images acquired with a series of different FAs, a T1 map can be calculated on a pixel-by-pixel basis by using a linear fitting method.

The actual FA α is location dependent because of radiofrequency (B1) inhomogeneity. Therefore, B1-corrected FA α is used in the pixel-by-pixel fitting process for calculating the VFA T1. A B1 mapping sequence was acquired prior to the VFA sequence acquisition with the following parameters: TR = 30 ms, TR extension= 120 ms, TE= 1.92 ms, flip angle= 60°, bandwidth= 383 Hz/pixel, FOV= 192 x 168 mm, matrix size= 96 x 35, slices number= 72, slice thickness= 5 mm, overlap between adjacent slices= 2.5 mm. Acquisition time for the B1 map was 10 minutes and 13 seconds.

Single-voxel spectroscopy was acquired using stimulated echo acquisition (STEAM) volume selection for spectral separation and T1 measurements. MRS data were acquired without water suppression after volume localised shimming using a knee coil with 16 signal averages and one pre-acquisition excitation. Local shimming (PB-volume) provided by the manufacturer was performed with shim size of 25x25x25 mm^3. The parameters of the sequence were: TE= 15 ms with an array of TRs (315, 600, 1000, 1500, 2000, 3000, 5000 ms) and mixing time (TM)~17 ms. Volume of

interests (VOIs) or STEAM boxes with voxel size of 8x8x8 mm^3 were positioned in the centre of each tube (used as a reference for postprocessing and analysis) with three-plane reconstructions from a mDixon Quant sequence used for the voxels' positioning. Two sets of acquisitions at two different centre frequencies (one set on the main fat peak and one set on the water peak) were performed for each tube. The positioning of VOIs of the spectroscopy were saved as screenshots as a reference for positioning ROIs in the evaluation of MRI-based T1 and FF measurements.

8.2.4 MRI protocol for the clinical feasibility study

A 16-channel transmit-receive knee coil was used to scan the knee. A sagittal fast-spin echo single slice inversion recovery (FSE-SSIR) sequences was used for T1 mapping with the following parameters: TR/TE= 8000/30 ms with eight different inversion times (TIs) (50, 100, 200, 400, 800, 1600, 3200, 5000 ms), section thickness= 2.5 mm, matrix size= 352x352 mm, pixel size=0.625x0.625mm, BW= 623 Hz/pixel, echo train length= 15. For each scan, an SSIR image was acquired through a region that contained a BML.

8.2.5 MR images and spectroscopy analysis

The MRI data were transferred to a separate computer for offline postprocessing.

MRI-based FF and T1 were assessed using software developed in-house on Matlab (MathWorks, USA). A rectangular ROI was drawn in the centre of each phantom. For comparison, the ROIs were visually matched to the size and orientation of the MRS voxels.

MRS Spectral analysis used the Advanced Method for Accurate, Robust, and Efficient Spectral (AMARES) algorithm included in the jMRUI software package [201]. The spectral data of water (4.65 ppm) and multiple fat spectral peaks (0.90, 1.30, 1.60,

2.06, 2.82, and 5.26 ppm) were reconstructed and corrected for phase, baseline, and frequency shift. A manually selected resonance frequency and line width of water and fat peaks were used as starting values in the nonlinear least squares fitting algorithm. Peak fitting was performed for the spectra at each individual TR. The computed areas under each spectral peak were plotted against TRs, and a monoexponential saturation recovery was used for the fitting with the equation below:

$S_I = S_0 (1-\exp(-(TR - (TE/2) - TM)/T1))$

Where S_I is the peak spectral area for a given TR, S_0 is the equilibrium value, TR is the repetition time, TE is the echo time, and TM is the mixing time.

The FF (as a percentage) was calculated using combined spectra (water peak acquired with centre frequency of water and the methylene peak acquired using the centre frequency of the main fat peak). The peak area of water signal obtained from the spectroscopy with TR of 5000 ms (S_{5000}) was corrected for T1 effects by calculating the theoretic peak area with TR=∞ [S_0], by using the calculated T1 relaxation times, as follows:

$S_0 = S_{5000} / (1-\exp(-(5000-(TE/2) - TM)/T1))$

The signal amplitude of the methylene fat (1.3 ppm) with TR 5000 ms was corrected by the ratio of the methylene peak to the total fat peak (obtained from 100% peanut oil in the phantoms or normal bone marrow of human subject). These corrected values were then used to calculate MRS fat fraction as below:

$\text{Fat fraction} = 100\ \% \cdot I_{fat} / (I_{fat} + I_{water})$

To evaluate the repeatability of MRI- and MRS-based fat fraction and T1 measurements in a participant, three different regions of interests (VOIs) or STEAM

boxes (voxel size 8x8x8 mm^3) were positioned within a BML, normal-appearing marrow close to a BML, and normal marrow well away from BMLs with three-plane reconstructions from a 3D mDixon Quant sequence and sagittal PDFS images used for the voxels' positioning. The positioning of VOIs of the spectroscopy were saved (as screenshots) as a reference for positioning ROIs for the second scan and for the comparison between sequences. Positioning of the VOIs is shown in Figure 8.2.

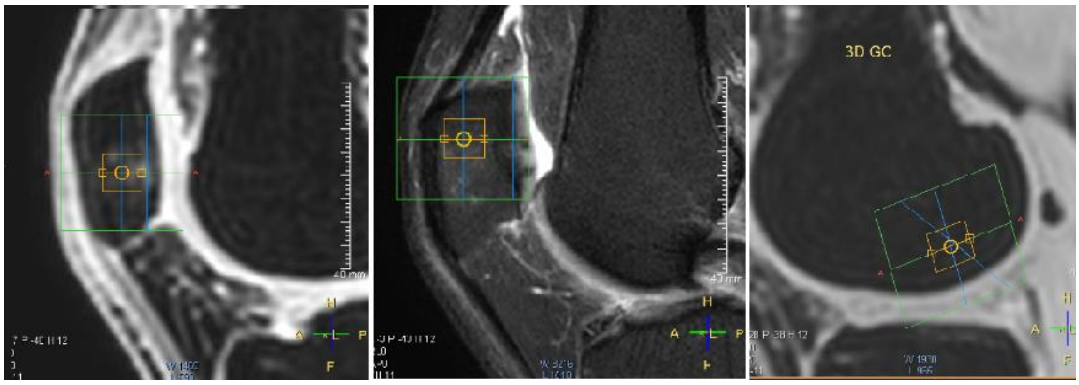

(a) (b) (c)

Figure 8.2. VOIs positioning for MR spectroscopy of the participant. STEAM box was positioned in the BML of the patella (a) on water-only mDixon Quant image. VOI of normal-appearing marrow nearby BML in the patella (b) shown on PDFS image, and VOI of subchondral bone marrow of the lateral femoral condyle (c) on the water-only mDixon Quant image.

Further, mDixon Quant FF and SSIR FF methods were also compared by comparing FF values from 10 different ROIs taken from different locations in the knee. Ten different ROIs (square shape) of normal-appearing and abnormal bone marrow with the size ranging from 24 to 64 mm^2 were carefully drawn on the mDixon Quant fat fraction map to avoid overlapping between ROIs. Similar ROIs were then drawn on the biexponential SSIR FF image by matching the same ROIs for size and location as closely as possible. The comparison was performed from images from the second visit.

For the clinical feasibility study of 6 knee OA subjects, mono- and biexponential fits of inversion recovery images were performed to calculate T1 and FF. ROIs of BMLs and normal-appearing marrow were defined by a radiologist experienced in BML

segmentation (HN). On the inversion recovery image with TI= 200 ms for each subject, the ROI of the BML was defined as the area determined to be the maximum extent of BML, while an ROI of normal-appearing bone marrow (oval ROI with minimum size of 2 cm^2) was also defined (either in the distal femur or proximal tibia outside BML) on the same image of each subject. The ROIs were then copied to the monoexponential T1 and SSIR fat fraction maps to calculate T1 and FF, respectively. T1 and FF values for each patient were calculated as median values of pixels within the ROIs and the values across all patients were also reported as median and interquartile range. The biexponential fitting for the clinical feasibility study used the known T1 value of normal marrow at 3T from a previous study (381.2 ms) [202].

8.2.6 Statistical analyses

The T1 and FF values over all voxels in each ROI of the phantoms were reported as mean ± standard deviation (SD). To assess the bias of measurement or accuracy of the MRI measurements these were evaluated with Bland-Alman plots; the bias (overall mean difference) between the MRI and MRS assessments and 95% confidence intervals around the mean difference were determined. The correlations between MRI-based and MRS-based fat fractions of the phantoms were assessed using Pearson correlation coefficients (r), as well as the correlation between T1 of inversion recovery and VFA sequences.

T1 and FF values in the clinical feasibility study were reported as median and interquartile range (IQR). The difference in T1 and FF values between BML and normal bone marrow from all knees was tested using non-parametric test (Wilcoxon signed rank test). Statistical significance was set at $p< 0.05$.

8.3 Results

8.3.1 Fat fraction and T1 relaxation times assessed in the phantom

Figure 8.3 shows examples of MR spectra of the phantom acquired using the STEAM sequence. A scatterplot between known FF of the phantom (both fat-water and fat-water-bone phantoms) and MR spectroscopy FF is shown in figure 8.4. The Pearson correlation coefficient shows a very strong correlation [183] between fat fraction assessed using MR spectroscopy with known FF of the phantoms (all components) (r= 0.992, p< 0.05). Bland-Altman analysis of MRS FF and known FF showed mean bias of -3.8 % ± 3.5 % (95% CI -5.6 to -2.0).

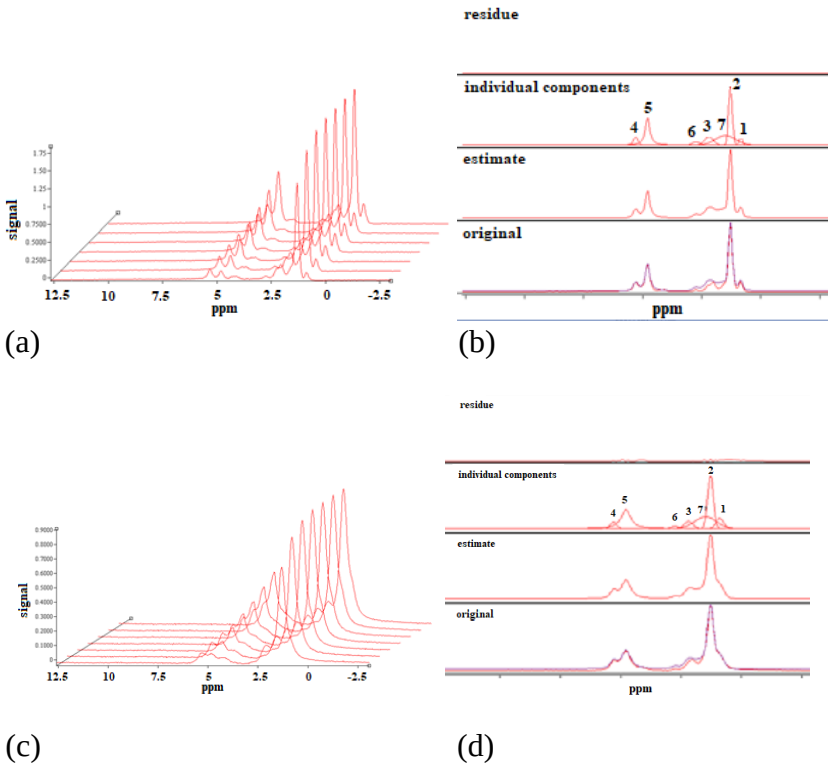

Figure 8.3. Examples of MR spectra acquired in the phantom with 58.6% FF by weight. (a) is MR spectra at a series of different TR from the VOI of the 58.6% FF phantom with no bone and (c) the spectra from the 58.5% FF of FWB phantom. Various peaks are indicated for fat at 0.90 (1), 1.30 (2), 1.60 (7), 2.06 (3); 2.82 (6), and 5.26 (4) ppm, and the water peak is indicated at 4.65 (5) ppm. The results of measured spectra fitted in jMRUI (AMARES) software for the longest TR are shown in (b) and (d). Broad linewidth of the water resonance (c) in the FWB phantom.

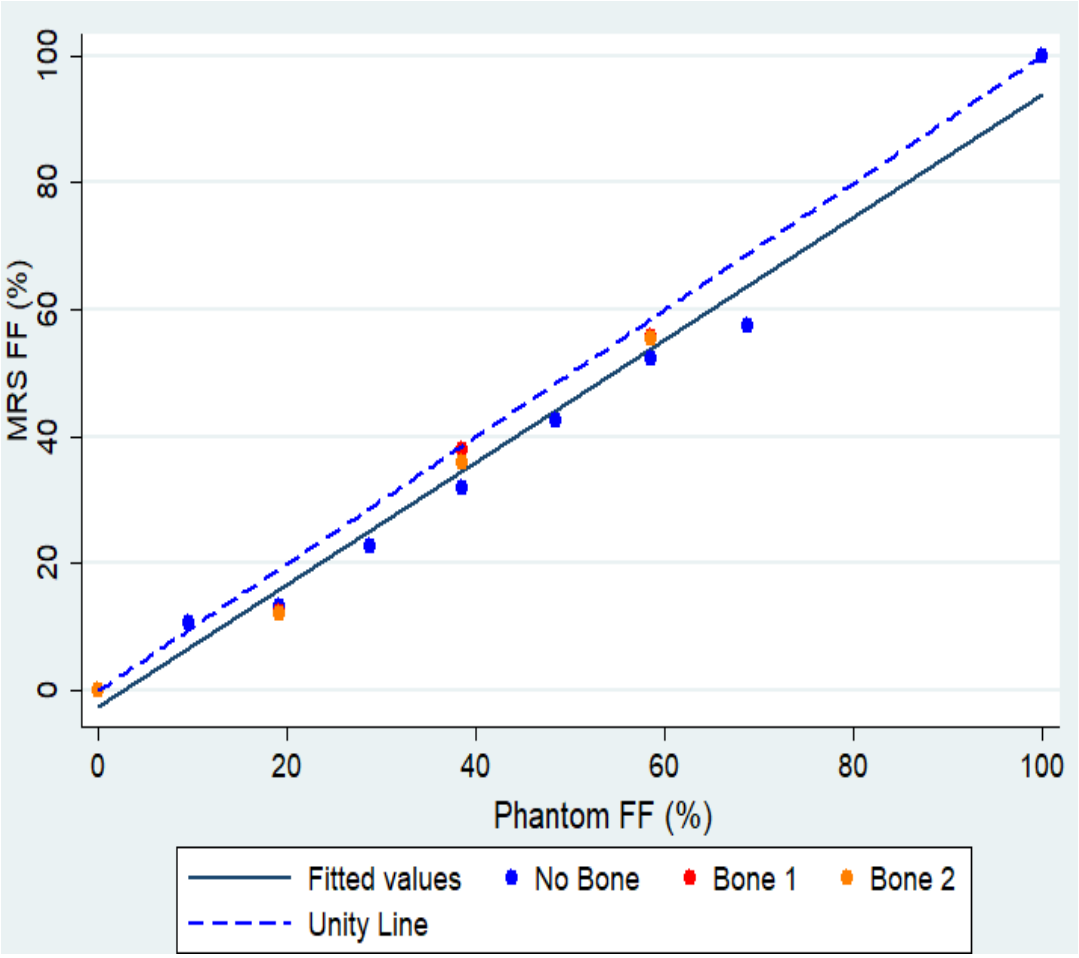

Figure 8.4. Scatterplot of MRS FF measurements and known FF of the phantom without and with bone granules. MRS FF agree closely with known FF phantom in the absence (No bone) and presence of bone (Bone 1 and Bone 2). Dashed line indicates perfect agreement and solid line represents the correlation (trend) line for phantom with and without bone. Bone 1 and bone 2 are FWB phantoms with lower (100 mg/ cm^3) and higher bone concentrations (150 mg/cm^3), respectively.

mDixon Quant FF and SSIR FF maps of the phantom are shown in figure 8.5. The mDixon Quant FF map with rectangular ROIs in each tube is shown in figure 8.5b.

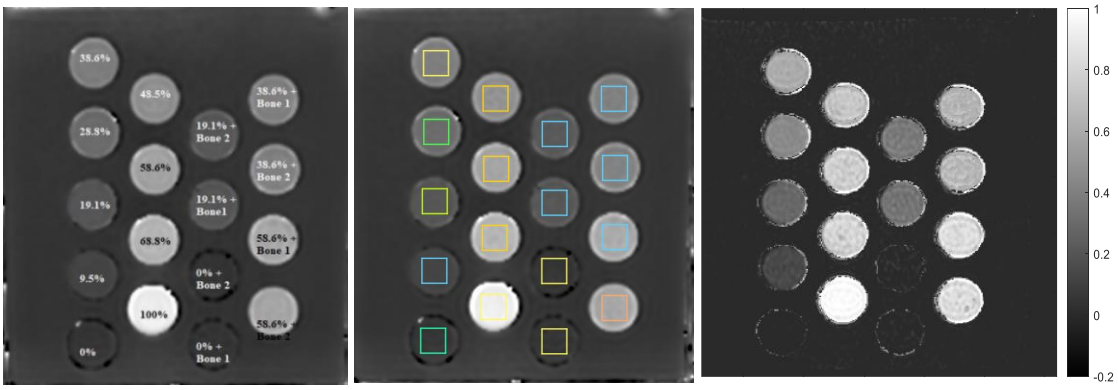

(a) (b) (c)

Figure 8.5. MR images of oil-water and oil-water-bone phantoms. Fat fraction map of mDixon Quant (a and b) and biexponential SSIR FF (c) of the phantom. Labels indicate reference FF values that vary between 0 and 100%. Bone 1 (100 mg/cm^3) and bone 2 (150 mg/cm^3) are two different concentrations of bone added to 0%, 19.1%, 38.6%, and 58.6 % FF. (b) shows Rectangular ROIs drawn in the centre of each tubes on the mDixon Quant FF map.

Figure 8.6 shows the scatterplot between phantom FF and FF values measured using the mDixon Quant sequence. Fat fraction assessed using the mDixon Quant sequence was very strongly correlated with phantom known FF ($r= 0.999$, $p< 0.05$). The presence of bone (low and high concentrations) showed relatively little impact on MRS FF measurements. mDixon Quant FF of the phantom (with and without bones) was also very strongly correlated with FF as assessed using MR spectroscopy ($r= 0.991$; $p< 0.05$), see figure 8.7.

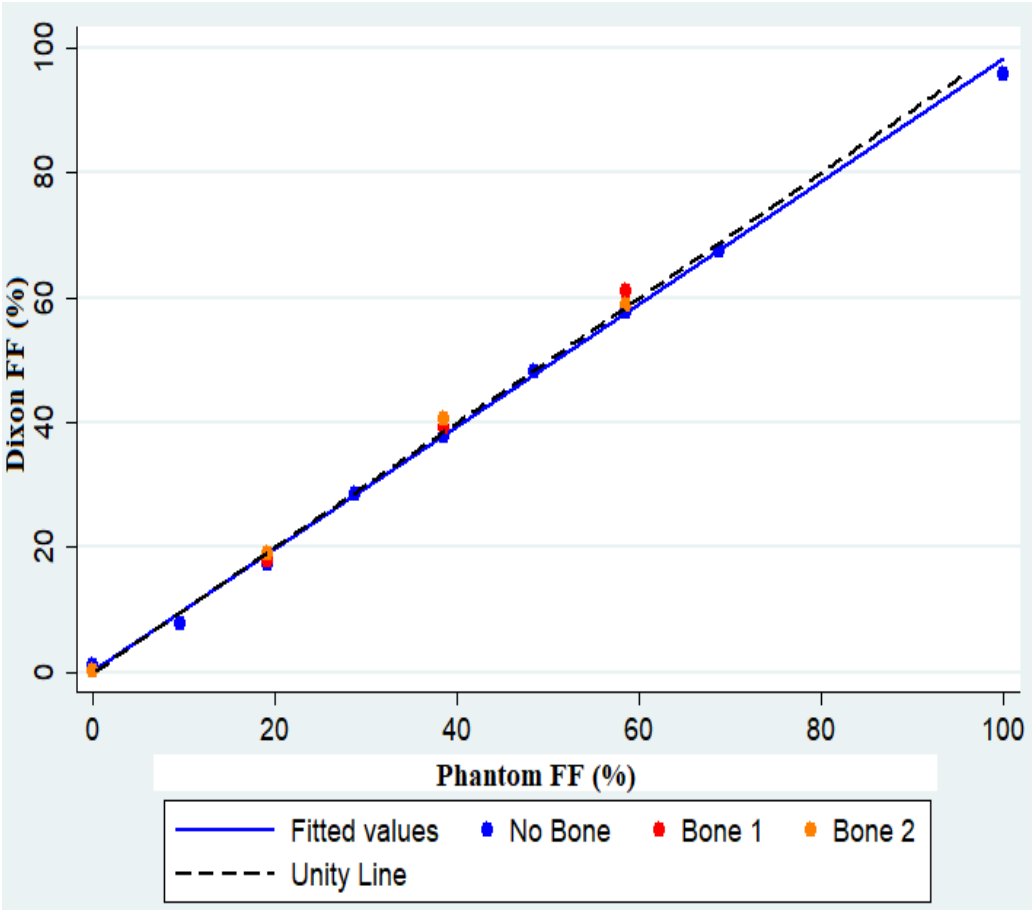

Figure 8.6. Scatterplots of fat fraction measurements of the fat-water and fat-water-bone phantoms using mDixon Quant sequence vs. known fat fraction. Fat fraction measurements from the mDixon Quant sequence correlated very strongly with the known FF of the phantoms. The solid line represents the trend line for all the phantoms and dashed line (unity line) indicates perfect agreement.

For the comparison between MRS and mDixon Quant FF values, the ROIs of the mDixon Quant sequences were visually matched to the size and location of the MRS voxels. Figure 8.7 shows the scatterplot between MRS and mDixon Quant FF.

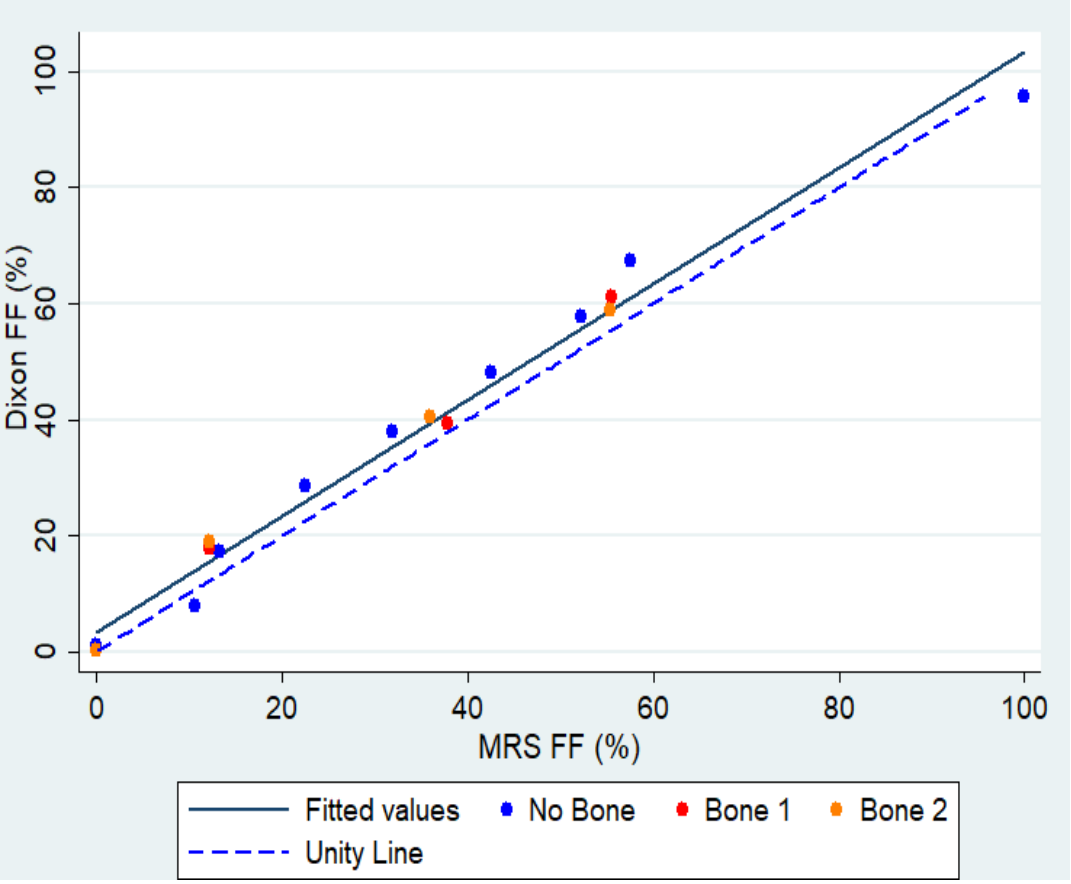

Figure 8.7. Scatterplot of fat fraction values of the phantoms between MRS and mDixon Quant sequences. The graph shows very strong correlation between mDixon Quant FF and MRS FF measurements. The dotted line represents the trend line and dashed line indicates perfect agreement.

The overall FF values measured using the mDixon Quant sequence were slightly lower than known phantom FF values with mean bias of -0.4 ± 1.6 % (95% CI -1.2 to 0.4). Compared to MRS FF, mDixon Quant FF values were slightly higher with mean bias of 3.4 ± 3.6 (95% CI 1.6 to 5.3).

Figure 8.8 shows the scatterplot between the known phantom FF and FF estimated using biexponential T1 fitting of the SSIR sequence. The graph showed a very strong correlation with known FF of the phantom with Pearson correlation coefficient of 0.955 ($p< 0.05$) but the agreement was less than that between the phantom FF and mDixon Quant (Fig.8.6) or MR spectroscopy (Fig.8.4). Bland-Altman analysis of

SSIR FF and known phantom FF values showed mean bias of 16.2 ± 11.4 % (95% CI 10.3 to 22.1). Overall, SSIR FF shows higher FF values in the phantom, both in the absence and in the presence of bone. The bone had a greater effect on SSIR FF than on mDixon Quant FF.

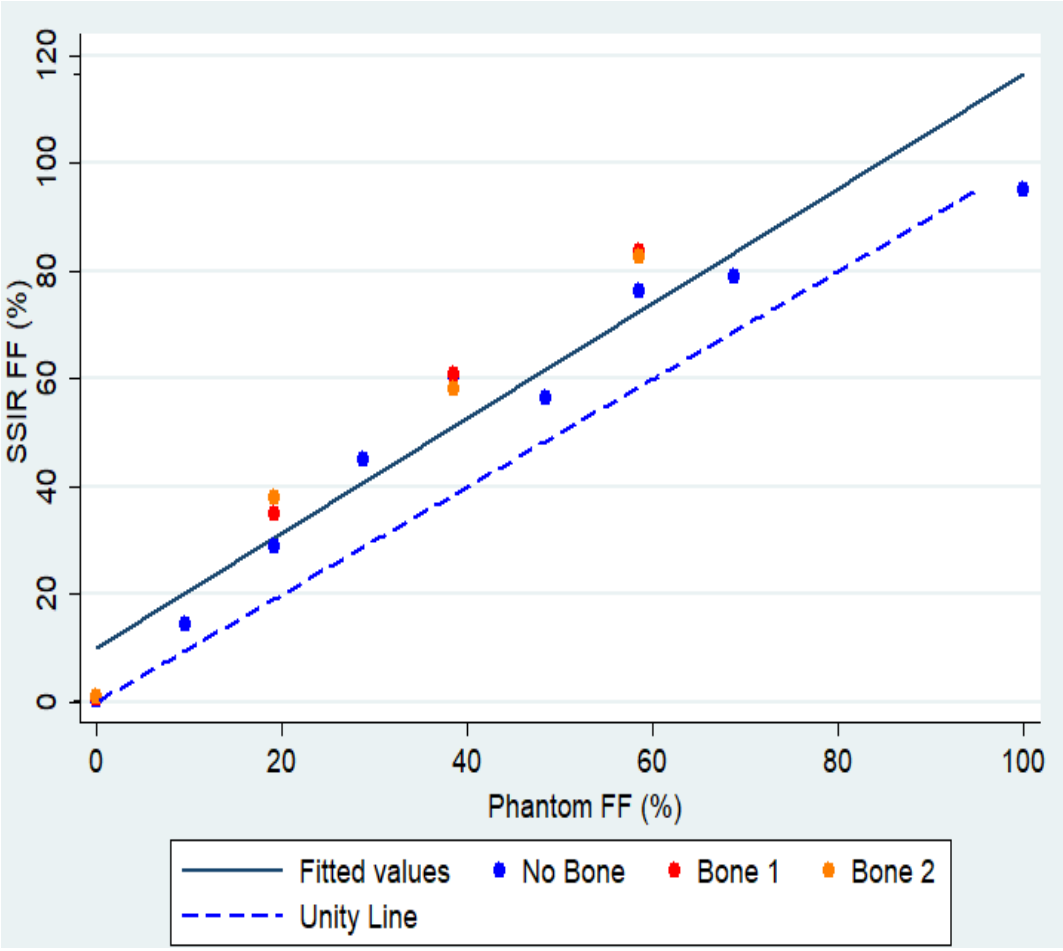

Figure 8.8. Scatter plot of fat fraction values between SSIR FF measurements and known FF of the phantom. The solid lines represent the trend line and dashed lines indicate perfect agreement.

Examples of monoexponential and biexponential T1 fitting using SSIR images are presented in figure 8.9.

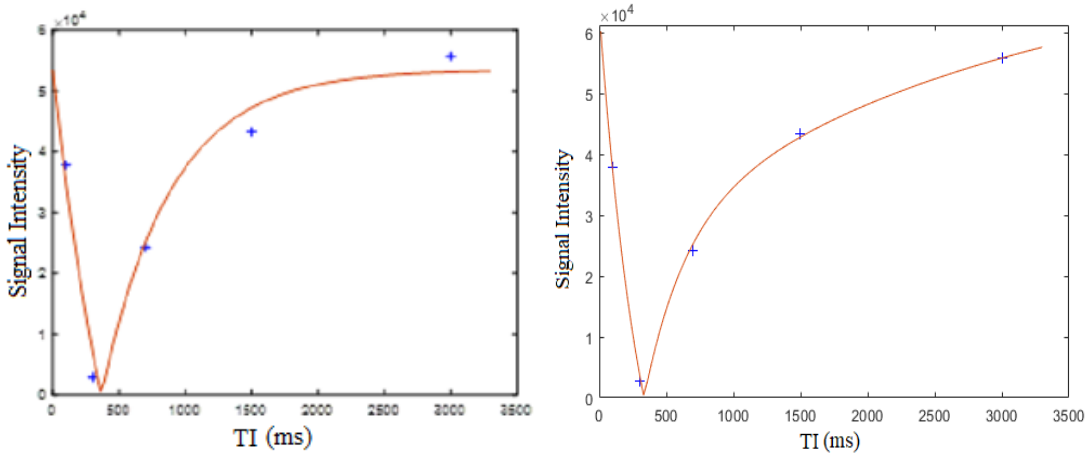

(a) (b)

Figure 8.9. Examples of single pixel fit for 38.6% FF (a) monoexponential (b) biexponential fitting showing the expected improved fitting with the biexponential fit.

There was also a very strong correlation between SSIR FF and MRS FF (Pearson r= 0.932; p< 0.05) as shown in figure 8.10. Bland-Altman analysis of SSIR FF and MRS FF showed a mean bias of 18.2 ± 12.3 (95% CI 12 to 24.6). Compared to the mDixon Quant sequence, SSIR FF were significantly higher than mDixon Quant FF (Wilcoxon signed-rank test, p< 0.05) with mean difference of 12.8% (95% CI 8.3 to 17.3). A scatterplot between SSIR FF and mDixon Quant FF is shown in figure 8.11.

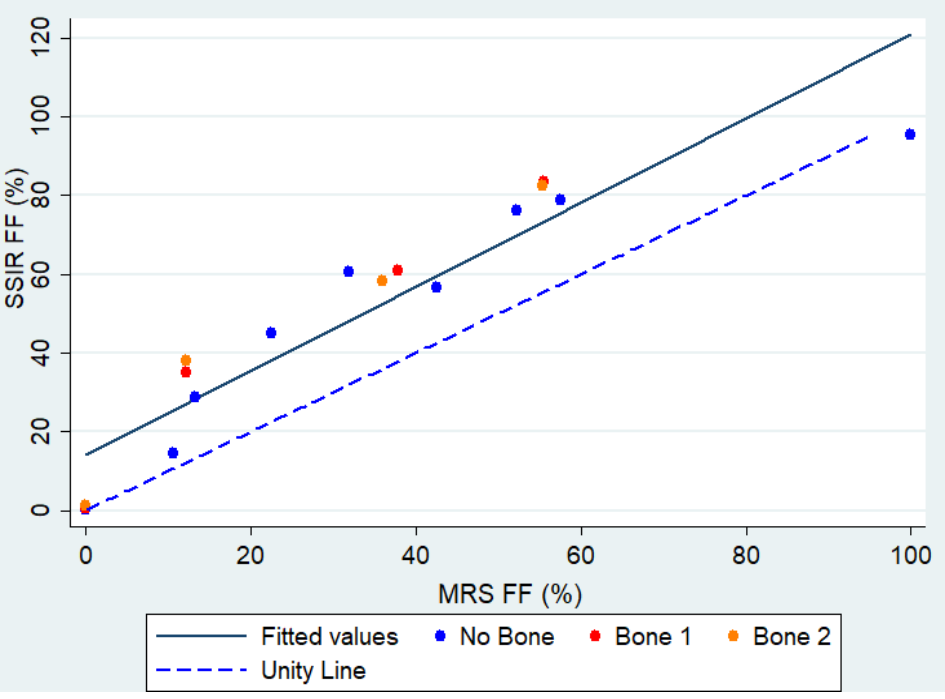

Figure 8.10. Scatterplot of fat fraction values between SSIR FF and MRS FF. The solid lines represent the trend line and dashed lines indicate perfect agreement.

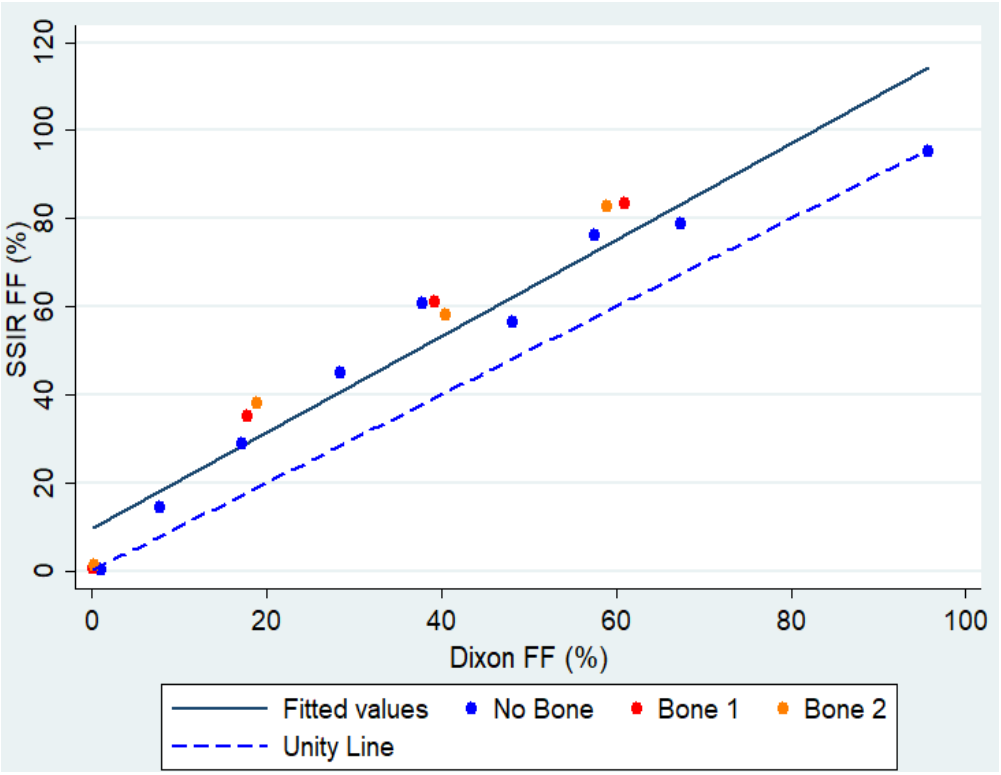

Figure 8.11. Scatterplot of fat fraction values of the phantom measured using the mDixon Quant sequence and the biexponential T1 of SSIR sequence. The dotted lines represent the trend line and dashed lines indicate perfect agreement.

Figure 8.12 shows T1 maps from SSIR and VFA sequences. T1 values of the phantoms obtained from the SSIR technique are shown in figure 14. Generally, T1 values decrease with increased fat concentration but are relatively flat from 38.5 to 68.6 % FF. T1 values were shorter with the addition of bone granules compared to the phantom components without bone granules.

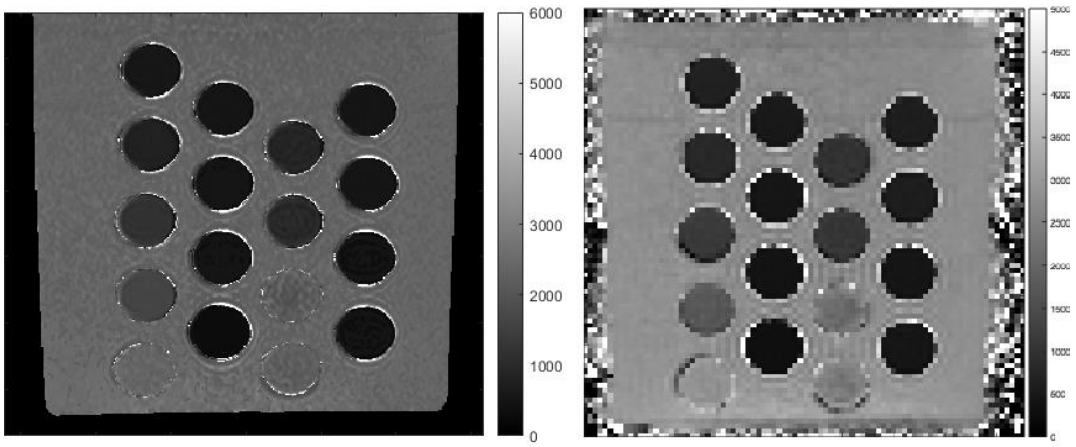

(a) (b)

Figure 8.12. T1 maps of the phantom acquired using SSIR (a) and VFA sequences (b).

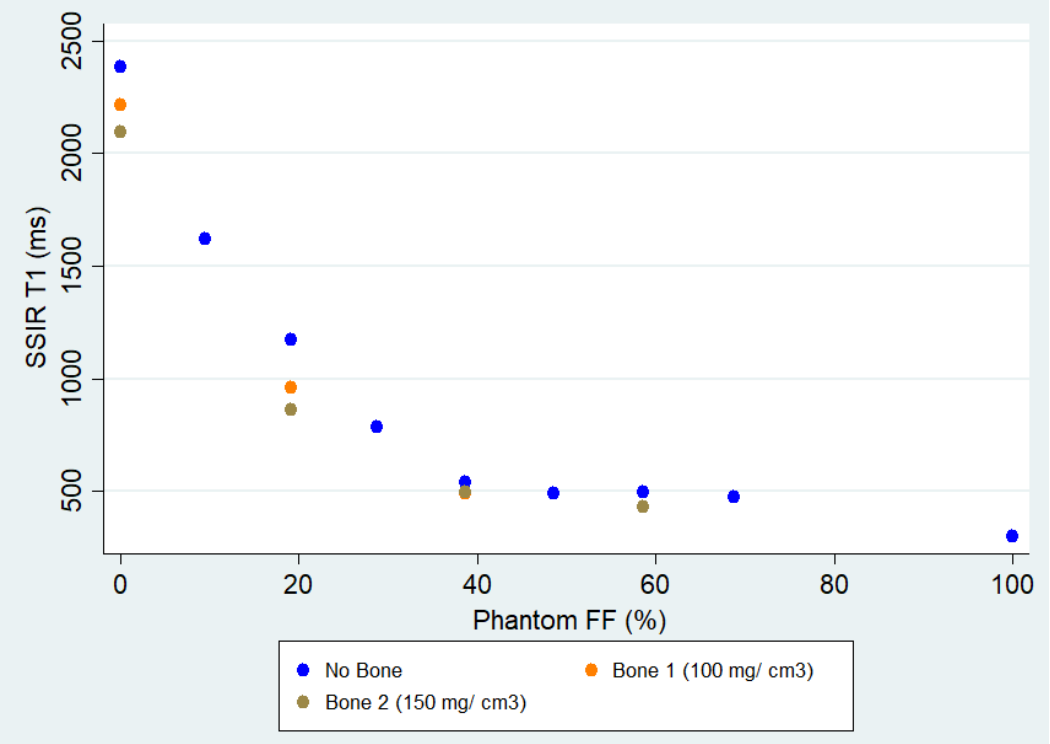

Figure 8.13. T1 values of the phantoms measured by monoexponential T1 fitting of the inversion recovery images. Bone 1 (100 mg/cm^3) and Bone 2 (150 mg/cm^3) are two different concentrations of bone added to 0%, 19.1%, 38.6%, and 58.6 % FF.

T1 relaxation times of the phantoms obtained using the 3D GE VFA sequence is shown in figure 8.14. T1 values of the phantom obtained using the VFA sequence decrease with increased fat concentration but are relatively flat from 58.4 to 68.6% FF. T1 values were shorter with the addition of bone granules compared to the phantom without bone granules.

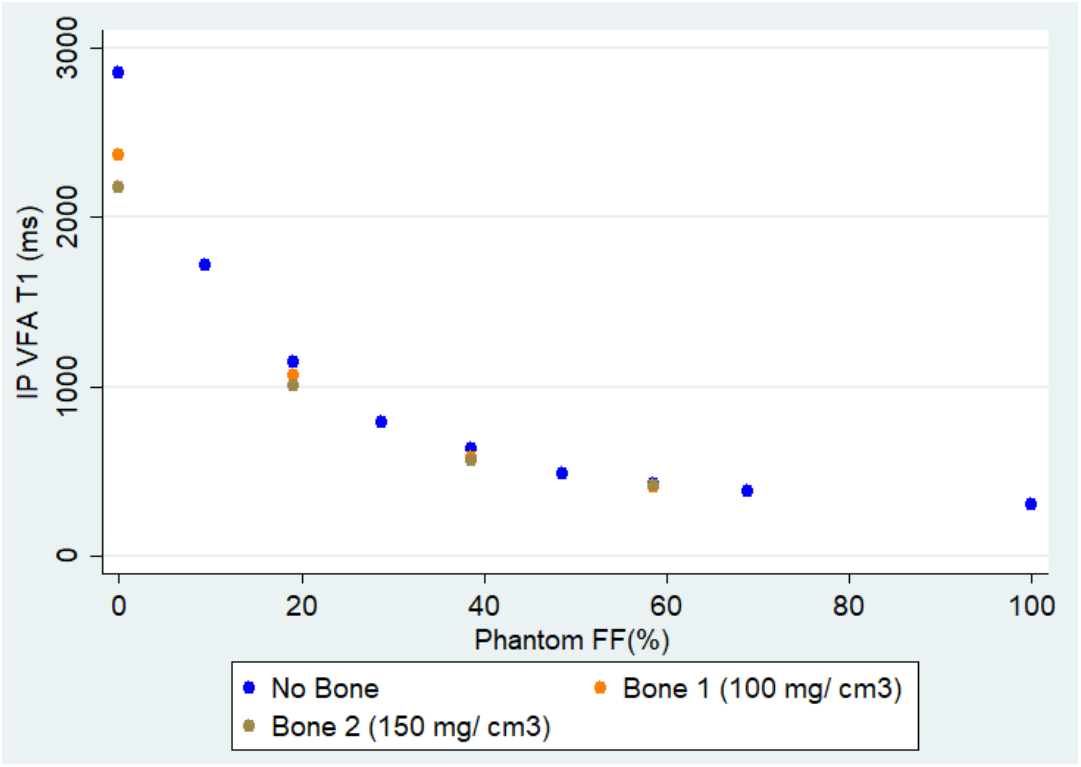

Figure 8.14. T1 relaxation times of the phantom using the 3D VFA technique. Bone 1 (100 mg/cm^3) and bone 2 (150 mg/cm^3) are two different concentrations of bone added to 0%, 19.1%, 38.6%, and 58.6 % FF.

The correlation between T1 relaxation times of the phantoms measured using the VFA and monoexponential SSIR techniques is shown in figure 8.15. The scatterplot of VFA against SSIR shows a very strong correlation with Pearson correlation coefficient (r)= 0.993 ($p< 0.05$). Bland-Altman analysis of VFA and SSIR T1 showed mean bias of 62.7 ± 125.5 ms (95% CI -1.8 to 127.3). For example, the VFA T1 relaxation time of 100% FF phantom is slightly higher than when assessed using SSIR (301.3 vs 297.1 ms).

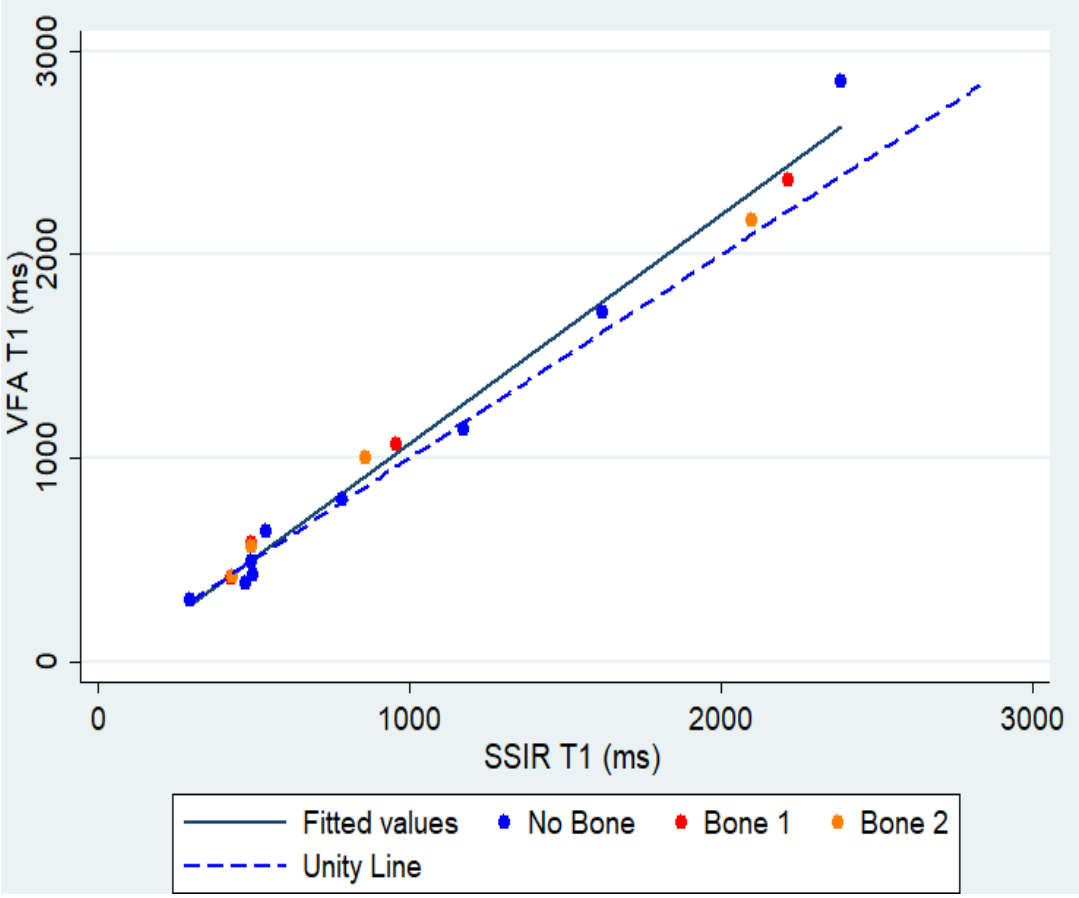

Figure 8.15. Comparison between T1 measurements of the phantom made with 3D VFA and monoexponential T1 from SSIR sequences shows a very strong linear correlation. The solid line represents the trend line and dashed line indicates perfect agreement.

8.3.2 FF and T1 measurements in a participant with BML

The single slice inversion recovery images of the knee are shown in figure 8.16.

Results from the repeatability study of FF and T1 measurements on different MRI and MRS techniques from the same participant scanned at two different times are shown in tables 8.1 and 8.2.

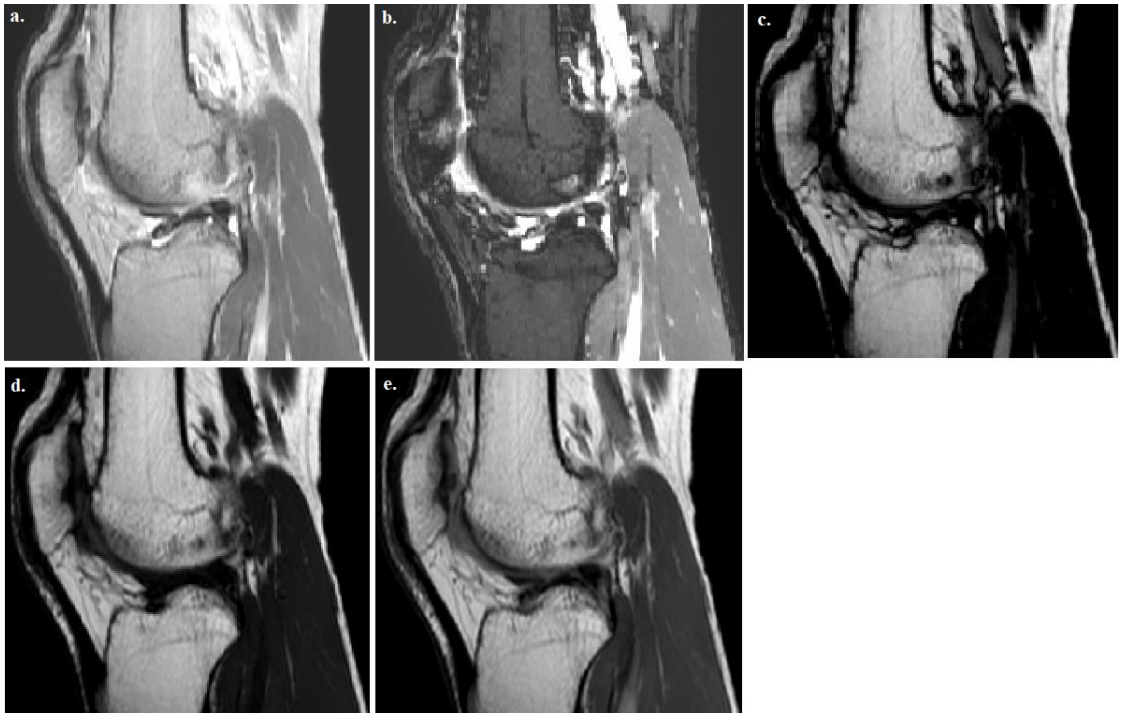

Figure 8.16. Sagittal images of single slice inversion recovery sequence of the knee joint from a participant with 5 different TI series. (a) to (e) correspond to SSIR images with TI of 100, 300, 700, 1500, and 3000 ms.

For fat fraction comparison with spectroscopy (table 8.1), the size and location of the ROIs on six adjacent slices of the mDixon Quant sequences were visually matched to the VOIs in the MRS, as shown in figure 8.2. The single slice limited matching of the SSIR and spectroscopy; normal marrow was measured in the subchondral bone marrow of the trochlea instead of the lateral femoral condyle.

	First Scan			Second Scan		
Regions	**mDixon Quant FF (%)**	**SSIR FF (%)**	**MRS FF (%)**	**mDixon Quant FF (%)**	**SSIR FF (%)**	**MRS FF (%)**
BML	70.5	68.4	64.9	71.5	69.1	67.1
Normal-appearing marrow near BML	89.8	90.7	87.9	90.8	92.6	98.9
Normal marrow	93.1	90.4	97.9	93.7	94.1	98.2

Table 8.1. Fat fraction measurements of BML and normal marrow of the participant using MRI and MRS methods

For comparison of T1 between SSIR and VFA, ROIs on the SSIR image were matched to ROIs on 2 slices of the VFA images (table 8.2).

	First Scan		Second Scan	
Regions	**SSIR T1 (ms)**	**IP VFA T1 (ms)**	**SSIR T1 (ms)**	**IP VFA T1 (ms)**
BML	576.5	631	558.8	631.8
Normal-appearing marrow near BML	413.6	467.6	403.8	427.2
Marrow	396	415.5	392.1	408.8

Table 8.2. T1 relaxation times of BML and normal marrow of the participant on SSIR and VFA sequences

Examples of monoexponential and biexponential T1 fitting curves from a BML in the participant are shown in figure 8.17.

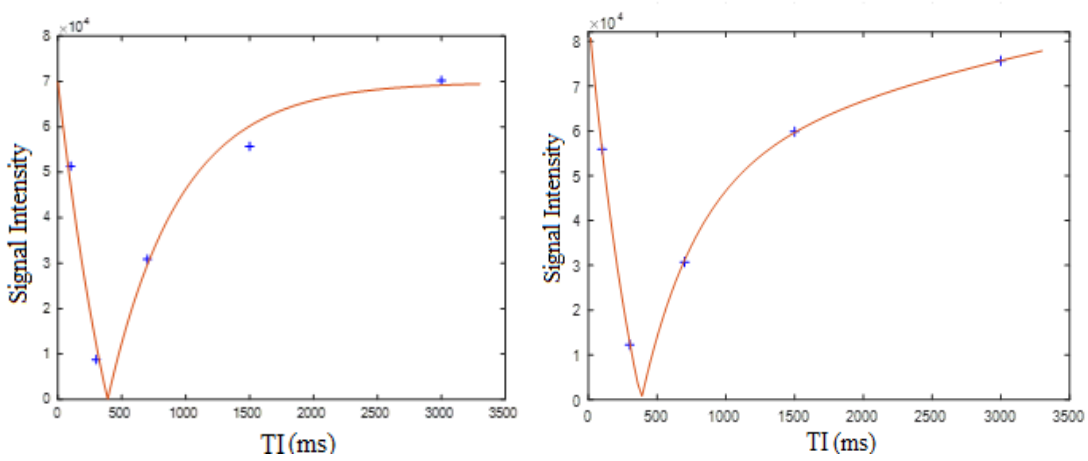

(a) (b)

Figure 8.17. Example of single pixel fit from the BML of a participant (a) monoexponential (b) biexponential showing the expected improved fitting with the biexponential fit.

Examples of MR spectra obtained from rectangular VOIs in the BML, and normal marrow of the participant are shown in figure 8.18.

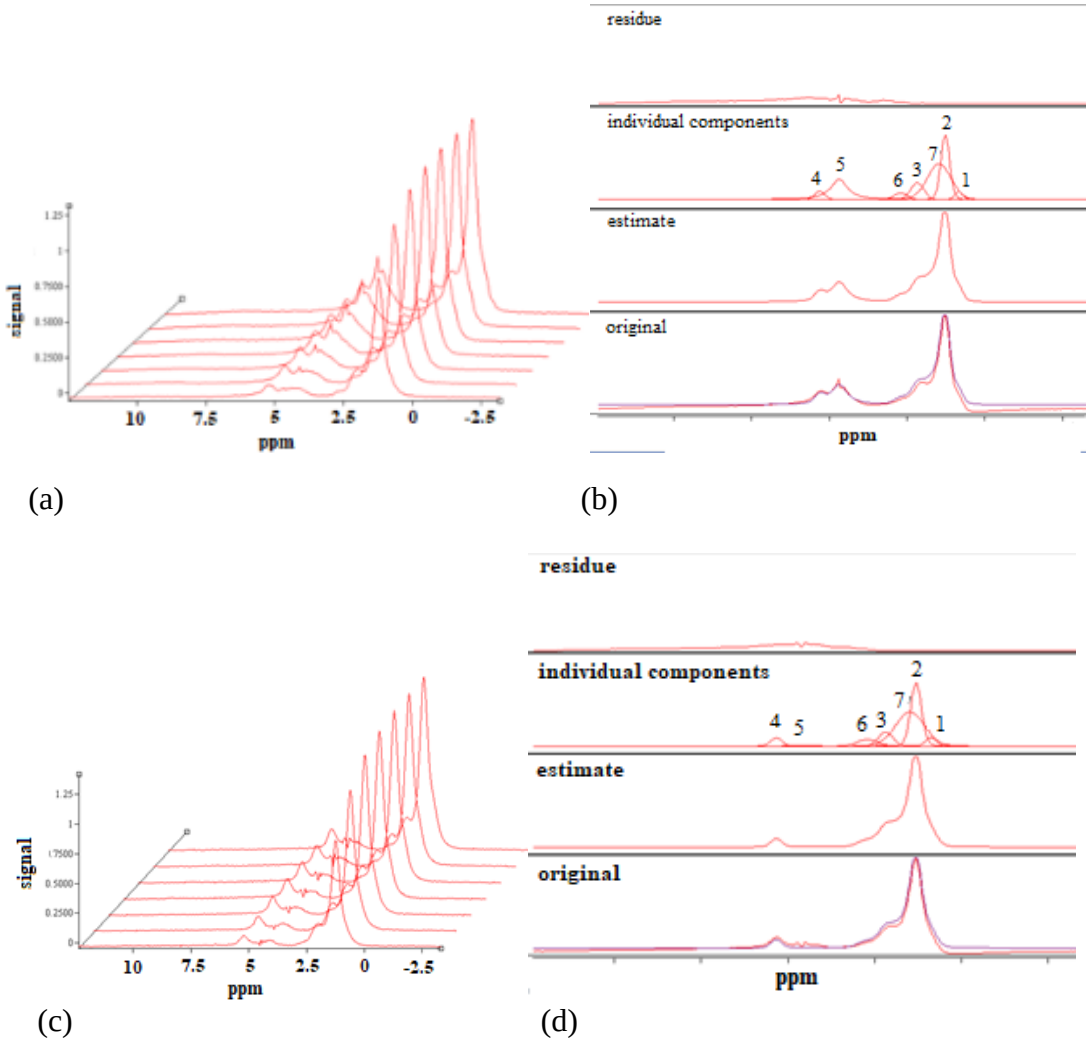

Figure 8.18. Single voxel MRS. (a) and (b) show the spectra from the BML and normal bone marrow, respectively. MR spectra series at different TR obtained by using STEAM (TR= 310, 600, 1000, 1500, 2000, 3000, and 5000 ms) from the VOIs displayed in figure 2. Various peaks are indicated for fat at 0.90 (1), 1.30 (2), 1.60 (7), 2.06 (3); 2.82 (6), and 5.26 (4) ppm, and the water peak is indicated at 4.65 (5) ppm. The measured spectra were fitted in jMRUI (AMARES) software, the longest TR are shown in (b) and (c).

Comparison between mDixon Quant and SSIR FF for 10 different locations (matched ROIs) is shown in figure 8.19. There was a very strong linear correlation linear between mDixon Quant FF and SSIR FF ($r= 0.980$; $p< 0.05$) with a mean bias of 0.5 ± 3.0 % (95% CI -1.7 to 2.6).

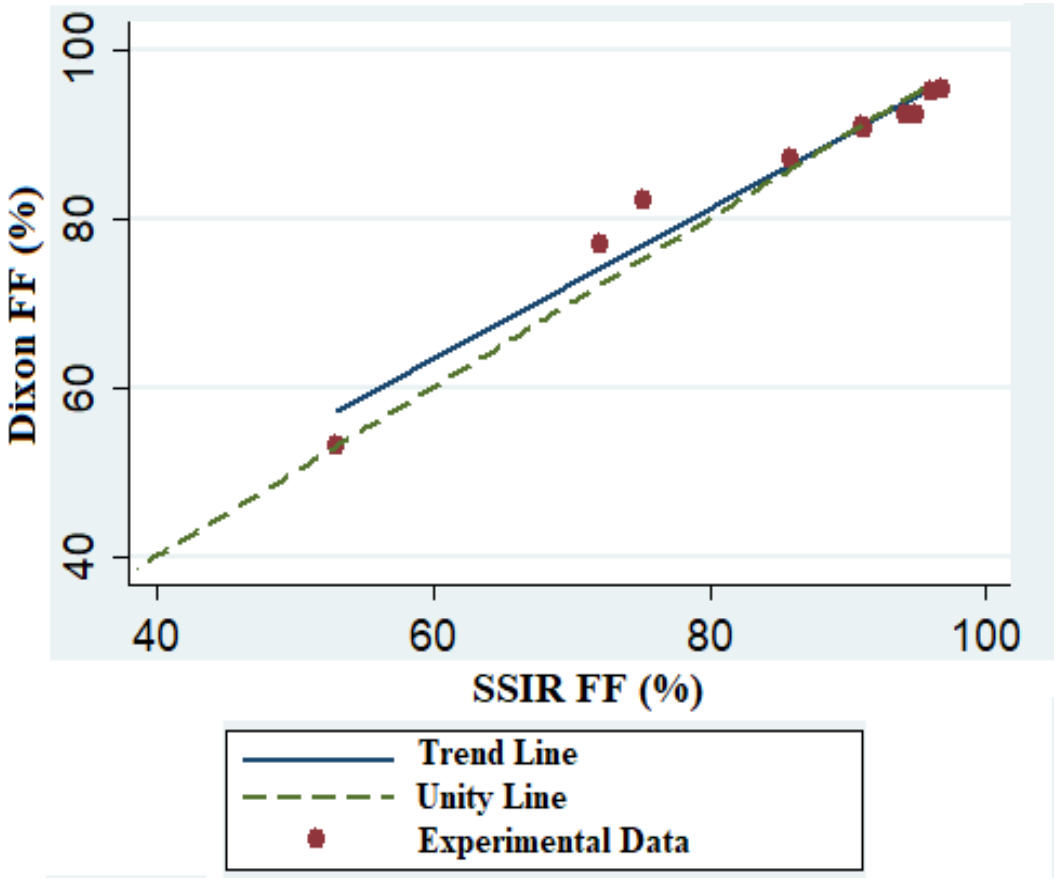

Figure 8.19. Comparison between mDixon Quant FF and SSIR FF shows a strong linear correlation. The solid line represents the trend line and dashed line indicates perfect agreement.

8.3.3 Clinical feasibility study

There were six symptomatic knee OA patients (two men and four women), mean age 58.5 years (SD ± 6.6). Examples of a BML on in SSIR T1 and FF map are shown in figure 8.20.

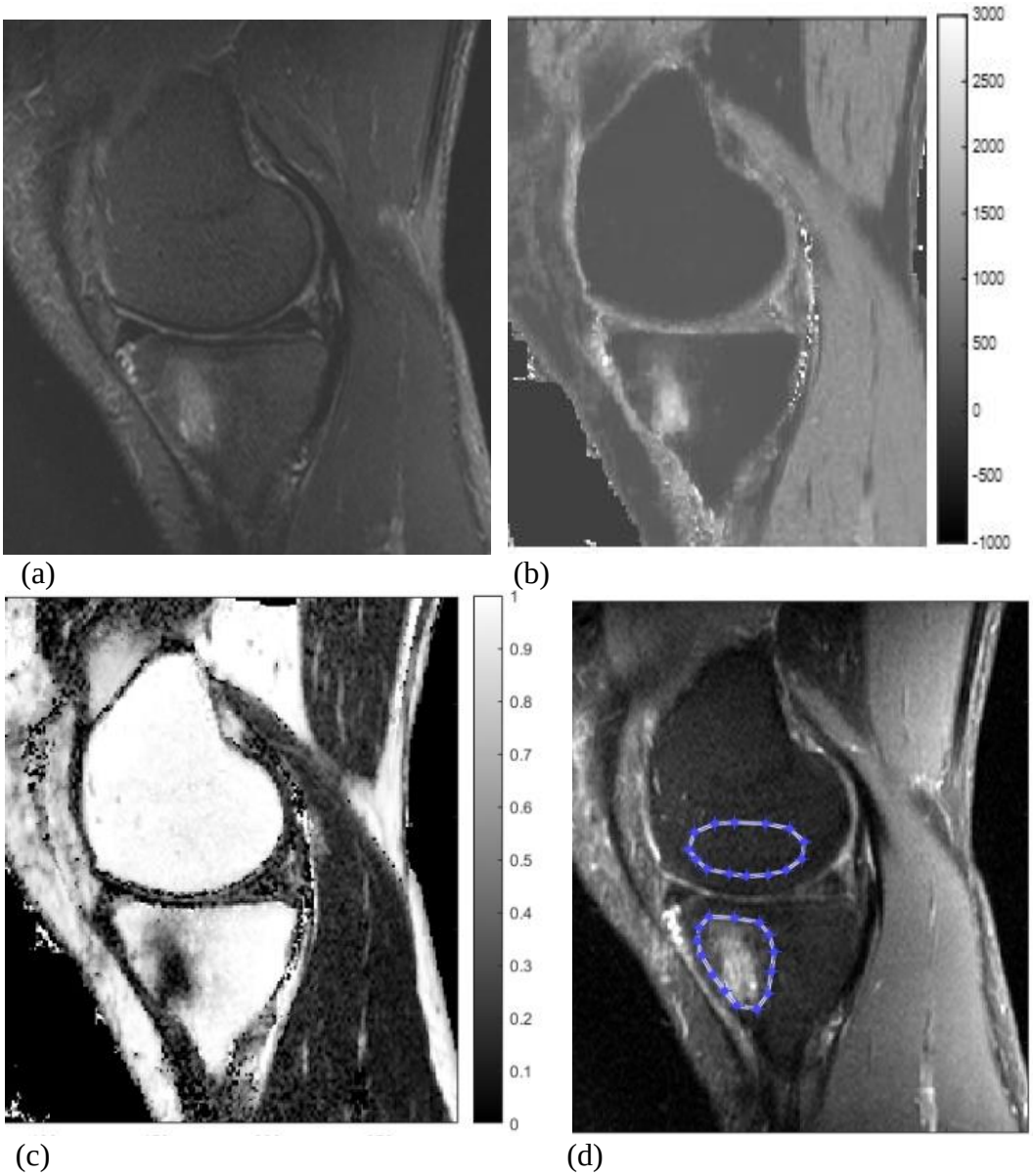

Figure 8.20. Sagittal images of knee OA patient on STIR image (a), monoexponential SSIR T1 (b) and biexponential FF maps (c) show subchondral BML in the tibia. (d) shows ROIs of the BML and normal bone marrow which were drawn on the inversion recovery image with TI= 200 ms.

Results of T1 values of monoexponential fitting of inversion recovery sequences of knee OA patients are shown in figure 8.21. T1 for each patient was calculated as the median value of pixels within the ROIs and the value across all patients was reported as median and interquartile range (IQR). T1 values for normal-appearing marrow were similar across all patients, ranging from 388.4 to 411.3 ms with median 399.0 ms (Interquartile range [IQR] 395.8 – 410.2). The median T1 of BMLs was significantly higher at 798.1 ms ($p < 0.05$, IQR 528.6 – 911.1), see figure 8.21.

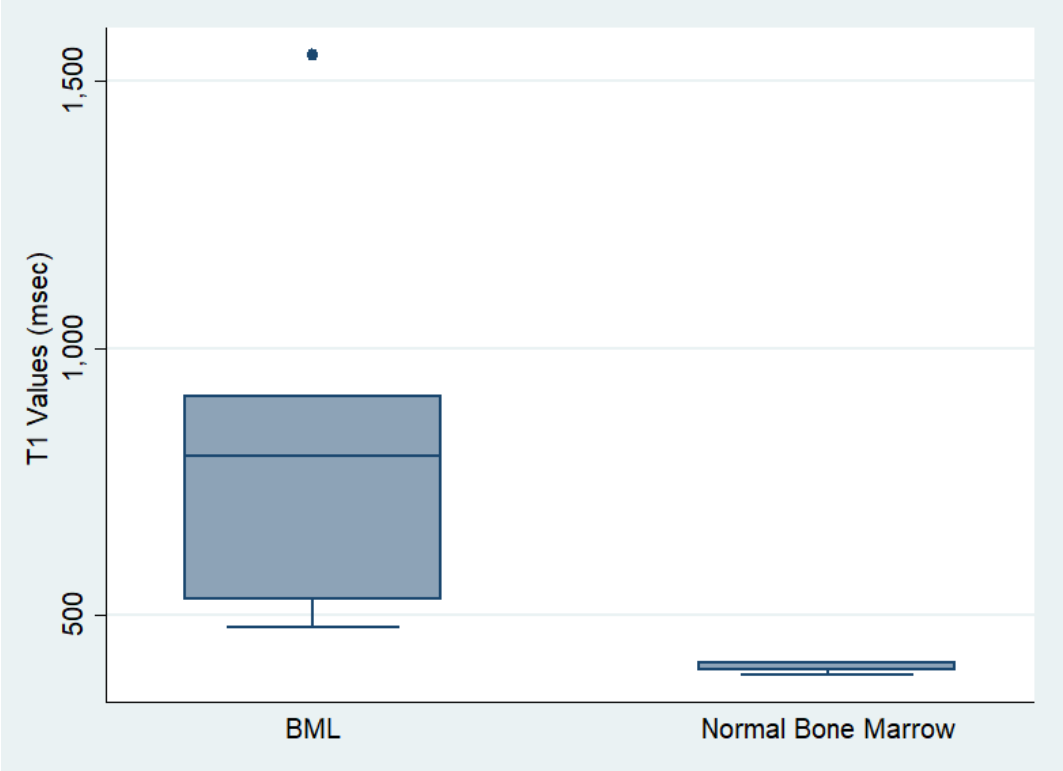

Figure 8.21. Boxplots of T1 relaxation times of BML and normal bone marrow measured using monoexponential fit of inversion recovery images. The boxes represent the interquartile range, the horizontal lines in the boxes represent the median values.

The boxplots show the range and distribution of T1 values for BML and normal bone marrow. There is a greater variability for T1 values of BMLs, ranging from 477.6 to 1550.1 ms, though the boxplots of BMLs and normal marrow do not overlap.

Based on the biexponential fit method, FF of subjects' BMLs was significantly lower (Wilcoxon sign-ranked test $p < 0.05$) than normal bone marrow (52.7% [IQR 42.7 – 75.2] vs 90.8% [IQR 89.3 – 91.8]), see figure 8.22.

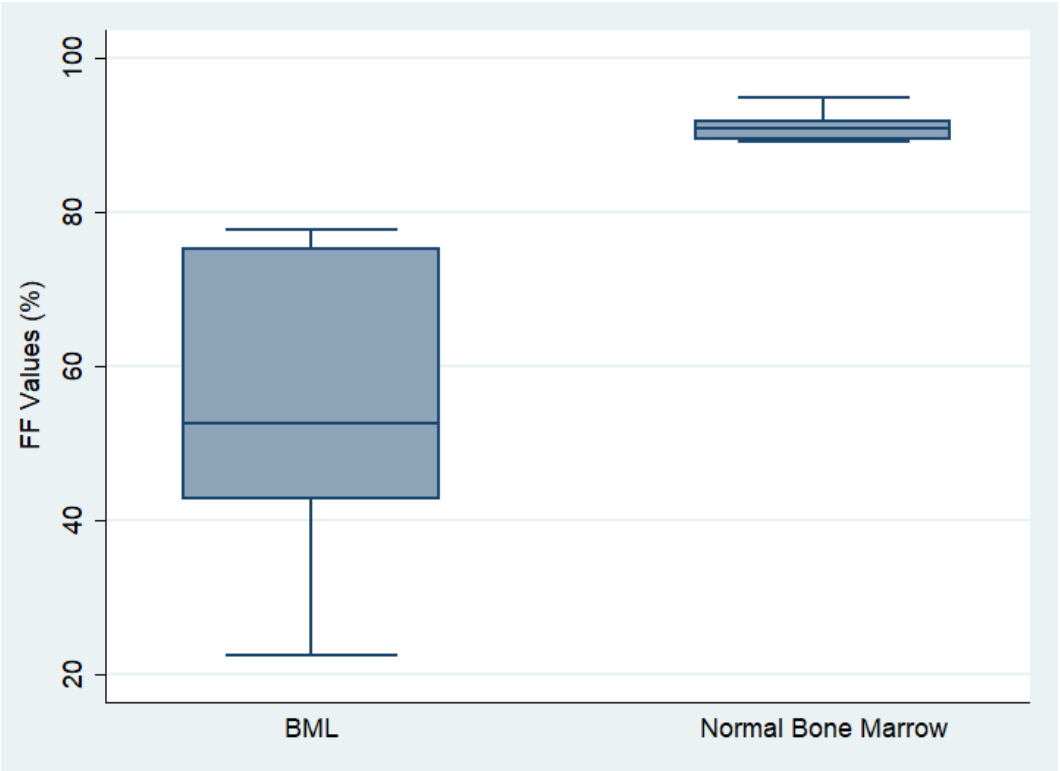

Figure 8.22. Boxplots of fat fraction values (as percentage) within the ROIs of BML and normal bone marrow. The boxes represent the interquartile range of the FF values and the horizontal lines in the boxes are the median values.

The graph shows that the range of FF for normal bone marrow were relatively narrow, ranging from 89.1 to 94.8%. Although the range of FF values of BMLs were wider from 22.6 to 77.7 %, values of BML and normal marrow do not overlap.

8.4 Discussion

This study looked at MR spectroscopy fat fraction (MRS FF), mDixon Quant fat fraction (mDixon Quant FF), T1 estimates (from VFA and SSIR), and novel biexponential inversion recovery T1-based estimation of fat fraction (SSIR FF) in a fat-water-bone phantom (FWB phantom) and a subject with a bone marrow lesion. SSIR T1 and SSIR FF were also measured in a small number of OA knee patients to compare values in BMLs and normal-appearing marrow. The present study found that mDixon Quant FF was accurate for fat fraction quantifications over a wide range of FF

of fat-water emulsions with and without the presence of bone granules when compared to the gold standard of spectroscopy.

Preliminary in vivo study of knee OA patients using a monoexponential inversion recovery method showed significantly longer T1 relaxation times in BMLs than nearby normal-appearing bone marrow (figure 8.21). The reduction of T1 with bone and a wide range of FF in the FWB phantom was also shown (figure 8.13 and 8.14). T1 values of the FWB phantom assessed using 3D VFA T1 mapping were slightly higher compared to monoexponential SSIR with a strong linear relationship between them (figure 8.15).

A novel, alternative technique for estimating FF using a biexponential T1 model with single slice inversion recovery (SSIR FF) was also assessed. The results showed SSIR FF was also significantly lower in BML than normal-appearing bone marrow (figure 8.22). There was a good agreement between mDixon Quant FF and SSIR FF on a single participant with a BML (r= 0.980; figure 8.19). However, in the FWB phantom, SSIR FF was less well correlated with MRS FF than mDixon Quant FF was (r=0.932, figure 8.10 vs r=0.991, figure 8.7).

Although fat fraction quantification with both mDixon Quant and biexponential SSIR methods were strongly correlated with MRS FF, the best agreement between MRI and MRS in vitro was achieved using the mDixon Quant sequence. On average, the difference between mDixon Quant FF and MRS FF was very small, whereas the difference between SSIR FF and MRS FF was considerably larger.

8.4.1 mDixon Quant FF

The results of the analysis confirmed that estimates of FF from mDixon Quant MRI sequences suitable for knee imaging are similar to those obtained using MR

spectroscopy in the FWB phantom. Dixon imaging has been extensively validated in phantoms, focusing particularly on sequences and phantoms relevant to liver imaging [116]. Similar to our results, a previous FWB phantom study using Dixon sequences showed excellent correlation with true FF values and little effect of variation of bone concentration [108]; however, spectroscopy was not included, and the authors recommended that comparison with MR spectroscopy should ideally be performed as gold standard. In addition, the current study extends that work by applying it to a higher resolution sequence suitable for knee assessment.

In the study there was a very strong correlation between mDixon Quant and MRS with only a small bias, with mDixon Quant FF slightly higher than MRS FF. Good agreement with MRS is in keeping with previous results of a study using lower resolution sequences, including in fat-iron phantoms [203].

Preliminary results of the present study from a single participant showed good scan-scan reproducibility for mDixon Quant imaging (table 8.1). Results from spectroscopy of normal-appearing marrow near BML were less reproducible, which may be due to difficulty in reproducibly positioning the large spectroscopy voxel at a boundary. Although marrow near BML visually looked normal the mDixon Quant sequence was able to detect lower FF compared to normal bone marrow far away from BML, suggesting it may be a sensitive measure of bone marrow change.

The mDixon Quant sequence has several advantages over MR spectroscopy for fat fraction estimation as it can measure fat content throughout the knee with high spatial resolution in clinically feasible acquisition times. It is now widely available on clinical scanners with automated fat fraction calculation. Furthermore, postprocessing is considerably easier and faster than with MRS.

8.4.2 T1 relaxation time measurements

There were significant differences in T1 values between BMLs and normal-appearing marrow using a monoexponential T1 fit of SSIR images in patients with knee OA. Previous work on MRI T1 relaxometry of subchondral bone marrow and BMLs in knee OA is limited. T1 of normal bone marrow of the knee in the present study is close to the value reported in a study on 5 healthy younger individuals using a spin-echo inversion recovery sequence (399.0 vs 381.2 ms) [202]. T1 relaxation time measurements have been used for assessing a number of diseases involving bone marrow, including Gaucher [143], sickle cell [204, 205], anorexia nervosa [206], leukaemia [207], and polycythaemia vera [208]. More recently T1 relaxation time measurement has been successfully used in ankylosing spondylitis where T1 was shown to increase with increasing disease activity and decrease following treatment, suggesting that monoexponential T1 measurement may be useful for quantifying bone marrow oedema [139]. The current study suggests that T1 measurement may also be useful in knee OA.

Monoexponential T1 estimates of bone marrow combine effects of the T1 of the water, the short T1 of the fat, and their relative proportions. The present study showed large decreases of T1 with FF in the range of low FF (0 – 38.5%), although the relationship was quite flat around 50-70% FF (figure 8.14). Previous in vivo studies have also shown a decrease in T1 with increasing fat fraction [143, 206, 209, 210]. Monoexponential T1 mapping described in this study also showed a decrease in T1 with the presence of different bone granule concentrations, so may depend on trabecular bone as well as bone marrow composition. The findings using monoexponential T1 measurement of 100% FF phantom (peanut oil) in this study are

in reasonable agreement with a previous study of peanut oil [202] that used inversion recovery to calculate T1 (297.1 vs 280 ms).

There was a strong linear relationship between T1 values of the phantom assessed using 3D VFA and SSIR sequences (figure 8.16), although T1 values assessed using 3D VFA were slightly longer (62.7 ms). The T1 relaxation time for the 100 % FF phantom using the VFA method was slightly higher than from the SSIR method (301.3 vs 297.1 ms). Similarly, slightly longer T1 relaxation times were observed in the BML and normal marrow of the participant (table 8.2). The 2 sequences gave similar T1 estimates despite well-known potential limitations in trabecular bone of VFA T1 and B1 mapping using gradient echo sequences optimised for a single water component in soft tissue, due to the short T2*, the short T1 of fat and phase differences between fat and water; in this study, short echo times were used with the main fat and water peak in-phase for the VFA sequence. Compared to the SSIR method, one of the major advantages of the VFA sequence is that it permits measurement of T1 from a 3D volume in a relatively short time. The 3D sequence can also reduce through-slice chemical shift. Chemical shift, including in-plane effects are likely to be more important in BMLs (including at their sharp subchondral margin) than in diffuse disease (e.g., in liver), although high bandwidths were used in the current study to help reduce this. The SSIR sequence used also differs from the VFA (and mDixon Quant) sequence as it is more heavily T2 weighted, with the consequence that shorter T2 moieties (e.g., fibrosis) may not be included in the measurement; further work will be required to determine whether this is beneficial or not.

8.4.3 SSIR FF estimation

SSIR FF was significantly lower in BML than normal-appearing bone marrow in knee OA patients. FF values of normal bone marrow using biexponential T1 mapping are within the range of the preliminary study of FF using a mDixon Quant sequence (see chapter 7). In that study 17 subjects with painful knee OA were assessed and the mean FF of normal bone marrow was 92.1 % (SD= ±2.5). Further, similar to the results of the biexponential T1 mapping, mDixon Quant FF values of BMLs were significantly lower (72.5 % ± 8.6) than FF of normal bone marrow. Previous MR spectroscopic imaging studies have also reported an increase of water content within BMLs in knee OA subjects compared to normal bone marrow of healthy subjects (Chapter 7). Therefore, increased water component within BMLs may explain the reduced fat fraction and increased T1 relaxation time.

To the best of our knowledge, fat fraction estimation using biexponential T1 mapping has not been done previously on BMLs in knee osteoarthritis. Quantitative biexponential mapping has been widely used to map T2 values in vivo [199] and T2 has been used to calculate fat and water fractions of diseased muscle [198]. Biexponential mapping is designed to separate the different contributions of the fat and water T1/T2 components to allow to the fat and water fractions in each voxel to be quantified.

The biexponential inversion recovery FF of the phantom was reasonably well correlated with mDixon Quant FF. Compared to MRS FF, SSIR FF tended to overestimate the FF in the phantom although better agreement was found in a participant with a BML (figure 8.19). Poorer results in the phantom may be due in part to the fast spin echo SSIR sequence with a longer echo time and T2 and J-coupling

effects leading to increased fat signal and overestimation of FF compared to the mDixon Quant sequence or spectroscopy. This may be less pronounced in-vivo as T2 relaxation times of BMLs may be longer than those of agar [211, 212]; T2 values of BMLs are poorly characterised, however BMLs are widely accepted to be well visualised at longer TEs such as those used here (Chapter 2). Another potential cause of lower agreement between mDixon Quant and SSIR FF estimates in the phantom is the bicomponent fat fraction model which assumes independent T1 relaxation times for water (variable) and fat (fixed). Previous phantom work that used safflower oil (Latin name *Carthamus tinctorius* belonging to the sunflower family Asteraceae [213]) looking at the effect of fat fraction on fat T1 differed, developing a more complicated model for different peaks but suggesting changes to the main methylene fat peak T1 were small, may depend on the precise details of the emulsion [214], with little effect in vivo [215]. This could be addressed by allowing the T1 of fat to vary in the model, although this may reduce robustness.

Overall, the initial results from SSIR FF show some promise for BML assessment, though it requires further MR validation including in a phantom with a longer T2 that better matches the T2 of BML and/or using shorter effective echo times. Further correlation studies with well validated techniques, such as mDixon Quant or MR spectroscopy across multiple patients are necessary. The optimisation of biexponential mapping for practical use is also important, for example using Look-Locker techniques may allow accurate relaxation curve characterisation across the whole knee in clinically feasible scan times.

There are some limitations to be considered in interpreting the results. The phantom has a number of limitations as a model for subchondral bone marrow lesions in the knee. The small number of phantom components with bone granules (0 %, 19.1 %,

38.6 %, and 58.6 %) could be addressed in future studies by adding bone granules to more fat fractions. There are differences in T1 relaxation times of peanut oil and fatty arrow and potential differences in T1 between agar in the phantom and the unknown and likely spatially dependent T1 of the water component within BMLs. The T2 values of the water component in the phantom may be shorter than in BMLs, the bone granules used in the phantom contain only mineral with no collagen and the trabecular structure is not accurately modelled [108]. The distribution of fat in the phantom emulsion may be different from that in marrow adipocytes and the phantoms may not be perfectly homogeneous [108]. The phantom was imaged at room temperature rather than body temperature. Variations in temperature may influence the chemical shift between fat and water [216] and have an effect on the results of the phantom study.

Unlike some previous studies that focussed on liver, the present study included a full range of fat fractions, however there was large gap between 68.6% and 100% FF due to limitations of oil-water phantom composition as mentioned in previous work, even more so with the addition of bone granules [108]. This region of high FF (60 to 100 % FF) is important for BMLs (Figure 7.2), although the results in a single participant with a BML with FF in this range helps to overcome this limitation. A further limitation is that MR spectroscopy was performed with T1 correction but not T2 correction, although TE was chosen to be short while still allowing for accurate VOI definition.

Spectroscopic, mDixon Quant, and VFA techniques were only compared in a single participant with BML. The number of OA subjects studied was small though despite this we were able to show a significant difference between normal bone marrow and BMLs. The fixed T1 of fat came from a younger population [202]. The study did not investigate the T1 value of normal bone marrow in the knee of subjects without OA.

The approach which was taken used a single slice inversion recovery image and may not represent the true 3D properties of BMLs. Direct comparison of regions of interest on the inversion recovery sequence to the spectroscopy VOI was limited by the single slice, however ROIs could be better matched to the 3D mDixon Quant images. The acquisition times for the inversion recovery sequences in the present study was relatively long as multiple inversion times were required for biexponential fitting, limiting the application of the technique in clinical studies. For monoexponential fitting, the VFA sequence appears promising and allows coverage of the whole knee. Finally, this study did not evaluate the correlation of fat fraction and T1 values with any clinical symptoms or treatment effects.

The quantitative measurements presented in this study potentially offer more informative methods for the assessment of BMLs and may complement conventional MR imaging and BML volume measurements. Further research focusing on the feasibility and reliability of MRI-based fat fraction and T1 quantification in a larger number of subjects and different MR scanners is needed. Another interesting application in individuals with symptomatic knee OA would be to compare these measurements with conventional quantitative MRI volume-based measurements, cross-sectionally or longitudinally.

In conclusion, the results of this study support the value of mDixon Quant imaging for providing 3D high-resolution fat fraction maps of the knee as an accurate method for a wide range of fat fractions and different concentrations of bone. In addition to good reliability, it has advantages over methods such as spectroscopy as it provides high spatial resolution over a large field of view in feasible acquisition times.

T1 measurements show potential for BML assessment and quantitative discrimination of BML from normal marrow; further work is needed to develop clinically feasible protocols and determine whether T1 provides additional useful information over fat fraction measurements using mDixon Quant imaging. The novel T1-based estimate of fat fraction also appears feasible for discriminating BMLs from normal marrow and avoids some of the potential limitations of gradient echo mDixon Quant techniques. However, further development and validation is needed before it can compete with mDixon Quant imaging.

T1-based MR imaging techniques provide additional quantitative measurements to standard MR imaging and offer an alternative approach for the assessment of BMLs in knee OA.

Chapter 9

Discussion

Chapter 9

Discussion

9.1 Summary

In this chapter, the main findings from the research outlined in the thesis are summarised. Discussion of the findings in relation to the literature and important limitations are considered in individual results chapters (chapters 4-8). In this chapter the novelty of the findings and potential influence for clinical research studies are considered and also areas for future research.

9.2 Novel findings

The studies presented here have shown some novel findings to help improve the current approach of quantitative MRI-based BML assessment in knee OA. The data also provide some initial evidence of potential utility of the mDixon Quant sequence, 3D VFA T1 mapping, and biexponential T1-based fat fraction mapping as potential compositional measurements of BMLs.

9.2.1 Volumetric and compositional assessments of BMLs

In this thesis, a number of conventional MRI sequences have been directly compared for volumetric assessment of BMLs. The key finding of the comparison study between different conventional MRI sequences is that non-contrast enhanced fluid sensitive sequences (PDFS and STIR sequences), contrast enhanced T1-w sequence with fat suppression, and 3D GE mDixon Quant water only images all gave broadly similar measures for BML volume. PDFS or IWFS sequences are commonly used for BML size assessment, not least because they are part of the OAI protocol. The results here

broadly support the use of PDFS/ IWFS sequences for assessing BML volume. STIR images showed similar performance to PDFS for measuring BML volume, in keeping with prior recommendations, suggesting that future studies could use STIR as an alternative to PDFS for assessing BML volume. Water-only mDixon Quant images have also shown similar performance compared to PDFS for BML volume measurements. The broad agreement between PDFS and water-only mDixon Quant images in this study is consistent with previous work concluding 3D GE Dixon sequence was a suitable alternative for assessing bone marrow oedema in the hands of patients with rheumatoid arthritis after intravenous gadolinium-based contrast agent [186].

BML composition remains poorly understood and conventional volume measurements are limited in their assessment of BMLs as they provide no insight into changes deep within the lesion. Here, a new approach to the assessments of BMLs in knee OA using mDixon Quant sequence is presented. The results of FF measurements of mDixon Quant sequence in a small number of knee OA patients found that FF values were significantly lower in BMLs than normal-appearing marrow. The data suggests that FF measurements can depict changes in bone marrow composition in areas within BML, which can be viewed as increased water content and reduced normal fat marrow.

FF measured using the mDixon Quant sequence is relatively straightforward to understand and has the potential to provide useful insights into the pathophysiology of symptoms, natural history, and response to treatment of BMLs. It is relatively robust, more consistent across positions, and times and is less sensitive to field inhomogeneities. Preliminary study in Chapter 7 showed correlation with BML volume measurements using conventional MRI sequence providing some evidence of

validity for assessing longitudinal change and offers an alternative to BML volume measurement for longitudinal studies of BMLs.

9.2.2 Phantom study

The phantom study in chapter 8 extends previous work [108] by applying mDixon Quant sequence to a higher resolution sequence suitable for knee assessment and by using MR Spectroscopy as the reference, confirming the accuracy of FF estimates from the mDixon Quant sequence.

9.2.2.1 mDixon Quant imaging

Fat fraction assessed using 3D GE mDixon Quant imaging of the fat-water-bone (FWB) phantom was strongly correlated with fat fraction assessed using MR spectroscopy suggesting it is an accurate measure of fat fraction. Although MRS enables us to measure fat content with high accuracy, it requires more complex data processing and highly specialised/ trained personnel and time consuming. It evaluates only a single voxel that may lead to misinterpretation in the case of heterogeneous fat content within BML. Compared to MR spectroscopy, mDixon Quant images which cover the entire joint can be acquired with high resolution in reasonable times and are straightforward to acquire on many clinical scanners.

9.2.2.2 T1 imaging

Using a phantom, T1 values using SSIR and VFA methods mostly decreased as fat fraction increased. There was a strong correlation between VFA T1 and SSIR T1 in FWB phantoms, suggesting VFA is a potential alternative to SSIR T1 measurements allowing faster whole knee joint coverage.

In addition, a preliminary study of a small number of patients with knee OA in chapter 8 showed a significant difference between T1 of BMLs and normal-appearing marrow, suggesting that T1 estimates may be a potential alternative compositional measurement. This was the first study to look at inversion recovery sequences in the setting of knee OA to evaluate T1 relaxation times.

9.2.2.3 SSIR FF measurement

Assessment of FF of the FWB phantom using mDixon Quant imaging was more strongly correlated with composition assessed using MR spectroscopy than was SSIR-FF. A good correlation was found between SSIR FF and mDixon Quant FF in a single subject with a BML. Further, a preliminary study of SSIR FF in a small number of knee OA patients showed that fat fraction was significantly lower in BMLs than in normal bone marrow.

9.3 Possible future studies

9.3.1 Gradient echo MRI sequences for volumetric assessment of BMLs

T1-weighted FFE images could not detect the full extent of BMLs seen on PDFS images. However, BML size from 3D GE mDixon Quant images used in chapter 6 was broadly similar to size assessed using PDFS and the measurements from the sequences were correlated. The finding differs from previous reports which tended to advise against gradient echo images [77, 177], albeit based on data from different sequences. A number of features of the mDixon Quant images discussed in Chapter 7 may make them more sensitive to detect BMLs than FS T1-w FFE, including reduced effects of short T2* due to trabecular bone (commonly put forward as the reason for gradient echo insensitivity), reduced T1 sensitivity (the importance of which is demonstrated in chapter 8), high bandwidth and robust fat-water separation.

T1-w GE echo images may not fully visualise BMLs, and care must be taken in choosing the parameters for gradient echo imaging based on work presented here. It may be possible to further mitigate this, e.g., with longer repetition times or T1 correction to further reduce T1 effects; further work is needed to investigate if this is worthwhile.

In contrast to sequences where T1 weighting reduces signal from long T1 tissues, STIR images reduce signal from short T1 tissues. STIR images showed similar performance to PDFS for measuring BML volume, in keeping with prior recommendations [15, 82], suggesting that future studies could use STIR as an alternative to PDFS for assessing bone marrow lesion volume. mDixon Quant water-only images may also be adequate with appropriate choice of parameters.

The sensitivity of STIR and mDixon Quant for measuring BML volume also has implications for the compositional imaging of T1 and fat fraction measurements. If STIR and mDixon Quant were unable to image the full extent of BMLs, it would be less likely that the compositional mDixon Quant FF and T1 techniques would be able to assess the full range of BML composition, particularly at the edges where BML composition is likely to be closest to normal marrow.

9.3.2 Compositional MRI

9.3.2.1 3D GE mDixon Quant imaging

3D GE mDixon Quant imaging currently appears the most promising technique to enhance the current approaches of BML assessments in osteoarthritis despite previous concerns about gradient echo imaging in the literature. This technique is potentially useful for both volumetric and compositional assessment of BMLs and amenable to

use with semi-automated image analysis systems with reduced manual segmentation requirements.

The work in the thesis focused on GE mDixon Quant imaging. However, spin-echo (SE) mDixon Quant imaging has also been widely used as an alternative to conventional imaging with similar contrast for assessing bone marrow [167-169, 175, 217] and can also be used to derive fat fractions. One study using SE Dixon images has shown equivalent results of fat fractions to GE Dixon imaging in vertebrae, however, both sequences used 2-point Dixon imaging without T2* compensation [217]. Further work will be needed to compare FSE mDixon Quant and 3D GE mDixon quant for assessing BMLs. Furthermore, SE images lack some other advantages e.g., 3D imaging.

9.3.2.2 SSIR-based T1 and FF measurements

T1 values measured using the SSIR method were significantly higher in BMLs than in normal-appearing marrow. To our knowledge, this is the first study to look at T1 values using inversion recovery sequences in the setting of knee OA. This provides additional evidence that T1 may be a useful compositional technique, supporting previous work showing STIR is sensitive (Chapter 5), T1-weighted sequences are discriminatory [85] and T1 is useful for monitoring bone marrow changes in other diseases [143, 204-208, 218], including bone marrow oedema in ankylosing spondylitis [139]. T1 measurement of BMLs is, however, less well developed than mDixon Quant fat fraction. The single slice sequences used are not able to assess the entire BML.

Although the novel T1-based MRI technique shows some promise, it is less well-validated and will require substantial further development and validation work. T1

quantification with VFA gradient echo images gave similar results in phantoms compared to SSIR but given the variable performance of gradient echo imaging for assessment of BML volume, further work will be necessary to determine if they are suitable for imaging in knee osteoarthritis. Longitudinal T1 studies are yet to be undertaken, unlike mDixon Quant imaging (Chapter 5).

T1 is less straightforwardly linked to the underlying pathophysiological changes than mDixon Quant fat fraction, although fat fraction is likely to be an important determinant of T1 as in phantoms (chapter 8). Using a biexponential model, fat fraction was estimated from the SSIR recovery curve. This novel approach generated SSIR-FF which showed significant differences between BMLs and normal marrow, perhaps not surprisingly given the differences in monoexponential T1 described above. Results in a single participant correlated well with mDixon Quant imaging, however phantom results were less successful, possibly contributed to by limitations of the phantom for this application discussed in chapter 8. The motivation for this work was to develop a measure of fat fraction from spin-echo imaging which would be less sensitive to problems of gradient echo images which have led to them being advised against for BML assessment [77]. However, unlike other gradient echo sequences, the optimised mDixon Quant sequence appears much more similar to spin echo techniques for visualising BMLs, so this may be less important. Consequently, while the novel T1-based fat fraction estimation does offer some promise, the 3D GE mDixon Quant technique is currently better developed and validated for studying BMLs.

9.3.2.3 Combined T1 and mDixon Quant techniques

In this thesis, 3D GE mDixon Quant imaging and T1 mapping techniques were studied independently. An alternative spin echo technique for fat fraction estimation was investigated from T1 mapping, assuming a fixed T1 of fat, in part motivated by concerns about the reliability of 3D GE mDixon Quant imaging in trabecular bone. However, the results of this thesis support the validity of 3D GE mDixon Quant imaging of bone marrow and it would therefore seem reasonable to consider using it for T1 measurement in future studies of BMLs. This would potentially allow more accurate and independent estimation of fat and water T1 relaxation times in bone marrow to determine whether water T1 relaxation time provides any additional useful information in addition to that from fat fraction. This could be done using a number of different approaches including: (1) Using the fat fraction from mDixon Quant imaging as an input for the biexponential fit of the T1 relaxation curve. This would allow either estimation of both fat and water T1, or if the fat T1 is fixed, more robust, faster estimation of the water T1 relaxation time. Care would be needed to match the mDixon Quant and T1 mapping sequences e.g., for similar echo times, so the fat fractions for both techniques would be comparable. (2) T1 calculation from water-only VFA mDixon Quant images [219]. (3) magnitude-only VFA mDixon Quant assuming shorter fat T1 to resolve fat water ambiguity [209, 220, 221]. (4) MR fingerprinting using sequences with varying parameters and dictionary references derived from Bloch equation simulations [198, 222-227].

9.4 Clinical validation studies

The focus of the comparison studies between different MRI sequences was on the reliability and sensitivity in detection of BML size. Because of the standardised

imaging protocol, the influence of contrast dose or timing of contrast enhanced sequence on BML volume and other imaging sequence parameters which may potentially have an impact on outcome were not examined and for which further studies are needed. Further, this study was cross-sectional, and it did not look at predictive ability and sensitivity to change which are important in determining an optimum imaging sequence. Future clinical studies exploring the impact of a range of MRI sequence parameters on BML volume, including TR and TE in PDFS sequences, the dose of contrast agent and the timing of the acquisition following contrast injection would help inform optimum parameters to use when using these sequences.

Clinical validation studies are also needed to determine the sensitivity to change in BML volume using mDixon Quant sequence. Also, studies could look at the predictive ability of BMLs, assessed using conventional and mDixon Quant sequences, for clinical outcomes including pain and function. It is possible that one or more of these imaging sequences may be more sensitive to change and for predicting outcome, in which case there would be a strong argument for using those sequences in clinical research studies.

In relation to compositional MRI methods, the number of subjects studied in this thesis is relatively small. The reproducibility of fat fraction quantification of mDixon Quant was evaluated only on one subject. The reduced fat content of BMLs compared to normal marrow reported in Chapters 7 and 8 highlights the need for further clinical studies including:

(1) Scan-rescan reliability studies of mDixon Quant MR imaging. These studies are crucial to assess the consistency of the findings when repeated measurements are made to aid interpretation of the significance of changes including in individual patients.

(2) Comparison between fat fraction measurements at different centres and on different MRI scanners would be useful to understand whether measurements can be directly compared, for example from different clinical scanners or multi-centre studies.

(3) Cross sectional studies looking at the distribution of fat fraction across BMLs and whether or not these are homogenous and if not how that changes over time. This would help to understand the underlying pathophysiology of BMLs.

(4) Comparative clinical-pathological studies looking at how fat fraction imaging relates to underlying histologic change using specimens obtained at joint replacement surgery within BMLs. This would further improve the understanding of the pathophysiology underlying BMLs. This would also potentially allow imaging to better characterise BMLs changes in osteoarthritis in translational studies.

(5) Comparison of sensitivity to change of fat fraction with conventional volume measurements to determine if fat fraction measurements can improve the ability of imaging to monitor change in disease progression and response to treatment.

(6) Longitudinal studies looking at predictive ability of BMLs assessed using mDixon Quant sequence for clinical and structural outcomes, including pain, function, and progressive joint space narrowing.

9.5 Conclusion

Most conventional fluid sensitive MRI sequences are reliable and sensitive for the assessment of BML size. 3D gradient echo mDixon Quant imaging appears a promising technique for the assessment of BMLs in osteoarthritis, including both volumetric and compositional assessment, despite previous concerns about gradient echo imaging in the literature. T1 mapping holds promise as a novel approach to

imaging BMLs but is currently less feasible and less well validated than mDixon Quant imaging.

Bibliography

[1] D. S. C. Mathers and B. Pfleger, "Global burden of osteoarthritis in the year 2000," *World Health Organization, www who int/healthinfo/statistics/bod_osteoarthritis pdf,* 2003.

[2] S. Swain *et al.*, "Trends in Incidence and Prevalence of Osteoarthritis in the United Kingdom: Findings from the Clinical Practice Research Datalink (CPRD)," *Osteoarthritis and Cartilage,* 2020.

[3] T. Vos *et al.*, "Years lived with disability (YLDs) for 1160 sequelae of 289 diseases and injuries 1990-2010: a systematic analysis for the Global Burden of Disease Study 2010," *The Lancet,* vol. 380, no. 9859, pp. 2163-2196, 2010.

[4] R. C. Lawrence *et al.*, "Estimates of the prevalence of arthritis and other rheumatic conditions in the United States: Part II," *Arthritis & Rheumatism,* vol. 58, no. 1, pp. 26-35, 2008.

[5] A. Litwic, M. H. Edwards, E. M. Dennison, and C. Cooper, "Epidemiology and burden of osteoarthritis," *British medical bulletin,* vol. 105, no. 1, pp. 185-199, 2013.

[6] S. A. Oliveria, D. T. Felson, J. I. Reed, P. A. Cirillo, and A. M. Walker, "Incidence of symptomatic hand, hip, and knee osteoarthritis among patients in a health maintenance organization," *Arthritis & Rheumatism: Official Journal of the American College of Rheumatology,* vol. 38, no. 8, pp. 1134-1141, 1995.

[7] B. R. Deshpande *et al.*, "Number of persons with symptomatic knee osteoarthritis in the US: impact of race and ethnicity, age, sex, and obesity," *Arthritis care & research,* vol. 68, no. 12, pp. 1743-1750, 2016.

[8] K. Maurer, *Basic Data on Arthritis: Knee, Hip, and Sacroiliac Joints for Adults, 25-74 Years, United States, 1971-1975* (no. 213). Department of Health, Education and Welfare, Public Health Service, Office …, 1979.

[9] M. Cross *et al.*, "The global burden of hip and knee osteoarthritis: estimates from the global burden of disease 2010 study," *Annals of the Rheumatic Diseases,* vol. 73, no. 7, pp. 1323-1330, 2014.

[10] K. D. Brandt, M. Doherty, and S. Lohmander, "The concept of osteoarthritis as failure of the diarthrodial joint," *Osteoarthritis,* pp. 69-69, 2003.

[11] D. T. Felson *et al.*, "The association of bone marrow lesions with pain in knee osteoarthritis," *Annals of internal medicine,* vol. 134, no. 7, pp. 541-549, 2001.

[12] D. T. Felson *et al.*, "Correlation of the development of knee pain with enlarging bone marrow lesions on magnetic resonance imaging," *Arthritis & Rheumatology,* vol. 56, no. 9, pp. 2986-2992, 2007.

[13] D. J. Hunter *et al.*, "Increase in bone marrow lesions associated with cartilage loss: a longitudinal magnetic resonance imaging study of knee osteoarthritis," *Arthritis & Rheumatology,* vol. 54, no. 5, pp. 1529-1535, 2006.

[14] F. W. Roemer *et al.*, "Change in MRI-detected subchondral bone marrow lesions is associated with cartilage loss: the MOST Study. A longitudinal multicentre study of knee osteoarthritis," *Annals of the Rheumatic Diseases,* vol. 68, no. 9, pp. 1461-1465, 2009.

[15] C. G. Peterfy, G. Gold, F. Eckstein, F. Cicuttini, B. Dardzinski, and R. Stevens, "MRI protocols for whole-organ assessment of the knee in osteoarthritis," *Osteoarthritis and cartilage,* vol. 14, pp. 95-111, 2006.

[16] F. W. Roemer *et al.*, "Short tau inversion recovery and proton density-weighted fat suppressed sequences for the evaluation of osteoarthritis of the knee with a 1.0 T dedicated extremity MRI: development of a time-efficient sequence protocol," *European radiology,* vol. 15, no. 5, pp. 978-987, 2005.

[17] M. E. Mayerhoefer, M. J. Breitenseher, J. Kramer, N. Aigner, C. Norden, and S. Hofmann, "STIR vs. T1-weighted fat-suppressed gadolinium-enhanced MRI of bone marrow edema of the knee: Computer-assisted quantitative comparison and influence of injected contrast media volume and acquisition parameters," *Journal of Magnetic Resonance Imaging,* vol. 22, no. 6, pp. 788-793, 2005.

[18] M. J. Callaghan *et al.*, "A randomised trial of a brace for patellofemoral osteoarthritis targeting knee pain and bone marrow lesions," *Annals of the Rheumatic Diseases,* vol. 74, no. 6, pp. 1164-1170, 2015.

[19] W. T. Dixon, "Simple proton spectroscopic imaging," *Radiology,* vol. 153, no. 1, pp. 189-194, 1984.

[20] S. H. Duewell *et al.*, "Musculoskeletal MR imaging at 4 T and at 1.5 T: comparison of relaxation times and image contrast," *Radiology,* vol. 196, no. 2, pp. 551-555, 1995.

[21] R. Altman *et al.*, "Development of criteria for the classification and reporting of osteoarthritis: classification of osteoarthritis of the knee," *Arthritis & Rheumatology,* vol. 29, no. 8, pp. 1039-1049, 1986.

[22] L. Murphy *et al.*, "Lifetime risk of symptomatic knee osteoarthritis," *Arthritis Care & Research: Official Journal of the American College of Rheumatology,* vol. 59, no. 9, pp. 1207-1213, 2008.

[23] D. T. Felson *et al.*, "Osteoarthritis: new insights. Part 1: the disease and its risk factors," *Annals of internal medicine,* vol. 133, no. 8, pp. 635-646, 2000.

[24] A. Palotie *et al.*, "Predisposition to familial osteoarthrosis linked to type II collagen gene," *The Lancet,* vol. 333, no. 8644, pp. 924-927, 1989.

[25] K. Chapman *et al.*, "A meta-analysis of European and Asian cohorts reveals a global role of a functional SNP in the 5' UTR of GDF5 with osteoarthritis susceptibility," *Human molecular genetics,* vol. 17, no. 10, pp. 1497-1504, 2008.

[26] W. Zhang, "Risk factors of knee osteoarthritis–excellent evidence but little has been done," *Osteoarthritis and cartilage,* vol. 18, no. 1, pp. 1-2, 2010.

[27] J. W.-P. Michael, K. U. Schlüter-Brust, and P. Eysel, "The epidemiology, etiology, diagnosis, and treatment of osteoarthritis of the knee," *Deutsches Arzteblatt International,* vol. 107, no. 9, p. 152, 2010.

[28] J. W. Bijlsma, F. Berenbaum, and F. P. Lafeber, "Osteoarthritis: an update with relevance for clinical practice," *The Lancet,* vol. 377, no. 9783, pp. 2115-2126, 2011.

[29] J. H. Kellgren and J. S. Lawrence, "Radiological assessment of osteo-arthrosis," *Annals of the Rheumatic Diseases,* vol. 16, no. 4, p. 494, 1957.

[30] W. Liao, Z. Li, T. Li, Q. Zhang, H. Zhang, and X. Wang, "Proteomic analysis of synovial fluid in osteoarthritis using SWATH-mass spectrometry," *Molecular medicine reports,* vol. 17, no. 2, pp. 2827-2836, 2018.

[31] D. Schiphof, M. Boers, and S. M. Bierma-Zeinstra, "Differences in descriptions of Kellgren and Lawrence grades of knee osteoarthritis," *Annals of the rheumatic diseases,* vol. 67, no. 7, pp. 1034-1036, 2008.

[32] H. J. Braun and G. E. Gold, "Diagnosis of osteoarthritis: imaging," *Bone,* vol. 51, no. 2, pp. 278-288, 2012.

[33] S. Amin *et al.*, "The relationship between cartilage loss on magnetic resonance imaging and radiographic progression in men and women with knee osteoarthritis," *Arthritis & Rheumatism: Official Journal of the American College of Rheumatology,* vol. 52, no. 10, pp. 3152-3159, 2005.

[34] F. W. Roemer *et al.*, "MRI-detected subchondral bone marrow signal alterations of the knee joint: terminology, imaging appearance, relevance and radiological differential diagnosis," *Osteoarthritis and cartilage,* vol. 17, no. 9, pp. 1115-1131, 2009.

[35] M. K. Javaid *et al.*, "Pre-radiographic MRI findings are associated with onset of knee symptoms: the most study," *Osteoarthritis and cartilage,* vol. 18, no. 3, pp. 323-328, 2010.

[36] E. R. Garwood, M. P. Recht, and L. M. White, "Advanced imaging techniques in the knee: Benefits and limitations of new rapid acquisition strategies for routine knee MRI," *American Journal of Roentgenology,* vol. 209, no. 3, pp. 552-560, 2017.

[37] D. Hayashi, F. W. Roemer, and A. Guermazi, "Magnetic resonance imaging assessment of knee osteoarthritis: current and developing new concepts and techniques," *Clin Exp Rheumatol,* vol. 37, no. Suppl 120, pp. 88-95, 2019.

[38] W. Oldendorf, "Advantages and Disadvantages of MRI," in *Basics of Magnetic Resonance Imaging*: Springer, 1988, pp. 125-138.

[39] R. M. Shulman and B. Hunt, "Cardiac implanted electronic devices and MRI safety in 2018—the state of play," *European Radiology,* vol. 28, no. 10, pp. 4062-4065, 2018.

[40] D. Sayed *et al.*, "A comprehensive practice guideline for magnetic resonance imaging compatibility in implanted neuromodulation devices," *Neuromodulation: Technology at the Neural Interface,* vol. 23, no. 7, pp. 893-911, 2020.

[41] C. Jaimes, D. Biaggotti, G. Sreedher, A. Chaturvedi, M. M. Moore, and A. R. Danehy, "Magnetic resonance imaging in children with implants," *Pediatric Radiology,* vol. 51, no. 5, pp. 748-759, 2021.

[42] A. J. Wilson, W. A. Murphy, D. C. Hardy, and W. G. Totty, "Transient osteoporosis: transient bone marrow edema?," *Radiology,* vol. 167, no. 3, pp. 757-760, 1988.

[43] P. Garnero, C. Peterfy, S. Zaim, and M. Schoenharting, "Bone marrow abnormalities on magnetic resonance imaging are associated with type II collagen degradation in knee osteoarthritis: a three-month longitudinal study," *Arthritis & Rheumatology,* vol. 52, no. 9, pp. 2822-2829, 2005.

[44] F. J. Baranyay *et al.*, "Association of bone marrow lesions with knee structures and risk factors for bone marrow lesions in the knees of clinically healthy, community-based adults," in *Seminars in arthritis and rheumatism*, 2007, vol. 37, no. 2: Elsevier, pp. 112-118.

[45] S. Ip *et al.*, "Frequency of bone marrow lesions and association with pain severity: results from a population-based symptomatic knee cohort," *The Journal of rheumatology,* vol. 38, no. 6, pp. 1079-1085, 2011.

[46] M. Sowers *et al.*, "Magnetic resonance-detected subchondral bone marrow and cartilage defect characteristics associated with pain and X-ray-defined knee osteoarthritis," *Osteoarthritis and Cartilage,* vol. 11, no. 6, pp. 387-393, 2003.

[47] S. K. Tanamas *et al.*, "Bone marrow lesions in people with knee osteoarthritis predict progression of disease and joint replacement: a longitudinal study," *Rheumatology,* vol. 49, no. 12, pp. 2413-2419, 2010.

[48] J. Carrino, J. Blum, J. Parellada, M. Schweitzer, and W. Morrison, "MRI of bone marrow edema-like signal in the pathogenesis of subchondral cysts," *Osteoarthritis and cartilage,* vol. 14, no. 10, pp. 1081-1085, 2006.

[49] M. D. Crema *et al.*, "Subchondral cystlike lesions develop longitudinally in areas of bone marrow edema–like lesions in patients with or at risk for knee osteoarthritis: detection with MR imaging—the MOST study," *Radiology,* vol. 256, no. 3, pp. 855-862, 2010.

[50] M. Crema *et al.*, "373 MRI-detected bone marrow edema-like lesions are strongly associated with subchondral cysts in patients with or at risk for knee osteoarthritis: the MOST study," *Osteoarthritis and Cartilage,* vol. 16, p. S160, 2008.

[51] L. Torres *et al.*, "The relationship between specific tissue lesions and pain severity in persons with knee osteoarthritis," *Osteoarthritis and cartilage,* vol. 14, no. 10, pp. 1033-1040, 2006.

[52] P. R. Kornaat *et al.*, "Osteoarthritis of the knee: association between clinical features and MR imaging findings," *Radiology,* vol. 239, no. 3, pp. 811-817, 2006.

[53] M. Zanetti, E. Bruder, J. Romero, and J. Hodler, "Bone marrow edema pattern in osteoarthritic knees: correlation between MR imaging and histologic findings," *Radiology,* vol. 215, no. 3, pp. 835-840, 2000.
[54] E. Saadat *et al.*, "Diagnostic performance of in vivo 3-T MRI for articular cartilage abnormalities in human osteoarthritic knees using histology as standard of reference," *European radiology,* vol. 18, no. 10, pp. 2292-2302, 2008.
[55] L. L. Laslett *et al.*, "Zoledronic acid reduces knee pain and bone marrow lesions over 1 year: a randomised controlled trial," *Annals of the Rheumatic Diseases,* vol. 71, no. 8, pp. 1322-1328, 2012.
[56] L. M. Wildi *et al.*, "Chondroitin sulphate reduces both cartilage volume loss and bone marrow lesions in knee osteoarthritis patients starting as early as 6 months after initiation of therapy: a randomised, double-blind, placebo-controlled pilot study using MRI," *Annals of the Rheumatic Diseases,* vol. 70, no. 6, pp. 982-989, 2011.
[57] R. Bitar *et al.*, "MR pulse sequences: what every radiologist wants to know but is afraid to ask," *Radiographics,* vol. 26, no. 2, pp. 513-537, 2006.
[58] E. M. Purcell, H. C. Torrey, and R. V. Pound, "Resonance absorption by nuclear magnetic moments in a solid," *Physical review,* vol. 69, no. 1-2, p. 37, 1946.
[59] C. Kaut and C. Westbrook, *MRI in Practice*. Blackwell Science, 1998.
[60] F. Bloch, "Nuclear induction," *Physical review,* vol. 70, no. 7-8, p. 460, 1946.
[61] B. M. Dale, M. A. Brown, and R. C. Semelka, "MRI: basic principles and applications," 2015.
[62] N. Bloembergen, E. M. Purcell, and R. V. Pound, "Relaxation effects in nuclear magnetic resonance absorption," *Physical review,* vol. 73, no. 7, p. 679, 1948.
[63] D. Weishaupt, V. D. Köchli, and B. Marincek, *How does MRI work?: an introduction to the physics and function of magnetic resonance imaging*. Springer Science & Business Media, 2008.
[64] R. Damadian, "Tumor detection by nuclear magnetic resonance," 1971.
[65] J. T. Bushberg and J. M. Boone, *The essential physics of medical imaging*. Lippincott Williams & Wilkins, 2011.
[66] M. A. Brown, R. C. Semelka, and B. M. Dale, *MRI: basic principles and applications*. John Wiley & Sons, 2015.
[67] G. Sakellariou *et al.*, "EULAR recommendations for the use of imaging in the clinical management of peripheral joint osteoarthritis," *Annals of the rheumatic diseases,* vol. 76, no. 9, pp. 1484-1494, 2017.
[68] M. G. Fox *et al.*, "ACR appropriateness Criteria® chronic knee pain," *Journal of the American College of Radiology,* vol. 15, no. 11, pp. S302-S312, 2018.
[69] L. S. Lee, P. K. Chan, W. C. Fung, V. W. K. Chan, C. H. Yan, and K. Y. Chiu, "Imaging of knee osteoarthritis: A review of current evidence and clinical guidelines," *Musculoskeletal care,* vol. 19, no. 3, pp. 363-374, 2021.
[70] G. B. Chavhan, P. S. Babyn, B. G. Jankharia, H.-L. M. Cheng, and M. M. Shroff, "Steady-state MR imaging sequences: physics, classification, and clinical applications," *Radiographics,* vol. 28, no. 4, pp. 1147-1160, 2008.
[71] O. Bieri and K. Scheffler, "Fundamentals of balanced steady state free precession MRI," *Journal of Magnetic Resonance Imaging,* vol. 38, no. 1, pp. 2-11, 2013.
[72] K. Scheffler and S. Lehnhardt, "Principles and applications of balanced SSFP techniques," *European radiology,* vol. 13, no. 11, pp. 2409-2418, 2003.
[73] T. A. Bley, O. Wieben, C. J. François, J. H. Brittain, and S. B. Reeder, "Fat and water magnetic resonance imaging," *Journal of Magnetic Resonance Imaging,* vol. 31, no. 1, pp. 4-18, 2010.
[74] D. J. Hunter *et al.*, "Responsiveness and reliability of MRI in knee osteoarthritis: a meta-analysis of published evidence," *Osteoarthritis and cartilage,* vol. 19, no. 5, pp. 589-605, 2011.

[75] C. G. Peterfy, E. Schneider, and M. Nevitt, "The osteoarthritis initiative: report on the design rationale for the magnetic resonance imaging protocol for the knee," *Osteoarthritis and cartilage,* vol. 16, no. 12, pp. 1433-1441, 2008.

[76] T. M. Link, "MR imaging in osteoarthritis: hardware, coils, and sequences," *Radiologic clinics of North America,* vol. 47, no. 4, pp. 617-632, 2009.

[77] L. Xu, D. Hayashi, F. W. Roemer, D. T. Felson, and A. Guermazi, "Magnetic resonance imaging of subchondral bone marrow lesions in association with osteoarthritis," in *Seminars in arthritis and rheumatism*, 2012, vol. 42: Elsevier, pp. 105-118.

[78] D. W. McRobbie, E. A. Moore, M. J. Graves, and M. R. Prince, "MRI From Picture to Proton," *Journal of Magnetic,* 2008.

[79] F. Del Grande *et al.*, "Fat-suppression techniques for 3-T MR imaging of the musculoskeletal system," *Radiographics,* vol. 34, no. 1, pp. 217-233, 2014.

[80] D. Hayashi *et al.*, "Semiquantitative assessment of subchondral bone marrow edema-like lesions and subchondral cysts of the knee at 3T MRI: a comparison between intermediate-weighted fat-suppressed spin echo and Dual Echo Steady State sequences," *Bmc Musculoskeletal Disorders,* vol. 12, no. 1, p. 198, 2011.

[81] M. R. Schmid, J. Hodler, P. Vienne, C. A. Binkert, and M. Zanetti, "Bone marrow abnormalities of foot and ankle: STIR versus T1-weighted contrast-enhanced fat-suppressed spin-echo MR imaging," *Radiology,* vol. 224, no. 2, pp. 463-469, 2002.

[82] F. K. Nielsen, N. Egund, A. Jorgensen, D. A. Peters, and A. G. Jurik, "Assessment of subchondral bone marrow lesions in knee osteoarthritis by MRI: a comparison of fluid sensitive and contrast enhanced sequences," *Bmc Musculoskeletal Disorders,* vol. 17, Nov 16 2016.

[83] J.-P. Raynauld, L. M. Wildi, F. o. Abram, T. Moser, J.-P. Pelletier, and J. Martel-Pelletier, "Reliability and sensitivity to change of IW-TSE versus DESS magnetic resonance imaging sequences in the assessment of bone marrow lesions in knee osteoarthritis patients: Longitudinal data from the Osteoarthritis Initiative (OAI) cohort," *Journal of Biomedical Science and Engineering,* vol. 6, no. 03, p. 337, 2013.

[84] M. Zhang, J. B. Driban, L. L. Price, G. H. Lo, and T. E. McAlindon, "Magnetic resonance image sequence influences the relationship between bone marrow lesions volume and pain: data from the osteoarthritis initiative," *BioMed research international,* vol. 2015, 2015.

[85] A. E. Wluka *et al.*, "Bone marrow lesions can be subtyped into groups with different clinical outcomes using two magnetic resonance imaging (MRI) sequences," *Arthritis research & therapy,* vol. 17, no. 1, p. 270, 2015.

[86] F. W. Roemer *et al.*, "Volumetric and semiquantitative assessment of MRI-detected subchondral bone marrow lesions in knee osteoarthritis: a comparison of contrast-enhanced and non-enhanced imaging," *Osteoarthritis and cartilage,* vol. 18, no. 8, pp. 1062-1066, 2010.

[87] D. Muratovic *et al.*, "Bone marrow lesions detected by specific combination of MRI sequences are associated with severity of osteochondral degeneration," *Arthritis research & therapy,* vol. 18, no. 1, p. 54, 2016.

[88] C. G. Peterfy *et al.*, "Whole-organ magnetic resonance imaging score (WORMS) of the knee in osteoarthritis," *Osteoarthritis and cartilage,* vol. 12, no. 3, pp. 177-190, 2004.

[89] P. R. Kornaat *et al.*, "MRI assessment of knee osteoarthritis: Knee Osteoarthritis Scoring System (KOSS)-inter-observer and intra-observer reproducibility of a compartment-based scoring system," *Skeletal radiology,* vol. 34, no. 2, pp. 95-102, 2005.

[90] D. J. Hunter, G. H. Lo, D. Gale, A. J. Grainger, A. Guermazi, and P. G. Conaghan, "The reliability of a new scoring system for knee osteoarthritis MRI and the validity of bone marrow lesion assessment: BLOKS (Boston-Leeds Osteoarthritis Knee Score)," *Annals of the Rheumatic Diseases,* vol. 67, no. 2, pp. 206-211, 2008.

[91] D. J. Hunter *et al.*, "Evolution of semi-quantitative whole joint assessment of knee OA: MOAKS (MRI Osteoarthritis Knee Score)," *Osteoarthritis and cartilage,* vol. 19, no. 8, pp. 990-1002, 2011.
[92] J. A. Lynch *et al.*, "Comparison of BLOKS and WORMS scoring systems part I. Cross sectional comparison of methods to assess cartilage morphology, meniscal damage and bone marrow lesions on knee MRI: data from the osteoarthritis initiative," *Osteoarthritis and cartilage,* vol. 18, no. 11, pp. 1393-1401, 2010.
[93] F. W. Roemer, M. D. Crema, S. Trattnig, and A. Guermazi, "Advances in imaging of osteoarthritis and cartilage," *Radiology,* vol. 260, no. 2, pp. 332-354, 2011.
[94] C. Ratzlaff *et al.*, "A rapid, novel method of volumetric assessment of MRI-detected subchondral bone marrow lesions in knee osteoarthritis," *Osteoarthritis and cartilage,* vol. 21, no. 6, pp. 806-814, 2013.
[95] R. Stahl *et al.*, "Osteoarthritis of the knee at 3.0 T: comparison of a quantitative and a semi-quantitative score for the assessment of the extent of cartilage lesion and bone marrow edema pattern in a 24-month longitudinal study," *Skeletal radiology,* vol. 40, no. 10, pp. 1315-1327, 2011.
[96] J. B. Driban *et al.*, "Quantitative bone marrow lesion size in osteoarthritic knees correlates with cartilage damage and predicts longitudinal cartilage loss," *Bmc Musculoskeletal Disorders,* vol. 12, no. 1, p. 217, 2011.
[97] J. P. Raynauld *et al.*, "Correlation between bone lesion changes and cartilage volume loss in patients with osteoarthritis of the knee as assessed by quantitative magnetic resonance imaging over a 24-month period," *Annals of the Rheumatic Diseases,* vol. 67, no. 5, pp. 683-688, 2008.
[98] C. F. Maier, S. G. Tan, H. Hariharan, and H. G. Potter, "T2 quantitation of articular cartilage at 1.5 T," *Journal of Magnetic Resonance Imaging: An Official Journal of the International Society for Magnetic Resonance in Medicine,* vol. 17, no. 3, pp. 358-364, 2003.
[99] N. M. Menezes, M. L. Gray, J. R. Hartke, and D. Burstein, "T2 and T1rho MRI in articular cartilage systems," *Magnetic Resonance in Medicine: An Official Journal of the International Society for Magnetic Resonance in Medicine,* vol. 51, no. 3, pp. 503-509, 2004.
[100] C. Taylor, J. Carballido-Gamio, S. Majumdar, and X. Li, "Comparison of quantitative imaging of cartilage for osteoarthritis: T2, T1ρ, dGEMRIC and contrast-enhanced computed tomography," *Magnetic resonance imaging,* vol. 27, no. 6, pp. 779-784, 2009.
[101] J. Schooler *et al.*, "Longitudinal evaluation of T1ρ and T2 spatial distribution in osteoarthritic and healthy medial knee cartilage," *Osteoarthritis and cartilage,* vol. 22, no. 1, pp. 51-62, 2014.
[102] I. Cameron, "Techniques of Fat Suppression," *MR Phys Ottawa Hosp,* vol. 501, 2013.
[103] S. T. Schindera, B. J. Soher, D. M. Delong, B. M. Dale, and E. M. Merkle, "Effect of echo time pair selection on quantitative analysis for adrenal tumor characterization with in-phase and opposed-phase MR imaging: initial experience," *Radiology,* vol. 248, no. 1, pp. 140-147, 2008.
[104] L. S. Tufts, K. Shet, F. Liang, S. Majumdar, and X. Li, "Quantification of bone marrow water and lipid composition in anterior cruciate ligament-injured and osteoarthritic knees using three-dimensional magnetic resonance spectroscopic imaging," *Magnetic resonance imaging,* vol. 34, no. 5, pp. 632-637, 2016.
[105] G. H. Glover, "Multipoint Dixon technique for water and fat proton and susceptibility imaging," *Journal of Magnetic Resonance Imaging,* vol. 1, no. 5, pp. 521-530, 1991.
[106] S. B. Reeder *et al.*, "Quantification of hepatic steatosis with MRI: the effects of accurate fat spectral modeling," *Journal of Magnetic Resonance Imaging: An Official Journal of*

the International Society for Magnetic Resonance in Medicine, vol. 29, no. 6, pp. 1332-1339, 2009.

[107] S. B. Reeder *et al.*, "Multicoil Dixon chemical species separation with an iterative least-squares estimation method," *Magnetic resonance in medicine,* vol. 51, no. 1, pp. 35-45, 2004.

[108] T. J. P. Bray, A. Bainbridge, S. Punwani, Y. Ioannou, and M. A. Hall-Craggs, "Simultaneous quantification of bone edema/adiposity and structure in inflamed bone using chemical shift-encoded MRI in spondyloarthritis," *Magnetic resonance in medicine,* vol. 79, no. 2, pp. 1031-1042, 2018.

[109] G. E. Gold *et al.*, "Articular cartilage of the knee: rapid three-dimensional MR imaging at 3.0 T with IDEAL balanced steady-state free precessionâ€"initial experience," *Radiology,* vol. 240, no. 2, pp. 546-551, 2006.

[110] C. M. Gerdes, R. Kijowski, and S. B. Reeder, "IDEAL imaging of the musculoskeletal system: robust waterâ€"fat separation for uniform fat suppression, marrow evaluation, and cartilage imaging," *American Journal of Roentgenology,* vol. 189, no. 5, pp. W284-W291, 2007.

[111] F. Schick *et al.*, "MRI of muscular fat," *Magnetic Resonance in Medicine: An Official Journal of the International Society for Magnetic Resonance in Medicine,* vol. 47, no. 4, pp. 720-727, 2002.

[112] F. W. Roemer, F. Eckstein, and A. Guermazi, "Magnetic resonance imaging-based semiquantitative and quantitative assessment in osteoarthritis," *Rheumatic Disease Clinics of North America,* vol. 35, no. 3, pp. 521-555, 2009.

[113] D. C. Karampinos, G. Melkus, T. Baum, J. S. Bauer, E. J. Rummeny, and R. Krug, "Bone marrow fat quantification in the presence of trabecular bone: initial comparison between water-fat imaging and single-voxel MRS," *Magnetic resonance in medicine,* vol. 71, no. 3, pp. 1158-1165, 2014.

[114] C. S. Gee *et al.*, "Validation of bone marrow fat quantification in the presence of trabecular bone using MRI," *Journal of Magnetic Resonance Imaging,* vol. 42, no. 2, pp. 539-544, 2015.

[115] D. C. Karampinos *et al.*, "Quantitative MRI and spectroscopy of bone marrow," *Journal of Magnetic Resonance Imaging,* vol. 47, no. 2, pp. 332-353, 2018.

[116] T. J. P. Bray, M. D. Chouhan, S. Punwani, A. Bainbridge, and M. A. Hall-Craggs, "Fat fraction mapping using magnetic resonance imaging: insight into pathophysiology," *The British journal of radiology,* vol. 91, no. 1089, p. 20170344, 2017.

[117] T. J. Bray *et al.*, "Association of bone mineral density and fat fraction with magnetic susceptibility in inflamed trabecular bone," *Magnetic resonance in medicine,* vol. 81, no. 5, pp. 3094-3107, 2019.

[118] H. H. Hu, H. W. Kim, K. S. Nayak, and M. I. Goran, "Comparison of fat-water MRI and single-voxel MRS in the assessment of hepatic and pancreatic fat fractions in humans," *Obesity,* vol. 18, no. 4, pp. 841-847, 2010.

[119] G. Li *et al.*, "Comparison of chemical shift-encoded water-fat MRI and MR spectroscopy in quantification of marrow fat in postmenopausal females," *Journal of Magnetic Resonance Imaging,* vol. 45, no. 1, pp. 66-73, 2017.

[120] S. H. Lee, H. J. Yoo, S.-M. Yu, S. H. Hong, J.-Y. Choi, and H. D. Chae, "Fat quantification in the vertebral body: Comparison of modified dixon technique with single-voxel magnetic resonance spectroscopy," *Korean journal of radiology,* vol. 20, no. 1, pp. 126-133, 2019.

[121] S. B. Reeder, I. Cruite, G. Hamilton, and C. B. Sirlin, "Quantitative assessment of liver fat with magnetic resonance imaging and spectroscopy," *Journal of Magnetic Resonance Imaging,* vol. 34, no. 4, pp. 729-749, 2011.

[122] M. A. Fischer, C. W. A. Pfirrmann, N. Espinosa, D. A. Raptis, and F. M. Buck, "Dixon-based MRI for assessment of muscle-fat content in phantoms, healthy volunteers and

patients with achillodynia: comparison to visual assessment of calf muscle quality," *European radiology,* vol. 24, no. 6, pp. 1366-1375, 2014.

[123] T. A. L. Wren, S. Bluml, L. Tseng-Ong, and V. Gilsanz, "Three-point technique of fat quantification of muscle tissue as a marker of disease progression in Duchenne muscular dystrophy: preliminary study," *American Journal of Roentgenology,* vol. 190, no. 1, pp. W8-W12, 2008.

[124] M. Maas *et al.*, "Quantification of bone involvement in Gaucher disease: MR imaging bone marrow burden score as an alternative to Dixon quantitative chemical shift MR imagingâ€"initial experience," *Radiology,* vol. 229, no. 2, pp. 554-561, 2003.

[125] A. J. Taylor, M. Salerno, R. Dharmakumar, and M. Jerosch-Herold, "T1 mapping: basic techniques and clinical applications," *JACC: Cardiovascular Imaging,* vol. 9, no. 1, pp. 67-81, 2016.

[126] G. E. Gold, E. Han, J. Stainsby, G. Wright, J. Brittain, and C. Beaulieu, "Musculoskeletal MRI at 3.0 T: relaxation times and image contrast," *American Journal of Roentgenology,* vol. 183, no. 2, pp. 343-351, 2004.

[127] J. B. Vogler 3rd and W. A. Murphy, "Bone marrow imaging," *Radiology,* vol. 168, no. 3, pp. 679-693, 1988.

[128] D. G. Mitchell, D. L. Burk Jr, S. Vinitski, and M. D. Rifkin, "The biophysical basis of tissue contrast in extracranial MR imaging," *American Journal of Roentgenology,* vol. 149, no. 4, pp. 831-837, 1987.

[129] J. l. K. Barral, E. Gudmundson, N. Stikov, M. Etezadiâ€Amoli, P. Stoica, and D. G. Nishimura, "A robust methodology for in vivo T1 mapping," *Magnetic resonance in medicine,* vol. 64, no. 4, pp. 1057-1067, 2010.

[130] N. Stikov, C. Tardif, J. K. Barral, I. Levesque, and G. B. Pikes, "T1 mapping: methods and challenges," in *Proceedings International Society for Magnetic Resonance in medicine*, 2011, p. 1.

[131] S. A. Hurley, V. L. Yarnykh, K. M. Johnson, A. S. Field, A. L. Alexander, and A. A. Samsonov, "Simultaneous variable flip angleâ€"actual flip angle imaging method for improved accuracy and precision of threeâ€dimensional T1 and B1 measurements," *Magnetic resonance in medicine,* vol. 68, no. 1, pp. 54-64, 2012.

[132] G. Liberman, Y. Louzoun, and D. Ben Bashat, "T1 mapping using variable flip angle SPGR data with flip angle correction," *Journal of Magnetic Resonance Imaging,* vol. 40, no. 1, pp. 171-180, 2014.

[133] Z. Li *et al.*, "A simple B 1 correction method for dynamic contrast-enhanced MRI," *Physics in Medicine & Biology,* vol. 63, no. 16, p. 16NT01, 2018.

[134] E. K. Fram *et al.*, "Rapid calculation of T1 using variable flip angle gradient refocused imaging," *Magnetic resonance imaging,* vol. 5, no. 3, pp. 201-208, 1987.

[135] P. B. Kingsley and W. G. Monahan, "Effect of increased repetition time TR on precision of inversion-recovery T 1 measurements," *Magnetic resonance imaging,* vol. 19, no. 2, pp. 279-282, 2001.

[136] S. Barbosa, L. Blumhardt, N. Roberts, T. Lock, and R. Edwards, "Magnetic resonance relaxation time mapping in multiple sclerosis: normal appearing white matter and the “invisible” lesion load," *Magnetic resonance imaging,* vol. 12, no. 1, pp. 33-42, 1994.

[137] K. Yoneyama, Y. Kitanaka, O. Tanaka, and Y. J. Akashi, "Cardiovascular magnetic resonance imaging in heart failure," *Expert review of cardiovascular therapy,* vol. 16, no. 4, pp. 237-248, 2018.

[138] S. Smith, N. Roberts, D. Percy, and R. Edwards, "Detection of bone marrow abnormalities in patients with Hodgkin's disease by T1 mapping of MR images of lumbar vertebral bone marrow," *British journal of cancer,* vol. 65, no. 2, p. 246, 1992.

[139] M. Lin, X. Chen, S. Yu, F. Gao, and M. Ma, "Monitoring the efficacy of tumor necrosis factor alpha antagonists in the treatment of Ankylosing spondylarthritis: a pilot study

based on MR relaxometry technique," *BMC Medical Imaging,* vol. 21, no. 1, pp. 1-9, 2021.

[140] H. Noorveriandi, M. J. Parkes, M. J. Callaghan, D. T. Felson, T. W. O'Neill, and R. Hodgson, "Assessment of bone marrow oedema-like lesions using MRI in patellofemoral knee osteoarthritis: comparison of different MRI pulse sequences," *The British Journal of Radiology,* vol. 94, no. 1124, p. 20201367, 2021.

[141] X. Li *et al.*, "Quantitative assessment of bone marrow edema-like lesion and overlying cartilage in knees with osteoarthritis and anterior cruciate ligament tear using MR imaging and spectroscopic imaging at 3 Tesla," *Journal of Magnetic Resonance Imaging,* vol. 28, no. 2, pp. 453-461, 2008.

[142] E. De Bisschop, R. Luypaert, O. Louis, and M. Osteaux, "Fat fraction of lumbar bone marrow using in vivo proton nuclear magnetic resonance spectroscopy," *Bone,* vol. 14, no. 2, pp. 133-136, 1993.

[143] L. Johnson *et al.*, "Quantitative chemical shift imaging of vertebral bone marrow in patients with Gaucher disease," *Radiology,* vol. 182, no. 2, pp. 451-455, 1992.

[144] E. R. Danielsen and B. Ross, *Magnetic resonance spectroscopy diagnosis of neurological diseases*. CRC Press, 1999.

[145] I. M. Burtscher and S. Holtås, "Proton MR spectroscopy in clinical routine," *Journal of Magnetic Resonance Imaging: An Official Journal of the International Society for Magnetic Resonance in Medicine,* vol. 13, no. 4, pp. 560-567, 2001.

[146] S. R. Maheshwari, G. M. Fatterpekar, M. Castillo, and S. K. Mukherji, "Proton MR spectroscopy of the brain," in *Seminars in Ultrasound, CT and MRI*, 2000, vol. 21, no. 6: Elsevier, pp. 434-451.

[147] A. A. Maudsley *et al.*, "Numerical simulation of PRESS localized MR spectroscopy," *Journal of magnetic resonance,* vol. 173, no. 1, pp. 54-63, 2005.

[148] R. B. Thompson and P. S. Allen, "Response of metabolites with coupled spins to the STEAM sequence," *Magnetic Resonance in Medicine: An Official Journal of the International Society for Magnetic Resonance in Medicine,* vol. 45, no. 6, pp. 955-965, 2001.

[149] A. P. Burlina, T. Aureli, F. Bracco, F. Conti, and L. Battistin, "MR spectroscopy: a powerful tool for investigating brain function and neurological diseases," *Neurochemical research,* vol. 25, no. 9, pp. 1365-1372, 2000.

[150] D. Schellinger *et al.*, "Normal lumbar vertebrae: anatomic, age, and sex variance in subjects at proton MR spectroscopy—initial experience," *Radiology,* vol. 215, no. 3, pp. 910-916, 2000.

[151] J. F. Griffith *et al.*, "Vertebral bone mineral density, marrow perfusion, and fat content in healthy men and men with osteoporosis: dynamic contrast-enhanced MR imaging and MR spectroscopy," *Radiology,* vol. 236, no. 3, pp. 945-951, 2005.

[152] T. Baum *et al.*, "Does vertebral bone marrow fat content correlate with abdominal adipose tissue, lumbar spine bone mineral density, and blood biomarkers in women with type 2 diabetes mellitus?," *Journal of Magnetic Resonance Imaging,* vol. 35, no. 1, pp. 117-124, 2012.

[153] L. Van Dussen, P. Lips, H. Van Essen, C. Hollak, and N. Bravenboer, "Heterogeneous pattern of bone disease in adult type 1 Gaucher disease: clinical and pathological correlates," *Blood Cells, Molecules, and Diseases,* vol. 53, no. 3, pp. 118-123, 2014.

[154] A. Cohen *et al.*, "Marrow adiposity assessed on transiliac crest biopsy samples correlates with noninvasive measurement of marrow adiposity by proton magnetic resonance spectroscopy (1 H-MRS) at the spine but not the femur," *Osteoporosis International,* vol. 26, no. 10, pp. 2471-2478, 2015.

[155] X. Li *et al.*, "Quantification of vertebral bone marrow fat content using 3 Tesla MR spectroscopy: reproducibility, vertebral variation, and applications in osteoporosis," *Journal of Magnetic Resonance Imaging,* vol. 33, no. 4, pp. 974-979, 2011.

[156] V. M. Pansini, A. Monnet, J. Salleron, G. Penel, H. Migaud, and A. Cotten, "Reproducibility of 1H MR spectroscopy of hip bone marrow at 3 Tesla," *Journal of Magnetic Resonance Imaging,* vol. 36, no. 6, pp. 1445-1449, 2012.
[157] D. T. Felson *et al.*, "The efficacy of a lateral wedge insole for painful medial knee osteoarthritis after prescreening: a randomized clinical trial," *Arthritis & Rheumatology,* vol. 71, no. 6, pp. 908-915, 2019.
[158] D. T. Felson *et al.*, "Bone marrow edema and its relation to progression of knee osteoarthritis," *Annals of internal medicine,* vol. 139, no. 5_Part_1, pp. 330-336, 2003.
[159] P. R. Kornaat *et al.*, "Osteoarthritis of the knee: association between clinical features and MR imaging findings," *Radiology,* vol. 239, no. 3, pp. 811-817, 2006.
[160] G. H. Lo *et al.*, "Bone marrow lesions and joint effusion are strongly and independently associated with weight-bearing pain in knee osteoarthritis: data from the osteoarthritis initiative," *Osteoarthritis and cartilage,* vol. 17, no. 12, pp. 1562-1569, 2009.
[161] P. E. Shrout and J. L. Fleiss, "Intraclass correlations: uses in assessing rater reliability," *Psychological bulletin,* vol. 86, no. 2, p. 420, 1979.
[162] T. K. Koo and M. Y. Li, "A guideline of selecting and reporting intraclass correlation coefficients for reliability research," *Journal of chiropractic medicine,* vol. 15, no. 2, pp. 155-163, 2016.
[163] R. A. Armstrong, "When to use the B onferroni correction," *Ophthalmic and Physiological Optics,* vol. 34, no. 5, pp. 502-508, 2014.
[164] P. Schober, C. Boer, and L. A. Schwarte, "Correlation coefficients: appropriate use and interpretation," *Anesthesia & Analgesia,* vol. 126, no. 5, pp. 1763-1768, 2018.
[165] J. H. Lee, J. P. Dyke, D. Ballon, D. M. Ciombor, G. Tung, and R. K. Aaron, "Assessment of bone perfusion with contrast-enhanced magnetic resonance imaging," *Orthopedic Clinics of North America,* vol. 40, no. 2, pp. 249-257, 2009.
[166] S. Mirowitz, P. Apicella, W. Reinus, and A. Hammerman, "MR imaging of bone marrow lesions: Relative conspicuousness on T1-weighted, fat-suppressed T2-weighted, and STIR images," *AJR. American journal of roentgenology,* vol. 162, no. 1, pp. 215-221, 1994.
[167] S. Brandão *et al.*, "Comparing T1-weighted and T2-weighted three-point Dixon technique with conventional T1-weighted fat-saturation and short-tau inversion recovery (STIR) techniques for the study of the lumbar spine in a short-bore MRI machine," *Clinical radiology,* vol. 68, no. 11, pp. e617-e623, 2013.
[168] H. J. Park *et al.*, "Usefulness of the fast spin-echo three-point Dixon (mDixon) image of the knee joint on 3.0-T MRI: comparison with conventional fast spin-echo T 2 weighted image," *The British journal of radiology,* vol. 89, no. 1062, p. 20151074, 2016.
[169] N. Van Vucht *et al.*, "The Dixon technique for MRI of the bone marrow," *Skeletal radiology,* vol. 48, no. 12, pp. 1861-1874, 2019.
[170] T. Kirchgesner, M. Stoenoiu, N. Michoux, P. Durez, and B. V. Berg, "Comparison between 3-point Dixon-and CHESS-based OMERACT-recommended MRI protocols in hands of patients with suspicion of early rheumatoid arthritis," *European Journal of Radiology,* vol. 134, p. 109412, 2021.
[171] P. Pezeshk, A. Alian, and A. Chhabra, "Role of chemical shift and Dixon based techniques in musculoskeletal MR imaging," *European journal of radiology,* vol. 94, pp. 93-100, 2017.
[172] M. Bastian-Jordan, S. Dhupelia, M. McMeniman, M. Lanham, and J. Hislop-Jambrich, "A quality audit of MRI knee exams with the implementation of a novel 2-point DIXON sequence," *Journal of medical radiation sciences,* vol. 66, no. 3, pp. 163-169, 2019.
[173] N. Sollmann, C. Rüther, S. Schön, C. Zimmer, T. Baum, and J. S. Kirschke, "Implementation of a sagittal T2-weighted DIXON turbo spin-echo sequence may

shorten MRI acquisitions in the emergency setting of suspected spinal bleeding," *European Radiology Experimental,* vol. 5, no. 1, pp. 1-11, 2021.

[174] H. Huang *et al.*, "Qualitative and quantitative assessment of sacroiliitis in axial spondyloarthropathy: can a single T2-weighted Dixon sequence replace the standard protocol?," *Clinical radiology,* vol. 75, no. 4, pp. 321. e13-321. e20, 2020.

[175] C. F. Lins *et al.*, "Six-point DIXON and Magnetic Resonance Spectroscopy Techniques in Quantifying Bone Marrow Fat in Sickle Cell Disease," *Academic radiology,* 2021.

[176] M. A. Bowes *et al.*, "Machine-learning, MRI bone shape and important clinical outcomes in osteoarthritis: data from the Osteoarthritis Initiative," *Annals of the rheumatic diseases,* vol. 80, no. 4, pp. 502-508, 2021.

[177] S. M. Mattap *et al.*, "How do MRI-detected subchondral bone marrow lesions (BMLs) on two different MRI sequences correlate with clinically important outcomes?," *Calcified tissue international,* vol. 103, no. 2, pp. 131-143, 2018.

[178] S. Seah *et al.*, "The relationship of tibial bone perfusion to pain in knee osteoarthritis," *Osteoarthritis and cartilage,* vol. 20, no. 12, pp. 1527-1533, 2012.

[179] J.-F. Budzik *et al.*, "Perfusion of subchondral bone marrow in knee osteoarthritis: A dynamic contrast-enhanced magnetic resonance imaging preliminary study," *European journal of radiology,* vol. 88, pp. 129-134, 2017.

[180] C. L. Daugaard *et al.*, "Perfusion in bone marrow lesions assessed on DCE-MRI and its association with pain in knee osteoarthritis: a cross-sectional study," *Skeletal radiology,* vol. 49, no. 5, pp. 757-764, 2020.

[181] B. A. de Vries *et al.*, "Quantitative subchondral bone perfusion imaging in knee osteoarthritis using dynamic contrast enhanced MRI," in *Seminars in arthritis and rheumatism*, 2020, vol. 50, no. 2: Elsevier, pp. 177-182.

[182] F. Hu *et al.*, "3D Multi-Echo Dixon technique for simultaneous assessment of liver steatosis and iron overload in patients with chronic liver diseases: a feasibility study," *Quantitative imaging in medicine and surgery,* vol. 9, no. 6, p. 1014, 2019.

[183] Y. Chan, "Biostatistics 104: correlational analysis," *Singapore Med J,* vol. 44, no. 12, pp. 614-9, 2003.

[184] M. Farrow *et al.*, "Quantitative MRI in myositis patients: comparison with healthy volunteers and radiological visual assessment," *Clinical Radiology,* vol. 76, no. 1, pp. 81. e1-81. e10, 2021.

[185] C.-x. YANG, C.-n. MAO, and S.-z. WANG, "Magnetization Transfer Subtraction Picture in the Diagnosis of Degenerative Osteoarthritis of the Knee," *Chinese Journal of CT and MRI,* p. 02, 2013.

[186] T. Kirchgesner, M. Stoenoiu, N. Michoux, P. Durez, and B. V. Berg, "Contrast-enhanced T1-weighted Dixon water-and fat-only images to assess osteitis and erosions according to RAMRIS in hands of patients with early rheumatoid arthritis," *Diagnostic and Interventional Imaging,* 2021.

[187] C. M. Phan *et al.*, "MR imaging findings in the follow-up of patients with different stages of knee osteoarthritis and the correlation with clinical symptoms," *European radiology,* vol. 16, no. 3, pp. 608-618, 2006.

[188] E. C. Sayre *et al.*, "Associations between MRI features versus knee pain severity and progression: Data from the Vancouver Longitudinal Study of Early Knee Osteoarthritis," *PloS one,* vol. 12, no. 5, p. e0176833, 2017.

[189] D. T. Felson *et al.*, "Bone marrow lesions in knee osteoarthritis change in 6–12 weeks," *Osteoarthritis and cartilage,* vol. 20, no. 12, pp. 1514-1518, 2012.

[190] F. K. Nielsen, N. Egund, D. Peters, and A. G. Jurik, "Measurement of bone marrow lesions by MR imaging in knee osteoarthritis using quantitative segmentation methods–a reliability and sensitivity to change analysis," *BMC musculoskeletal disorders,* vol. 15, no. 1, p. 447, 2014.

[191] J. S. Gregory *et al.*, "MRI and the distribution of bone marrow fat in hip osteoarthritis," *Journal of Magnetic Resonance Imaging,* vol. 45, no. 1, pp. 42-50, 2017.
[192] M. M. Mukaka, "A guide to appropriate use of correlation coefficient in medical research," *Malawi Medical Journal,* vol. 24, no. 3, pp. 69-71, 2012.
[193] E. E. Bron *et al.*, "Image registration improves human knee cartilage T1 mapping with delayed gadolinium-enhanced MRI of cartilage (dGEMRIC)," *European radiology,* vol. 23, no. 1, pp. 246-252, 2013.
[194] G. Brix, S. Heiland, M. E. Bellemann, T. Koch, and W. J. Lorenz, "MR imaging of fat-containing tissues: valuation of two quantitative imaging techniques in comparison with localized proton spectroscopy," *Magnetic resonance imaging,* vol. 11, no. 7, pp. 977-991, 1993.
[195] R. Longo *et al.*, "Proton MR spectroscopy in quantitative in vivo determination of fat content in human liver steatosis," *Journal of Magnetic Resonance Imaging,* vol. 5, no. 3, pp. 281-285, 1995.
[196] F. Träber *et al.*, "Determination of H relaxation times of water in human bone marrow by fat-suppressed turbo spin echo in comparison to MR spectroscopic methods," *Journal of Magnetic Resonance Imaging,* vol. 6, no. 3, pp. 541-548, 1996.
[197] J. A. Rioux, I. R. Levesque, and B. K. Rutt, "Biexponential longitudinal relaxation in white matter: characterization and impact on T1 mapping with IR-FSE and MP2RAGE," *Magnetic resonance in medicine,* vol. 75, no. 6, pp. 2265-2277, 2016.
[198] B. Marty *et al.*, "Simultaneous muscle water T2 and fat fraction mapping using transverse relaxometry with stimulated echo compensation," *NMR in biomedicine,* vol. 29, no. 4, pp. 431-443, 2016.
[199] H. Shao *et al.*, "UTE bi-component analysis of T2* relaxation in articular cartilage," *Osteoarthritis and cartilage,* vol. 24, no. 2, pp. 364-373, 2016.
[200] M. A. Bernstein, K. F. King, and X. J. Zhou, *Handbook of MRI pulse sequences*. Elsevier, 2004.
[201] D. Stefan *et al.*, "Quantitation of magnetic resonance spectroscopy signals: the jMRUI software package," *Measurement Science and Technology,* vol. 20, no. 10, p. 104035, 2009.
[202] C. D. Jordan, M. Saranathan, N. K. Bangerter, B. A. Hargreaves, and G. E. Gold, "Musculoskeletal MRI at 3.0 T and 7.0 T: a comparison of relaxation times and image contrast," *European journal of radiology,* vol. 82, no. 5, pp. 734-739, 2013.
[203] K. Fukuzawa *et al.*, "Evaluation of six-point modified dixon and magnetic resonance spectroscopy for fat quantification: a fat–water–iron phantom study," *Radiological physics and technology,* vol. 10, no. 3, pp. 349-358, 2017.
[204] J. H. Liao *et al.*, "qMRI relaxometry of mandibular bone marrow: a monomodal distribution in sickle cell disease," *Journal of Magnetic Resonance Imaging,* vol. 37, no. 5, pp. 1182-1188, 2013.
[205] E. Elias *et al.*, "Quantitative MRI analysis of craniofacial bone marrow in patients with sickle cell disease," *American Journal of Neuroradiology,* vol. 34, no. 3, pp. 622-627, 2013.
[206] K. Ecklund *et al.*, "Bone marrow fat content in 70 adolescent girls with anorexia nervosa: Magnetic resonance imaging and magnetic resonance spectroscopy assessment," *Pediatric radiology,* vol. 47, no. 8, pp. 952-962, 2017.
[207] C. Thomsen, P. G. Sørensen, H. Karle, P. Christoffersen, and O. Henriksen, "Prolonged bone marrow T1-relaxation in acute leukaemia. In vivo tissue characterization by magnetic resonance imaging," *Magnetic resonance imaging,* vol. 5, no. 4, pp. 251-257, 1987.
[208] K. E. Jensen *et al.*, "Prolonged bone marrow T1-relaxation in patients with polycythemia vera," *Magnetic resonance imaging,* vol. 6, no. 3, pp. 291-292, 1988.

[209] C. Le Ster, J. Lasbleiz, S. Kannengiesser, R. Guillin, G. Gambarota, and H. Saint-Jalmes, "A fast method for the quantification of fat fraction and relaxation times: Comparison of five sites of bone marrow," *Magnetic resonance imaging,* vol. 39, pp. 157-161, 2017.
[210] B. R. Rosen *et al.*, "Hematologic bone marrow disorders: quantitative chemical shift MR imaging," *Radiology,* vol. 169, no. 3, pp. 799-804, 1988.
[211] R. M. D. Vre, R. Grimee, F. Parmentier, and J. Binet, "The use of agar gel as a basic reference material for calibrating relaxation times and imaging parameters," *Magnetic resonance in medicine,* vol. 2, no. 2, pp. 176-179, 1985.
[212] S. J. Matzat, E. J. McWalter, F. Kogan, W. Chen, and G. E. Gold, "T2 Relaxation time quantitation differs between pulse sequences in articular cartilage," *Journal of Magnetic Resonance Imaging,* vol. 42, no. 1, pp. 105-113, 2015.
[213] L. Dajue and H.-H. Mündel, *Safflower, Carthamus tinctorius L*. Bioversity International, 1996.
[214] V. Fortier and I. R. Levesque, "Longitudinal relaxation in fat-water mixtures and its dependence on fat content at 3 T," *NMR in Biomedicine,* p. e4629, 2021.
[215] G. Hamilton *et al.*, "In vivo breath-hold 1H MRS simultaneous estimation of liver proton density fat fraction, and T1 and T2 of water and fat, with a multi-TR, multi-TE sequence," *Journal of Magnetic Resonance Imaging,* vol. 42, no. 6, pp. 1538-1543, 2015.
[216] D. Hernando, S. D. Sharma, H. Kramer, and S. B. Reeder, "On the confounding effect of temperature on chemical shift-encoded fat quantification," *Magnetic resonance in medicine,* vol. 72, no. 2, pp. 464-470, 2014.
[217] R. Donners, A. Hirschmann, A. Gutzeit, and D. Harder, "T2-weighted Dixon MRI of the spine: A feasibility study of quantitative vertebral bone marrow analysis," *Diagnostic and Interventional Imaging,* 2021.
[218] M. Richards, J. A. Webb, S. Jewell, W. Gregory, and R. Reznek, "In-vivo measurement of spin lattice relaxation time (T 1) of bone marrow in healthy volunteers: the effects of age and sex," *The British journal of radiology,* vol. 61, no. 721, pp. 30-33, 1988.
[219] D. Tamada, T. Wakayama, H. Onishi, and U. Motosugi, "Multiparameter estimation using multi-echo spoiled gradient echo with variable flip angles and multicontrast compressed sensing," *Magnetic resonance in medicine,* vol. 80, no. 4, pp. 1546-1555, 2018.
[220] C. Le Ster, G. Gambarota, J. Lasbleiz, R. Guillin, O. Decaux, and H. Saint-Jalmes, "Breath-hold MR measurements of fat fraction, T1, and T2* of water and fat in vertebral bone marrow," *Journal of Magnetic Resonance Imaging,* vol. 44, no. 3, pp. 549-555, 2016.
[221] L. Marage, J. Lasbleiz, M. Fondin, M. Lederlin, G. Gambarota, and H. Saint-Jalmes, "Voxel-based mapping of five MR biomarkers in the wrist bone marrow," *Magnetic Resonance Materials in Physics, Biology and Medicine,* pp. 1-12, 2021.
[222] M. Cencini, L. Biagi, J. D. Kaggie, R. F. Schulte, M. Tosetti, and G. Buonincontri, "Magnetic resonance fingerprinting with dictionary-based fat and water separation (DBFW MRF): a multi-component approach," *Magnetic resonance in medicine,* vol. 81, no. 5, pp. 3032-3045, 2019.
[223] J. Ostenson, B. M. Damon, and E. B. Welch, "MR fingerprinting with simultaneous T1, T2, and fat signal fraction estimation with integrated B0 correction reduces bias in water T1 and T2 estimates," *Magnetic resonance imaging,* vol. 60, pp. 7-19, 2019.
[224] B. Marty, B. Coppa, and P. G. Carlier, "Monitoring skeletal muscle chronic fatty degenerations with fast T1-mapping," *European radiology,* vol. 28, no. 11, pp. 4662-4668, 2018.
[225] B. Marty and P. G. Carlier, "MR fingerprinting for water T1 and fat fraction quantification in fat infiltrated skeletal muscles," *Magnetic resonance in medicine,* vol. 83, no. 2, pp. 621-634, 2020.

[226] B. Marty, A. L. Lopez Kolkovsky, E. C. Araujo, and H. Reyngoudt, "Quantitative skeletal muscle imaging using 3D MR fingerprinting with water and fat separation," *Journal of Magnetic Resonance Imaging,* vol. 53, no. 5, pp. 1529-1538, 2021.

[227] B. Marty *et al.*, "Water-Fat Separation in MR Fingerprinting for Quantitative Monitoring of the Skeletal Muscle in Neuromuscular Disorders," *Radiology,* vol. 300, no. 3, pp. 652-660, 2021.